UNIVERSITÀ DEGLI STUDI DI CATANIA
DOTTORATO INTERNAZIONALE IN NEUROBIOLOGIA
XXV CICLO

BASI MOLECOLARI DEI DCP (DISORDINI CONFORMAZIONALI PROTEICI) A CARICO DEL SISTEMA NERVOSO: CONDIZIONI MICROAMBIENTALI E INTERRELAZIONI CELLULARI

Dott. Giuseppe Caruso

TESI DI DOTTORATO

Coordinatore: **Chiar.mo Prof. Roberto Avola**

Tutor: **Chiar.mo Prof. Vincenzo G. Nicoletti**

ANNO ACCADEMICO 2012-2013

INDEX

INTRODUCTION

PROTEIN CONFORMATIONAL DISORDERS (PCDs)

The biological function of a protein depends on its tridimensional structure, which is determined by its amino acid sequence during the process of protein folding (**Fig. 1**).

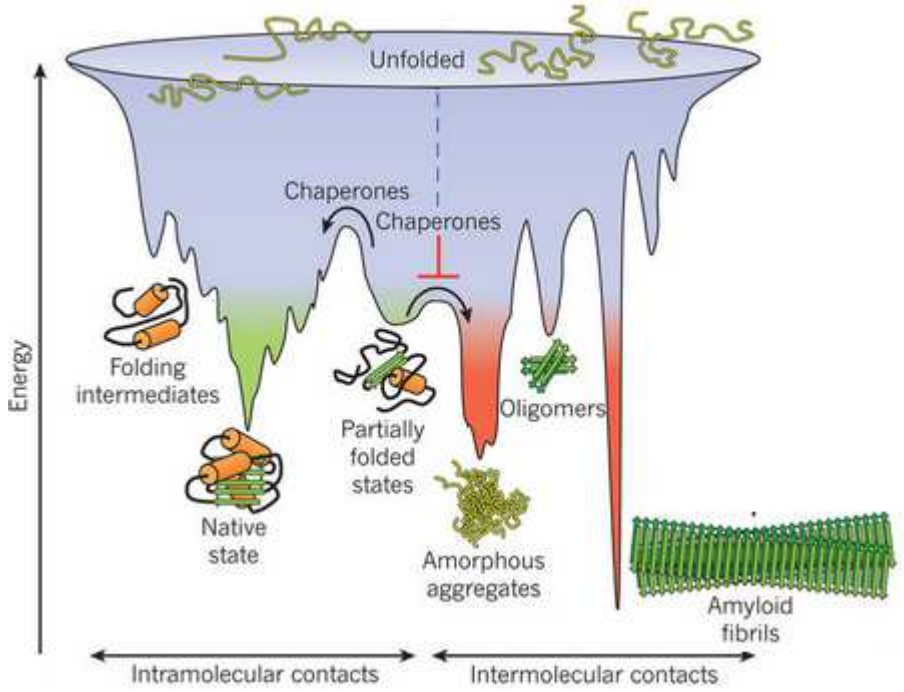

Figure 1 - Scheme of the funnel-shaped free-energy surface that proteins explore as they move towards the native state (green) by forming intramolecular contacts.

Several diseases have been shown to arise from protein misfolding and are grouped together under the name of protein conformational disorders (PCDs) [1-5].

The hallmark event in PCDs is a change in the secondary and/or tertiary structure of a normal protein without alteration of the primary structure. The conformational change may promote the disease by either gain of a toxic activity or by the lack of biological function of the natively folded protein [3,5] (**Fig. 2**).

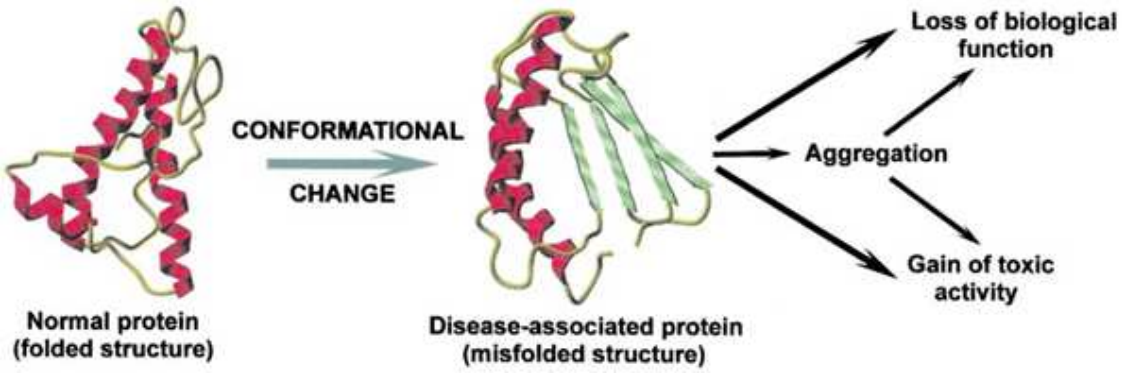

Figure 2 - Protein misfolding and disease.

Proteins that are normally soluble convert into insoluble aggregates that can form intractable and frequently toxic deposits in the brain, in skeletal and muscular tissue and in the heart and the liver [6].

The onset of aggregation may be triggered by any factor resulting in a rise of the concentration of the amyloidogenic precursor(s) such as a shift of the equilibrium between correctly folded and partially folded molecules towards the latter or an increase of the expression level of the affected protein and hence its whole equilibrium population comprising partially folded molecules [7](**Fig. 3**).

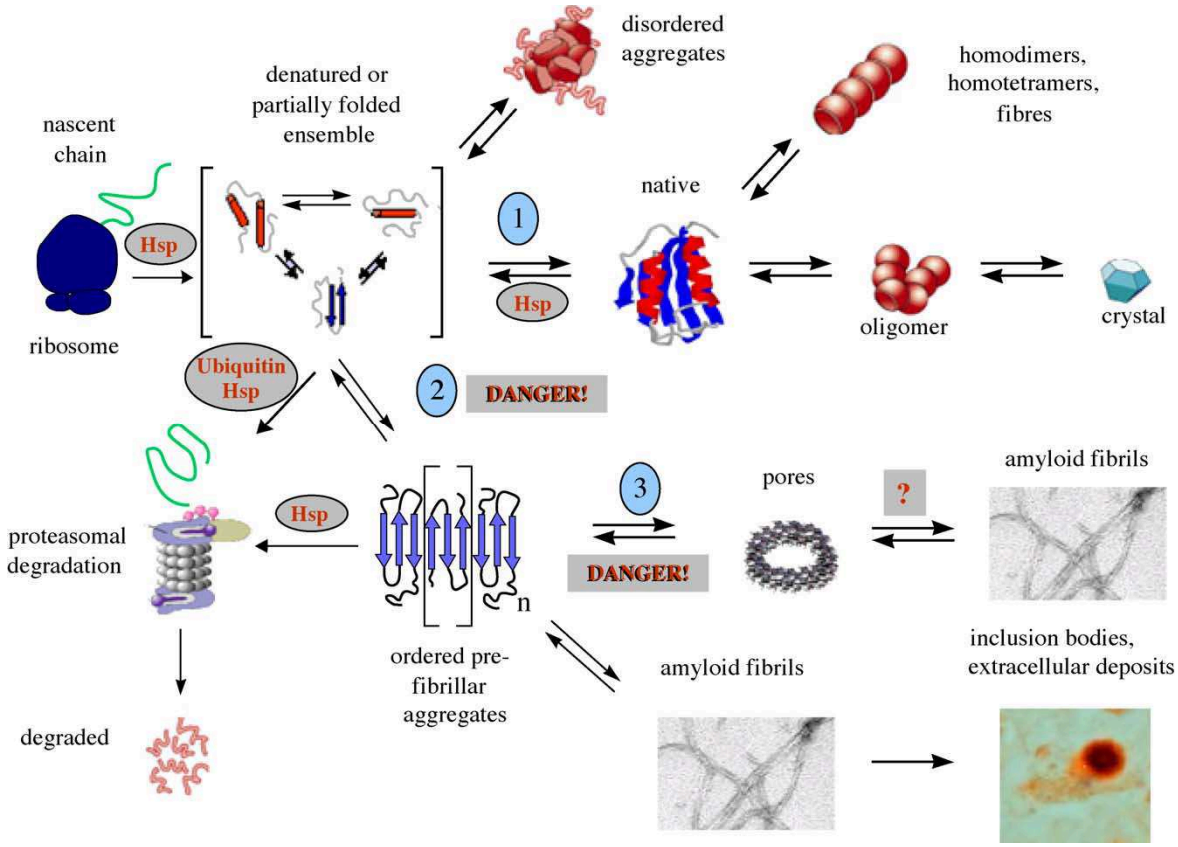

Figure 3 - The possible fates of newly synthesized polypeptide chains. Modifications of protein structure or medium conditions may favour protein-protein interactions into fibers or into crystalline lattices. Should these conditions be destabilising, the equilibrium (1) is shifted to the left thus increasing the population of partly folded molecules. Under normal conditions, these are refolded by the molecular chaperones or cleared by the ubiquitin-proteasome machinery. Should these machineries be impaired or the population of misfolded molecules overwhelm their buffering possibility, disordered aggregates arise or the aggregation path is undertaken. Equilibrium (2) is intrinsically shifted to the right and the nucleation of ordered aggregates is kinetically favoured by mutations increasing the mean hydrophobicity or propensity to beta structure or reducing the net charge of the misfolded/unfolded molecules. The formation of pre-fibrillar assemblies in the form of amyloid pores (equilibrium (3)) could be directly related to the cytotoxic effects of amyloids.

This may be the case of mutations, environmental changes or chemical modifications reducing the conformational stability of the protein. Alternatively, specific mutations may enhance aggregation simply by favouring kinetically the assembly of the unfolded

or partly folded monomers into the early oligomeric pre-fibrillar species (**Fig. 3**). Finally, protein aggregation may be favoured under conditions resulting in the impairment or overwhelming of the molecular machineries aimed at performing the quality control of protein folding.

The PCDs includes Alzheimer's disease (AD), transmissible spongiform encephalopathies (TSEs), serpin-de¢ciency disorders, haemolytic anemia, Huntington disease (HD), cystic fibrosis, diabetes mellitus type II, amyotrophic lateral sclerosis (ALS), Parkinson disease (PD), dialysis-related amyloidosis and many other diseases (**Table 1**).

PROTEIN INVOLVED	DISEASE
Amyloid-β	AD
α-Synuclein	PD
Amylin	Diabetes type II
SOD	ALS
β2-Microglobulin	Haemodialysis-related amyloidosis
Amyloid-A	Reactive amyloidosis
CFTR protein	Cystic fibrosis
Hemoglobin	Sickle cell anemia
Huntingtin	HD
PrP	Creutzfeldt-Jakob disease and relate disorders
Other proteins	Systemic and cerebral hereditary amyloidosis

Table 1 - List of some diseases that have been classi¢ed in the group of PCDs [2-5].

In most of PCDs the misfolded protein is rich in β-sheet conformation [4,5]. β-Sheets are one of the prevalent, repetitive secondary structures in folded proteins and are formed of alternating peptide pleated strands linked by hydrogen bonding between the NH and CO groups of the peptide bond. While in α-helices the hydrogen bonds are between groups within the same strand, in β-sheets the bonds are between one strand and another. Since the second β-strand can come from a different region of the same protein or from a different molecule, formation of β-sheets is usually stabilized by protein oligomerization or aggregation.

With the exception of cystic fibrosis and some forms of TSE, the end point of protein misfolding in PCD is aberrant protein aggregation and accumulation as amyloid-like deposits in diverse organs [2,3,8-10]. Despite the large differences in the structures of the proteins and peptides contributing to the aggregates found in the differing diseases, amyloid fibrils are surprisingly similar and share basic structural features. Typically, amyloid fibrils are straight, unbranched, 6-12 nm wide (but larger in some cases)

formed by a variable number of elementary filaments (protofilaments) around 1.5-2.0 nm in diameter, twisted around each other in a rope-like structure [11,12](**Fig. 4**).

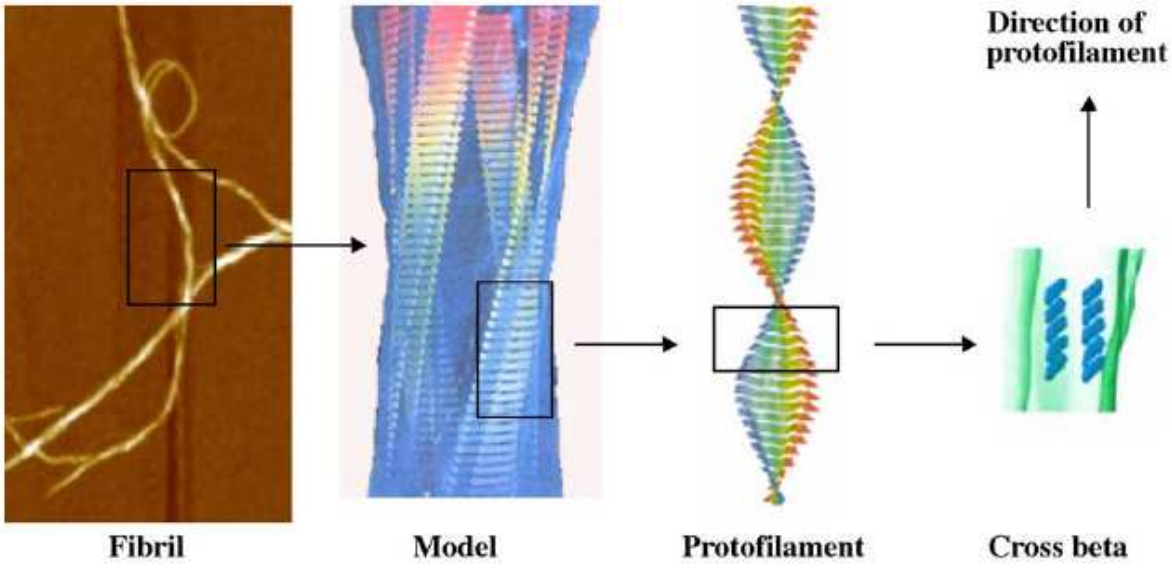

Figure 4 - Close-up view of the structural organization of an amyloid fibril. The four protofilaments are wound around each other and their core structure is a row of β-sheets where each strand runs perpendicular to the fibril axis.

The correlation and co-localization of protein aggregates with degenerating tissue and disease symptoms is a strong indication of the involvement of amyloid deposition in the pathogenesis of PCD [8-10]. Moreover, protein deposits have become a typical signature of PCD and their presence is used for definitive diagnosis [13,14].

Most PCDs have both an inherited and sporadic origin.

Studies with transgenic animal models have been useful in understanding the contribution of the misfolded protein in disease pathogenesis [15-21]. Transgenic mice that overexpress high levels of human amyloid precursor protein containing diverse mutations progressively develop many of the pathological hallmarks of AD, including cerebral amyloid deposits, neuritic dystrophy, astrogliosis, neuronal loss and cognitive and behavioral alterations [15,19,22,23].

A transgenic mouse model with high rates of expression of human islet amyloid polypeptide (IAPP) spontaneously developed diabetes mellitus by 8 weeks of age, which was associated with selective β death and impaired insulin secretion [20]. Small intra- and extracellular IAPP aggregates were present in islets of transgenic mice during the development of diabetes mellitus.

ALZHEIMER'S DISEASE (AD) AND B-AMYLOID

Alzheimer's disease (AD) is the most common agerelated neurodegenerative disorder, and one of the most devastating diagnoses that patients and their families can receive. The clinical symptoms result from the deterioration of selective cognitive domains, particularly those related to memory. Memory decline initially manifests as a loss of episodic memory. The dysfunction in episodic memory impedes recollection of recent events including autobiographical activities.

In 1907, Alois Alzheimer described two pathological alterations in the brain of a female patient suffering from dementia [24]. These two lesions represent the hallmark pathognomic features of the disease, and their observation during postmortem examination is still required for a diagnosis of AD. Alzheimer described a "peculiar substance" occurring as extracellular deposits in specific brain regions, which are now referred to as amyloid plaques (**Fig. 5 A**).

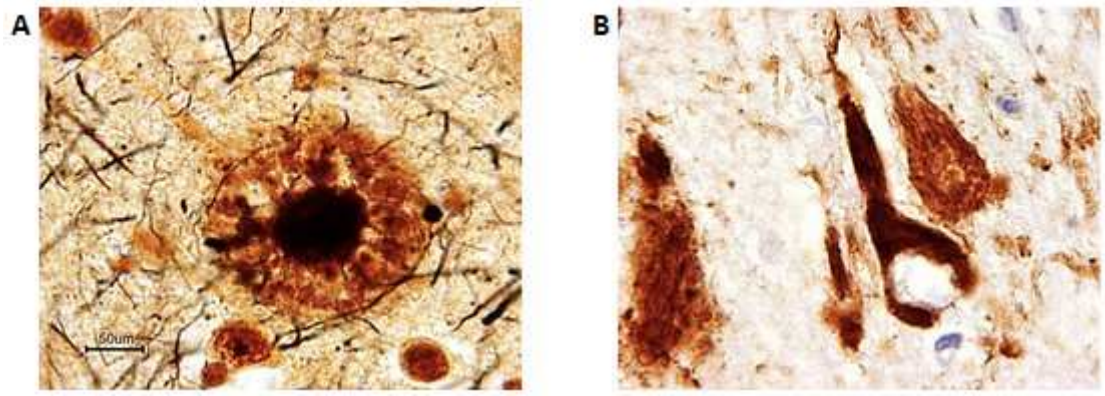

Figure 5 - Amyloid plaques (A), and neurofibrillary tangles (B).

It was not until the mid-1980s that it was discovered that the plaques consist of aggregates of a small peptide called amyloid-β (Aβ) [25,26]. The second lesion described by Alzheimer, neurofibrillary tangles (NFTs) (**Fig. 5 B**), occurs intraneuronally. NFTs are aggregates composed by the microtubule-associated protein tau that exhibits hyperphosphorylation and oxidative modifications. This protein has a fundamental role in the assemblage and activity of the microtubules, stabilizing the cytoscheletric structure, and participates in the axonal transport.

In AD patients, protein tau results to be hyperphosphorylated with consequent reduction of its ability to bind the microtubules and therefore it can aggregate and precipitate within the cell [27].

Numerous other structural and functional alterations ensue, including inflammatory

responses and oxidative stress [28-31]. The combined consequences of all the pathological changes, including the effects of the Aβ and tau pathologies, is severe neuronal and synaptic dysfunction and loss; at the time of death, the brain of a patient with AD may weigh one-third less than the brain of an age-matched, non-demented individual.

Basic science investigations were identifying microglia (brain-resident macrophage-typic cells) as proliferative brain cells recruited to AD-associated amyloid-β (Aβ) plaques [32,33] (**Fig. 6**).

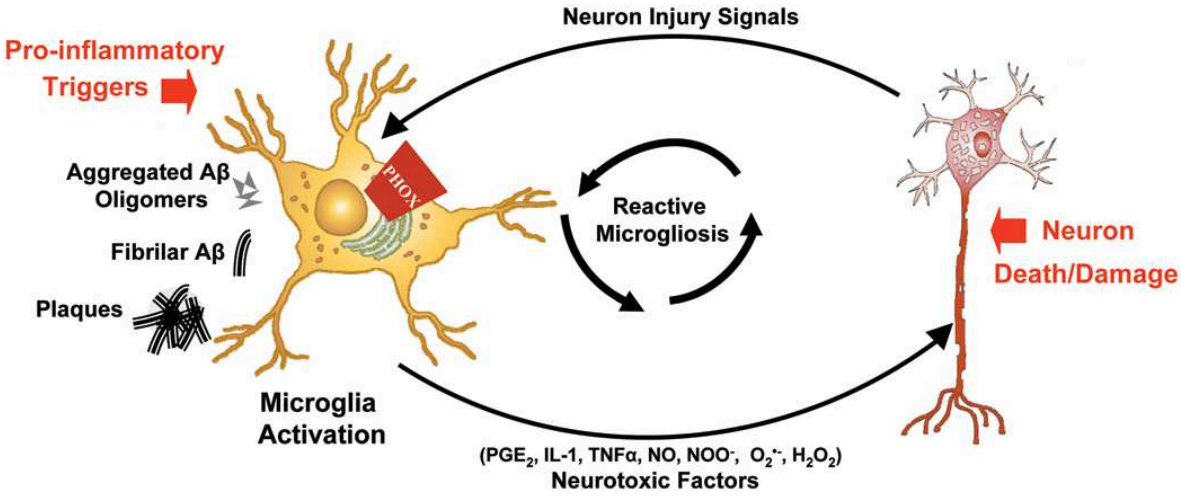

Figure 6 - Microglia-mediated neuron damage. Microglia activation has been implicated in the progressive nature of Alzheimer's disease. Microglia can become deleteriously activated in response to disease-specific stimuli (amyloid-β (Aβ) oligomers, Aβ fibrils, and senile plaques) to produce a catalogue of factors, such as reactive oxygen species and cytokines that are toxic to neurons. In addition to disease-specific pro-inflammatory stimuli, neuronal damage/death can also activate microglia to produce these toxic factors.

Histological and biochemical analyses have, over the years, convincingly demonstrated a myriad of classic immune molecules associated with AD brain parenchyma especially in and around AD-defining histological lesions, the senile plaques and neurofibrillary tangles. The long and growing list of these molecules include complement components [34,35]; inflammatory cytokines, especially interleukin 1 [32,36, 37] and interleukin 6 [37-41]; macrophage colony-stimulating factor (M-CSF) [42]; transforming growth factor-α [43]; C-reactive protein (CRP) and S100β [32,36,41]. In some studies, cytokine message has been found increased in AD brain, implying a local source for the cytokine [40,41].

The inflammatory markers found in late-stage AD brain might represent peripheral immune incursions secondary to severe AD pathology and BBB disruption; however, current knowledge of glial cell biology and two decades of observational study of AD brain belay the need to invoke strong peripheral immune origins for inflammatory

markers that are so readily observed in the AD brain. Aside from the fact that microglia proliferate endogenously in the brain, and are profligate sources of reactive oxygen species (ROS), cytokines, and eicosanoids, it is now clear that astrocytes and neurons are quite capable of locally synthesizing inflammatory cytokines and paracrine molecules. Astrocytes in particular synthesize high levels of PGE2, leukotrienes, cytokines, and chemokines which challenged with ROS, cytokine receptor ligands, or certain toxins [44-46]. Thus the brain is quite capable of initiating an innate and localized immunological response, such as seems to occur during the course of AD. At the same time that glia actively produce inflammatory factors, stressed astroglia suffer loss-of-functions of oxidative-sensitive enzyme activities and homeostatic behaviors, thus diminishing their ability to protect and nourish neurons, and to scavenge reactive paracrine factors [47].

Mitogen-activated protein kinase cascades such as the p38 module that largely regulate inflammatory gene expression are clearly activated in microglia and neurons in and around senile plaques [48].

Amyloid plaques may serve as neuroinflammatory foci both passively, by “capture” and slow release of lipophilic or amphipathic paracrine molecules, and by more active means wherein Aβ activates ambient glial cells. Aβ has been well-documented to promote microglial activation through action on scavenger receptors, chemokine receptors, receptors for advanced glycation end products (RAGE) and possibly by other means [49-51]. Aβ-activated glia can produce ROS/RNS and Aβ itself possesses interesting redox properties through its capacity to promote metal-catalyzed redox cycling reactions and ROS production in certain circumstances **[52]**.

Similar to the case for ROS/RNS, NFTs may be viewed as a toxic consequence of neuroinflammation as well as a driving force for the process. For instance, Neumann’s group has shown that tau accumulates in neurites of cultured neurons upon treatment with TNFα or co-culture with activated microglia, a process that seems to involve cytokine-stimulated ROS [53]. Recently, the MIF receptor CD74 has also been immunohistologically co-localized with NFTs [54], suggesting that tangle-bearing neurons might attract and/or capture activated microglia. Dysfunctional cytoskeletal tangles would be expected to compromise multiple aspects of neuron function to a degree possibly neurotoxic. Debris released during cell death and residual NFT

"ghosts" could plausible trigger further immune activation, thus exacerbating neuroinflammatory cycles.

Aβ is produced by endoproteolysis of the parental amyloid precursor protein (APP), which is achieved by the sequential cleavage of APP by groups of enzymes or enzyme complexes termed α-, β- and γ-secretases (**Fig. 7**).

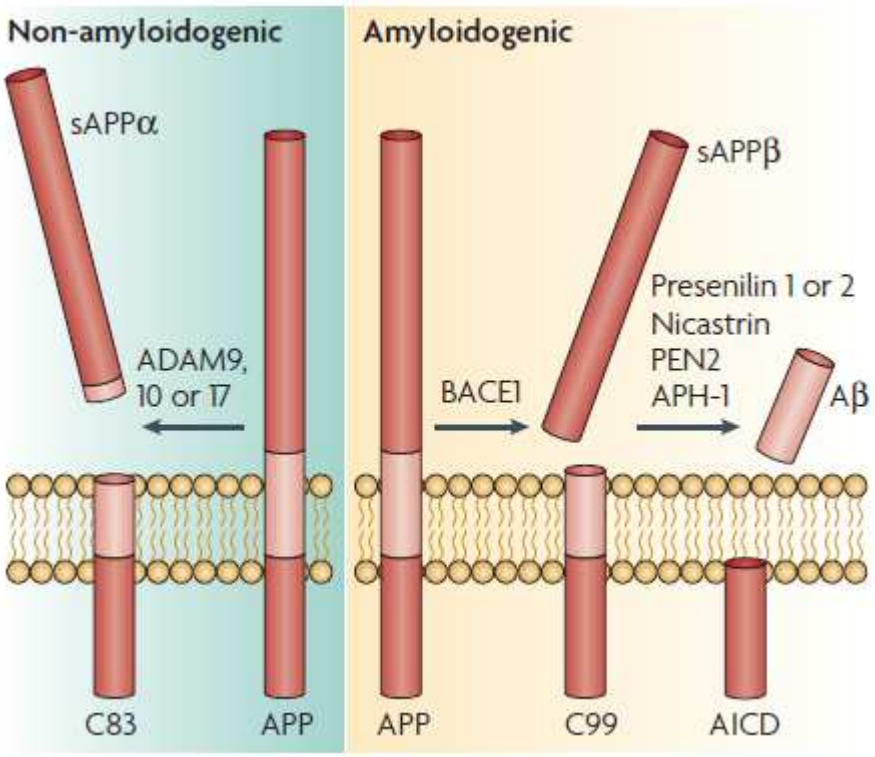

Figure 7 - APP proteolysis.

Three enzymes with α-secretase activity have been identified, all belonging to the ADAM family (a disintegrin- and metalloproteinase-family enzyme): ADAM9, ADAM10 and ADAM17 (also known as tumour necrosis factor converting enzyme) [55]. Several groups identified β-site APP-cleaving enzyme 1 (BACE1), which is a type I integral membrane protein belonging to the pepsin family of aspartyl proteases, as the β-secretase [56-58]. The γ-secretase has been identified as a complex of enzymes composed of presenilin 1 or 2, (PS1 and PS2), nicastrin, anterior pharynx defective and presenilin enhancer 2 [59-63].

The cleavage and processing of APP can be divided into a non-amyloidogenic pathway and an amyloidogenic pathway. In the prevalent non-amyloidogenic pathway, APP is cleaved by the α-secretase at a position 83 amino acids from the carboxy (C) terminus, producing a large amino (N)-terminal ectodomain (sAPPα) which is secreted into the extracellular medium [64]. The resulting 83-amino-acid C-terminal fragment (C83) is

retained in the membrane and subsequently cleaved by the γ-secretase, producing a short fragment termed p3 [65]. Importantly, cleavage by the α-secretase occurs within the Aβ region, thereby precluding formation of Aβ.

The amyloidogenic pathway is an alternative cleavage pathway for APP which leads to Aβ generation. The initial proteolysis is mediated by the β-secretase at a position located 99 amino acids from the C terminus. This cut results in the release of sAPPβ into the extracellular space, and leaves the 99-amino-acid C-terminal stub (known as C99) within the membrane, with the newly generated N terminus corresponding to the first amino acid of Aβ. Subsequent cleavage of this fragment (between residues 38 and 43) by the γ-secretase liberates an intact Aβ peptide. Most of the full-length Aβ peptide produced is 40 residues in length (Aβ40), whereas a small proportion (approximately 10%) is the 42 residue variant (Aβ42). The Aβ42 variant is more hydrophobic and more prone to fibril formation than Aβ40 [66], and it is this longer form that is also the predominant isoform found in cerebral plaques [67].

Mutations in three genes - APP, PS1 and PS2 - are known to cause autosomal dominant AD, which generally manifests with an early-onset pathogenesis [25]. One commonality of the disease-causing mutations in these genes is that they all affect the metabolism or stability of Aβ (**Fig. 8**).

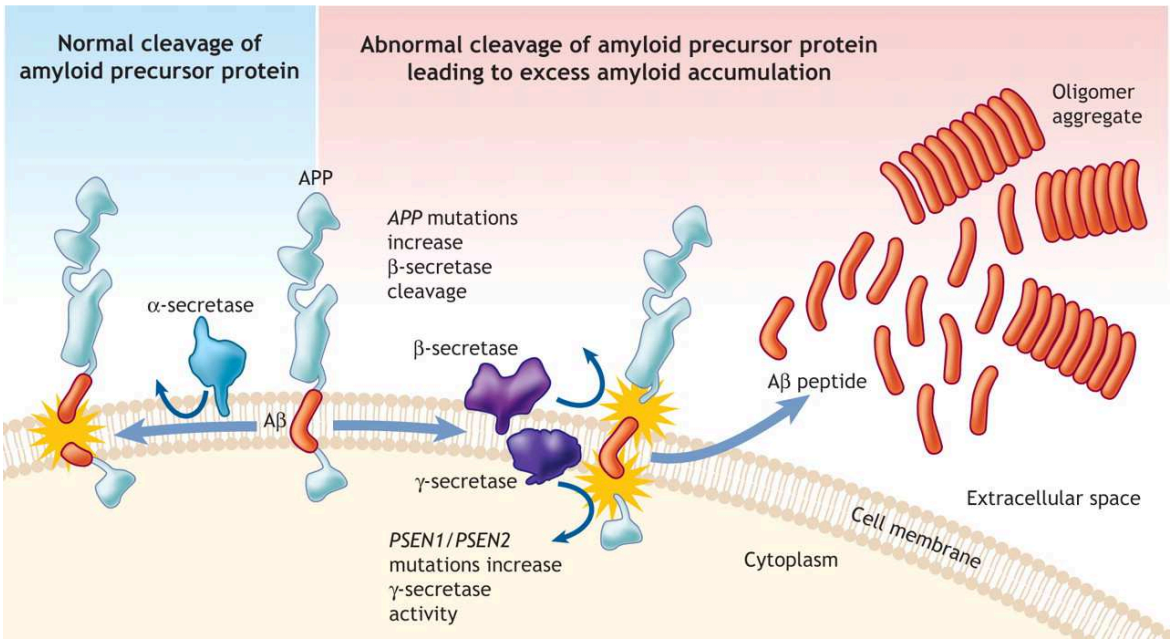

Figure 8 - Effect of mutations in the presenilin-1 and presenilin-2 genes (PSEN1 and PSEN2).

These genetic mutations have been used to generate transgenic mouse models of the disease. One common mutation in APP is known as the Swedish mutation (APP_{Swe}), in

which a double amino-acid change leads to increased cleavage of APP by the β-secretase [69]. Other mutations, such as the Arctic mutation (APP_{Arc}), increase the aggregation of Aβ, leading to early onset, aggressive forms of the disease [70] (**Fig. 9**).

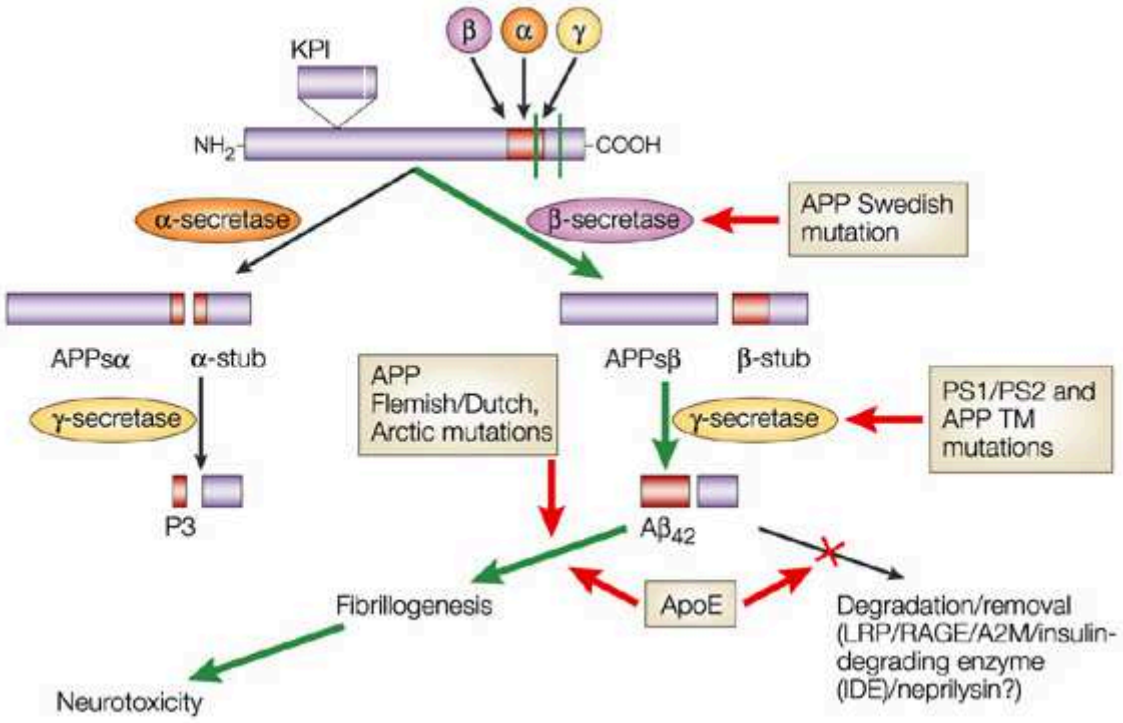

Figure 9 - Schematic of the proteolytic events and cleavage products that are generated during the processing of APP.

Mutations in the presenilins, such as the PS1M146V mutation, increase levels of Aβ42 [71,72], which aggregates more readily than Aβ40. Increased dosage of the APP gene also results in AD [73,74]. Similarly, Down syndrome, in which triplication of chromosome 21 (on which APP resides) occurs, leads to Aβ accumulation early in life [75,76].

Careful studies using C-terminal-specific antibodies against Aβ40 and Aβ42 have established that most of the intraneuronal Aβ ends at residue 42, and not at residue 40 [77].

The buildup of intracellular Aβ may be an early event in the pathogenesis of AD and Down syndrome. In patients with mild cognitive impairment (MCI), intraneuronal Aβ immunoreactivity has been reported in brain regions that are more prone to the development of early AD pathology, such as the hippocampus and the entorhinal cortex [77]. Similarly, it has been shown that the accumulation of intracellular Aβ precedes extracellular plaque formation in patients with Down syndrome [75]. These results suggest that the accumulation of intraneuronal Aβ is an early event in the progression of AD, preceding the formation of extracellular Aβ deposits. Indeed, it has been

demonstrated that intraneuronal Aβ levels decrease as extracellular plaques accumulate [76]. These conclusions are also consistent with results from transgenic mouse models, in which intracellular Aβ accumulation appears as an early event in the progression of the neuropathological phenotype, preceding the accumulation of extracellular Aβ plaques [78-85].

APP localizes to the plasma membrane [86] and has been postulated to have roles in cell adhesion [87] and cell movement [88], but APP has also been localized to the trans-Golgi network [89], endoplasmic reticulum (ER), and endosomal, lysosomal [86] and mitochondrial membranes [90] (**Fig. 10**).

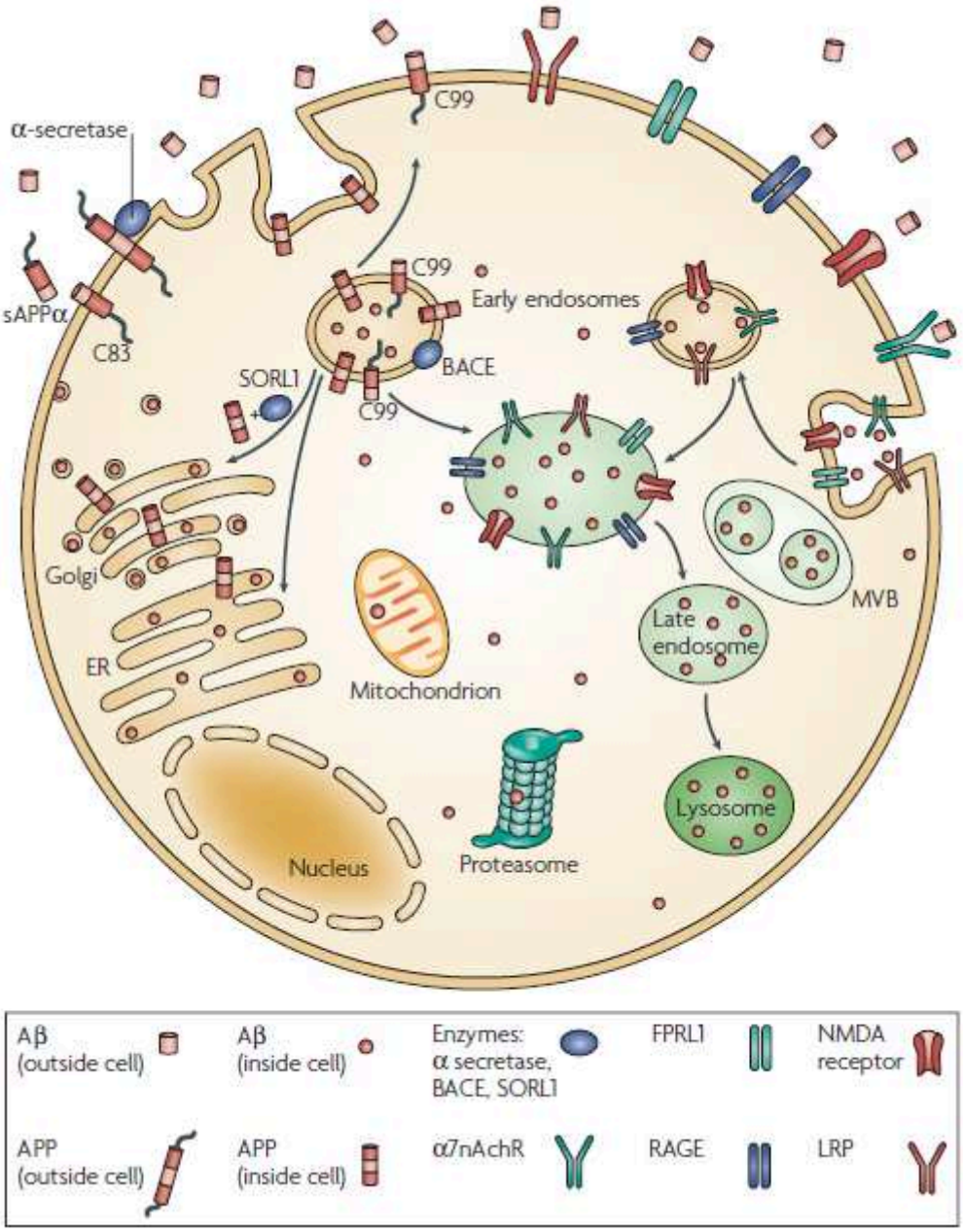

Figure 10 - Sites of cellular Aβ production.

The liberation of Aβ could potentially occur wherever APP and the β- and γ-secretases are localized, and it is likely that this occurs in several cellular compartments. Should Aβ cleavage occur within the confines of the cell, then that Aβ would be intracellular; if liberation of Aβ occurs at the plasma membrane or in the secretory pathway, then it would be released into the extracellular fluid. It is likely that both occur, but it seems that the vast majority of Aβ is secreted, suggesting that Aβ is predominantly produced at the plasma membrane, or as part of the secretory pathway, so that it is rapidly expelled from the cell.

In addition to Aβ being produced intracellularly, it is also possible that previously secreted Aβ, which forms the extracellular Aβ pool, could be taken up by cells and internalized into intracellular pools. Aβ can bind to various biomolecules, including lipids, proteins and proteoglycans. The binding of the various forms of Aβ to the plasma membrane has been studied, and a number of putative Aβ transporters have been identified [91-94]. Consequently, it is likely that some intracellular Aβ is derived from extracellular Aβ pools, and is taken up into the cells through receptors or transporters.

Aβ binds to the α7 nicotinic acetylcholine receptor (α7nAChR) with high affinity [95], and it has been shown that this binding results in receptor internalization and accumulation of Aβ intracellularly [93].

Apolipoprotein E (APOE) receptors, members of the low-density lipoprotein receptor (LDLR) family, modulate Aβ production and Aβ cellular uptake68. Another member of this family, LRP, binds to Aβ directly, or through ligands such as APOE, and undergoes rapid endocytosis, facilitating Aβ cellular uptake [91]. APOE*ε4 is the major genetic risk factor for AD, and it is notable that one of its functions appears to be to directly mediate the accumulation of intracellular Aβ.

In addition to LRP and nicotinic receptors, Aβ internalization has been reported through the scavenger receptor for advanced glycation end products (RAGE), in neurons and microglia [92,96,97]. Binding of Aβ to RAGE in neurons sets off a cascade of events that result in oxidative stress and NF-κB activation. This leads to increased production of macrophage-colony stimulating factor [98] and an enhanced microglial response. In addition to these downstream effects, it has been demonstrated that RAGE-Aβ complexes are internalized and that they co-localize with the lysosomal pathway in astrocytes in the brain of patients with AD [97].

It is plausible that intracellular Aβ has different roles in different cell types and that internalization in glial cells may be part of the regulatory system that seeks to control rising extracellular Aβ levels by taking the peptides up and degrading them. In neurons, the effects of intracellular Aβ are likely to be different. Neuronal Aβ uptake has also been shown to be mediated through NMDA (N-methyl-D-aspartate) receptors [99]. Blocking this NMDA receptor-Aβ internalization prevents pathogenicity, including increased microglial activation and cathepsin D levels [100].

Aβ is produced as a monomer, but readily aggregates to form multimeric complexes. These complexes range from low molecular weight dimers and trimers to higher molecular weight protofibrils and fibrils (**Fig. 11**).

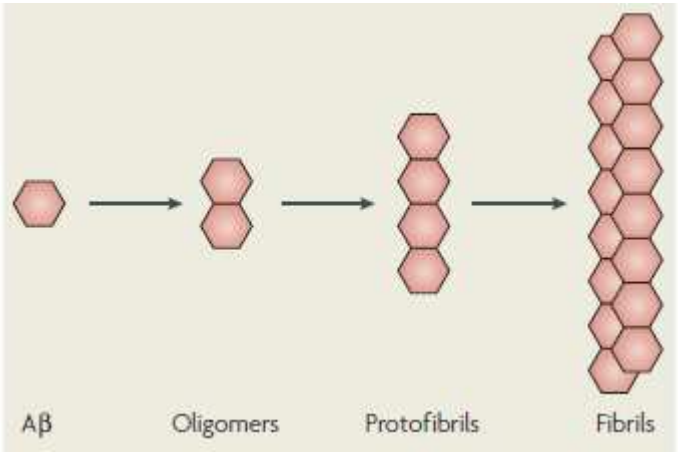

Figure 11 - Aβ assembly states.

The oligomeric species of Aβ have been found to be the most pathological, from dimers disrupting learning and memory, synaptic function and long term potentiation (LTP) [101,102], to dodecamers affecting cognition and memory in transgenic mouse models [103].

Supporting a crucial role for the formation of Aβ oligomers intracellularly, it has been shown that in tissue derived from human brain, Aβ oligomerization initiates within cells rather than in the extracellular space [104].

Aβ oligomerization has also been shown to occur during interactions with lipid bilayers, in particular cholesterol- and glycosphingolipid-rich microdomains known as lipid rafts [105,106]. As biological lipid membranes can modulate both protein folding dynamics and rates of protein aggregation, different lipid compositions in different subcellular compartment membranes may have a role in Aβ aggregation.

It may be that the relatively low levels of intracellular Aβ in the brain of patients with AD (compared with relatively high extracellular Aβ levels), are vital for the seeding of

toxic oligomers that give rise to pathological events and further seed extracellular plaque formation - for example, by secreting these oligomeric species into the extracellular space. Secreted oligomers may also facilitate other pathological events, such as disruption of synaptic transmission [102]. This means that intracellular Aβ could be sufficient to initiate and propagate the AD pathology.

In mouse-AD model, removal of extracellular Aβ plaques is shortly followed by the clearance of intraneuronal Aβ [107]. Notably, as the pathology re-emerges, intraneuronal Aβ appears first, followed by the extracellular plaques [108]. These observations show that clearance of extracellular Aβ also leads to the indirect reduction of intraneuronal stores. This finding indicates that extracellular Aβ may originate from intraneuronal pools and that a dynamic equilibrium exists between the two pools, such that when extracellular pools are removed, intraneuronal pools are sequestered out of the cell.

Amyloid-β (Aβ), produced intracellularly or taken up from extracellular sources, has various pathological effects on cell and organelle function (**Fig. 12**).

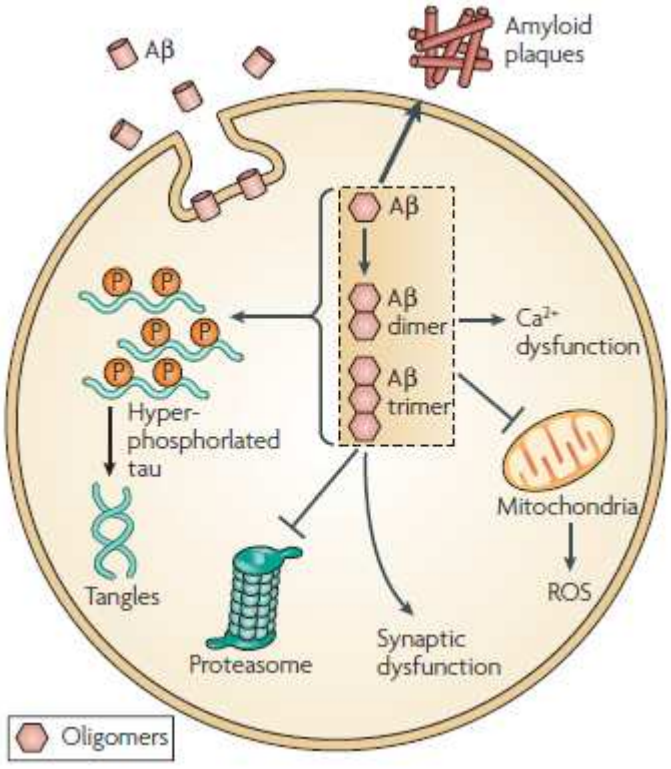

Figure 12 - Pathological effects of intraneuronal Aβ.

Intracellular Aβ can exist as a monomeric form that further aggregates into oligomers, and it may be any of these species that mediate pathological events *in vivo*, particularly within a dysfunctional neuron. Evidence suggests that intracellular Aβ may contribute

to pathology by facilitating tau hyperphosphorylation, disrupting proteasome and mitochondria function, and triggering calcium and synaptic dysfunction.

A number of factors have been shown to modulate intraneuronal Aβ in animal models of AD. One of the most interesting observations is the effect of aging.

For example, young 3xTg-AD mice accumulate both soluble and oligomeric Aβ within neuronal cell bodies, but the intraneuronal pool decreases at ages in which extracellular plaques manifest [108]. This finding also parallels studies in human brain tissue, including that from patients with AD and Down syndrome [75,76,109]. These studies suggest that the brain of patients with early stage AD might have more abundant intraneuronal Aβ, which then becomes extracellular as the disease progresses and neuronal death and lysis occur. Therefore, AD brains coming to autopsy are usually advanced end-stage brains, in which intraneuronal Aβ has relocated to the extracellular pool.

Other environmental and pharmacological factors can modulate the intraneuronal Aβ pool [110-113].

DIABETES MELLITUS TYPE 2 (T2DM) AND AMYLIN

Diabetes is a chronic disease that affects millions around the world, and is also the leading cause of kidney failure, nontraumatic lower limb amputation, and new cases of blindness among adults. Overall, it is the seventh leading cause of death and a major cause of heart disease and stroke.

Diabetes mellitus is often simply considered as diabetes, a syndrome of disordered metabolism with abnormally high blood glucose levels (hyperglycemia) [114].

The two most common forms of diabetes are type 1 diabetes (diminished production of insulin) and type 2 diabetes (impaired response to insulin and β dysfunction) (T2DM). Both lead to hyperglycemia, excessive urine production, compensatory thirst, increased fluid intake, blurred vision, unexplained weight loss, lethargy, and changes in energy metabolism. The distinction between type 1 and type 2 DM was clearly made in 1936 [115]. T2DM was first described as a component of metabolic syndrome in 1988 [116].

Type I diabetes is a rather straightforward condition where the body does not produce insulin, and, therefore, it must be supplemented for survival.

T2DM results from interaction between genetic, environmental and behavioral risk factors [117-118].

People living with T2DM are more vulnerable to various forms of both short- and long-term complications, which often lead to their premature death. This tendency of increased morbidity and mortality is seen in patients with T2DM because of the commonness of this type of DM, its insidious onset and late recognition, especially in resource-poor developing countries like Africa [119].

The incidence of T2DM varies substantially from one geographical region to the other as a result of environmental and lifestyle risk factors [120].

A 2011 Centre for Disease Control and Prevention (CDC) report estimates that DM affects about 25.8 million people in the US (7.8% of the population) in 2010 with 90% to 95% of them being T2DM [121].

T2DM is a complex heterogeneous group of metabolic conditions characterized by increased levels of blood glucose due to impairment in insulin action and/or insulin secretion [122] (**Fig. 13**).

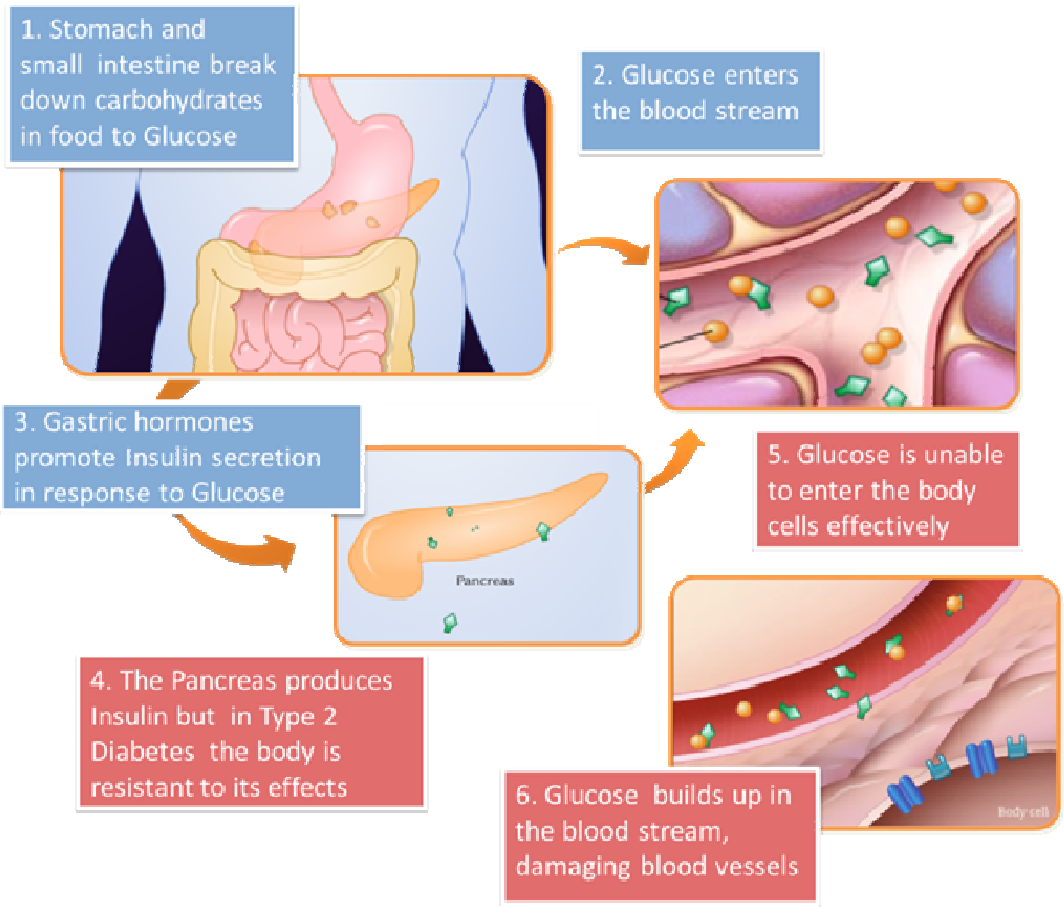

Figure 13 - The diagram describes the damaged metabolic process in T2DM.

Physiologically, the pancreatic βs constantly synthesize insulin, regardless of blood glucose levels (**Fig. 14**).

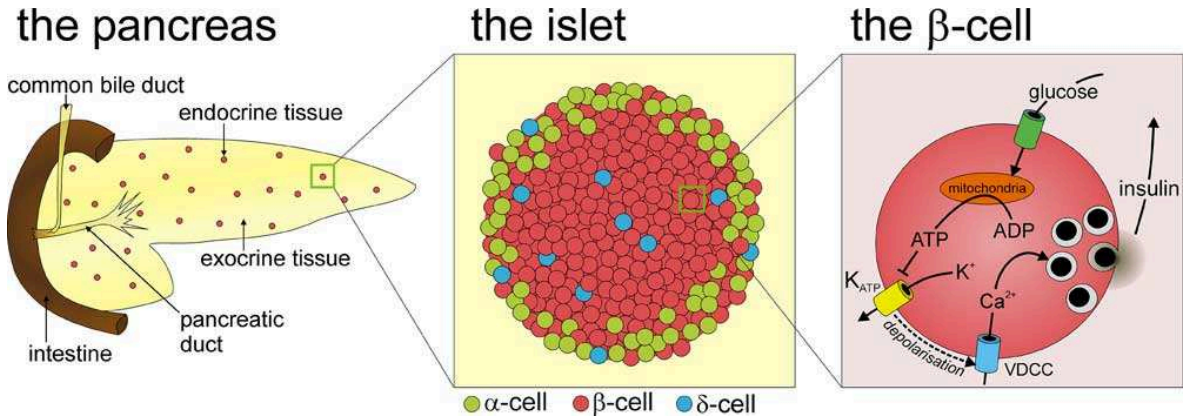

Figure 14 - Insulin production in the human pancreas. The human pancreas is located in the abdomen, next to the small intestine. βs are found next to blood vessels flowing through the pancreas and they release insulin into the blood stream.

Insulin is stored within vacuoles and released once triggered by an elevation of the blood glucose level. Insulin is the principal hormone that regulates uptake of glucose from the blood into most cells, including skeletal muscle cells and adipocytes. Insulin is also the major signal for conversion of glucose to glycogen for internal storage in liver and skeletal muscle cells. A drop in the blood glucose level results in a decrease in release of insulin from the βs and an increase in release of glucagon from the αs, which stimulates the conversion of glycogen to glucose. Following an overnight fast, glucose is largely produced by glycogenolysis and gluconeogenesis.

T2DM is characterized by insulin insensitivity as a result of insulin resistance, declining insulin production, and eventual pancreatic β failure [123,124]. This leads to a decrease in glucose transport into the liver, muscle cells, and fat cells. There is an increase in the breakdown of fat with hyperglycemia. The involvement of impaired α function has recently been recognized in the pathophysiology of T2DM [125].

Insulin resistance refers to suppressed or delayed responses to insulin. Insulin resistance is generally “post-receptor”, which refers to a problem with the cells that respond to insulin rather than a problem with insulin production. Some rare causes of diabetes include pregnancy, certain medications, or diseases such as maturity onset diabetes in the young (MODY).

A number of lifestyle factors are known to be important to the development of T2DM. These are physical inactivity, sedentary lifestyle, cigarette smoking and generous

consumption of alcohol [126]. Obesity has been found to contribute to approximately 55% of cases of type T2DM [127] (**Fig. 15**).

Figure 15 - Lifestyle factors important to the development of T2DM.

There is a strong inheritable genetic connection in T2DM, having relatives (especially first degree) with type 2 DM increases the risks of developing T2DM substantially. Concordance among monozygotic twins is close to 100%, and about 25% of those with the disease have a family history of DM [128]. Recently, genes discovered to be significantly associated with developing T2DM, include TCF7L2, PPARG, FTO, KCNJ11, NOTCH2, WFS1, CDKAL1, IGF2BP2, SLC30A8, JAZF1, and HHEX. KCNJ11 (potassium inwardly rectifying channel, subfamily J, member 11), encodes the islet ATP-sensitive potassium channel Kir6.2, and TCF7L2 (transcription factor 7-like 2) regulates proglucagon gene expression and thus the production of glucagonlike peptide-1 [129]. Moreover, obesity (which is an independent risk factor for type 2 DM) is strongly inherited [130]. Monogenic forms like Maturity-onset diabetes of the young (MODY), constitutes up to 5% of cases [131]. There are many medical conditions which can potentially give rise to, or exacerbate T2DM. These include obesity, hypertension, elevated cholesterol (combined hyperlipidemia), and with the condition often termed metabolic syndrome (it is also known as Syndrome X, Reaven's syndrome) [132]. Other causes include acromegaly, Cushing's syndrome, thyrotoxicosis, pheochromocytoma, chronic pancreatitis, cancer, and drugs [133]

Additional factors found to increase the risk of T2DM include aging [134], high-fat diets, and a less active lifestyle [135].

Amylin, also referred to as islet amyloid polypeptide (IAPP), is composed of 37 amino acid residues and contains a disulfide bridge between residues two and seven (**Fig. 16**).

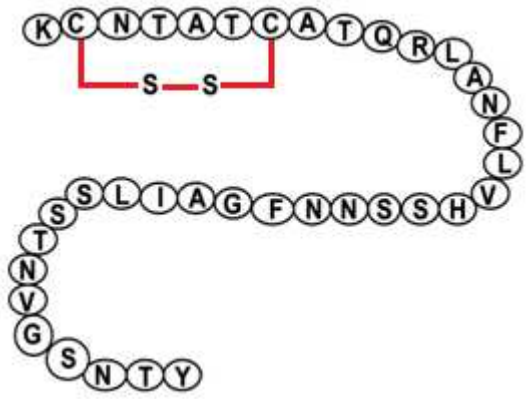

Figure 16 - Amino acid sequence of Amylin with cystine bond at position 2 and 7. The disulfide bond must be intact in order for Amylin to be biologically active.

Amylin is expressed on gene 12 by one single gene copy on the short arm of the chromosome [136]. Amylin is derived after an 89-amino acid long precursor protein, referred to as preProIAPP, which is cleaved at the N-terminal yielding ProIAPP and which is subsequently posttranslationally processed by the prohormone convertase (PC2) [137]. These processes occur in pancreatic β cells, and, hence, Amylin is secreted together with insulin in a 20 to 1 molar ratio of insulin to Amylin [138].

Initially, it was reported that Amylin works antagonistically to insulin by inhibiting glycogenesis and promoting glycolysis [139-142]. However, other studies have suggested that Amylin plays a critical role in glucose homeostasis by suppressing the release of glucagon from pancreatic α cells and, hence, prevents release of glucose from the liver, decreases gastric emptying, and stimulates the satiety center in the brain [138,143-146].

Since Amylin is coreleased with insulin, consuming an excess amount of carbohydrates and fat may lead to an elevated amount of Amylin being secreted that could eventually initiate Amylin aggregation, since it was found that a high carbohydrate or high fat diet promoted amyloid formation in transgenic mice [147-148].

Amylin aggregation has been suggested to occur in a stepwise manner, with soluble monomeric Amylin forming oligomeric structures, protofibrils, and eventually amyloid

fibrils, some of which are toxic to the pancreatic beta cells [149]. Destruction of the pancreatic beta cells results in decreased insulin production and manifests as type II diabetes.

The occurrence of islet amyloid fibril formation is less than 15% in non-diabetic patients, but is present in over 90% of diabetic subjects [150].

Amyloid is only seen in T2DM, because, in type 1 diabetics, the IAPP source is removed due to the destruction of the beta cells.

Since Amylin aggregation is central to this peptide acquiring cytotoxic properties, numerous researchers have over the last two decades either observed or proposed the molecular mechanism and region responsible for Amylin aggregation (**Table 2**), with a common feature among all studies being that the aggregates were in a β-sheet conformation.

Year	Amyloidogenic region	Predicted or observed
1990	20–29	Observed
1999	17–34, 24–37, 30–37	Observed
2000	20–29	Observed
2000	23–27 and 22–27	Observed
2001	22–29	Observed
2001	8–20	Observed
2002	14–18, 14–22, 14–20, 15–20, 15–19	Observed
2002	22–27	Observed
2003	12–17, 15–20	Observed
2005	12–17, 22–27, 31–37	Observed
2006	13–18	Predicted
2007	8–17, 28–37	Predicted
2007	12–18, 15–20, 22–28	Predicted
2009	8, 13, 17, 25, 27, 32*	Predicted

*Nucleation sites.

Table 2 - Observed and predicted amyloid forming regions of mylin.

Although in humans and a few other mammals such as primates [151] and cats [152] it might form amyloid deposits, in rats it does not form amyloid fibrils and it is not cytotoxic [153-154]. The human (hIAPP) and rat (rIAPP) sequences differ in only six out of 37 positions, five of which are located between residues 20-29. rIAPP contains three proline residues in this region at positions 25, 28 and 29, whereas the human sequence has none. Additional differences include the replacement of His18, Phe23 and Ile26 of the human sequence with Arg, Leu and Val, respectively, in rIAPP. Amyloidogenic hIAPP has been shown to be more toxic to cells than non-amyloidogenic rat IAPP [155].

The first study on the amyloidogenic region of Amylin was performed by Westermark *et al*. and based on the nonamyloidogenic nature of Amylin from different species and experimental data using synthetic peptides proposed that the 25-29 region is the shortest amyloidogenic region of Amylin [156]. With the exception of the 1-7 region of Amylin, the entire length of this peptide has at some stage been shown to have amyloidogenic properties (**Table 2**). Of note, it was found that the 22-27 region coiled around each other into typical amyloid fibrils [157] and also increased fibril formation [158]. In addition, the 11-20 region was found to bind to Amylin with the highest affinity when compared to peptides that were homologous to other regions of Amylin and that the 14-18 region is the core recognition site for Amylin binding [38].

The observation that His18 protonation might modulate aggregation of full-length hIAPP it was noteworthy [159] and is consistent with a described model of hIAPP fibrils, in which individual peptides form a planar S-shaped structure, involving residues 9-37, that is characterised by the presence of three b strands with His18 located in the turn between strands 1 and 2 [160]. The supposedly parallel in-register stacking of these basic building blocks would bring His18 close in space in neighbouring peptides. Such a structure would likely be strongly destabilized by electrostatic repulsion upon protonation of His18.

One of the earliest models for β-sheet formation was proposed by Jaikaran *et al*. (**Fig. 16 A**) [161].

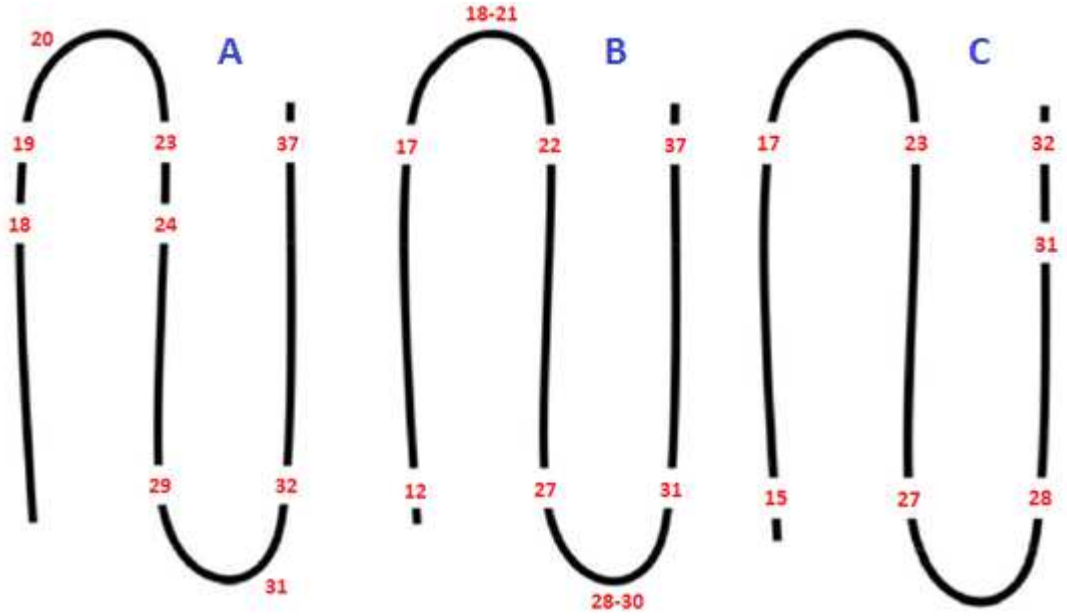

Figure 16 - Schematic representation of the β-sheet and β-turn regions of Amylin as predicted by (A) Jaikaran *et al.*, (B) Kajava *et al.*, and (C) Luca *et al.* [161-163].

According to this model, a β-turn is predicted at residues 31 thereby allowing the 24-29 and 32-37 regions to form an antiparallel β-sheet and at residue 20 which would allow the 18-23 region to extend the β-sheet [39]. This model also proposes that hydrophobic interactions are responsible for initiating the aggregation process and that hydrogen bonds stabilize the β-sheet structure [39]. A later study proposed that the 12-17, 22-27, and 31-37 regions form antiparallel β-sheets with the 18-21 and 28-30 regions forming the β-turns (**Fig. 16 B**) [162].

In addition, it was also suggested that the hydrophobic side chains in the 15-17 and 32 region interact with that of the 23-27 region whilst there is interstrand hydrophilic association between the 28-31 regions of Amylin strands (**Fig. 16 C**) [163]. It is noteworthy that there is considerable overlap between the β-sheet forming regions proposed by all three model-predicting studies. In addition, the predicted β-sheet forming regions contain the proposed nucleation sites for aggregation [164] as well as aromatic amino acids which have been reported to play a significant role in amyloid formation due to interactions between the planar aromatic structures which are also referred to as π-π interactions [165]. Taking all models into consideration, a proposed model of the β-sheet and β-turn regions of Amylin is illustrated in **Figure 17**.

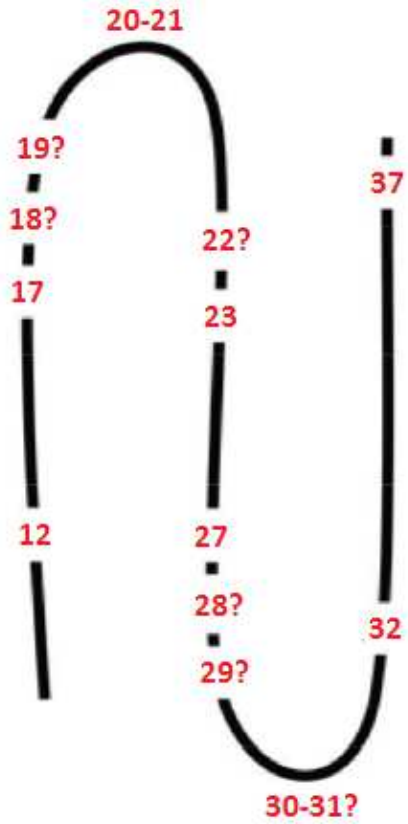

Figure 17 - Data integration for a comprehensive understanding of previous predictions.

This model proposes that the 12-17, 23-27, and 32-37 regionsmake up the β-sheet structure with regions 20-21 being constituents of the β-turn region. Residues 18, 19, 22, and 28-31 could either participate in forming the β-sheet or β-turn.

Thus, soluble monomeric Amylin can associate into soluble β-sheet oligomeric state [166] which further progresses to protofibrils and insoluble amyloid fibrils [167]. According to Kodali and Wetzel, the oligomer which is formed prior to the protofibril is defined as being a "metastable multimer in an amyloid formation reaction" [149]. These soluble intermediates were reported to have diameters between 2.7 and 4 nm, whilst protofibrils have a width of 5 nm and are "non-spherical filamentous structures lacking a periodic substructure that are often found at intermediate times during the formation of mature fibrils", and amyloid fibrils, are "relatively straight, unbranched protein fibrils, with diameters in the 10 nm range, and often (but not always) consist of multiple protofilaments twisted around the fibril axis" (**Fig.18**) [159,168].

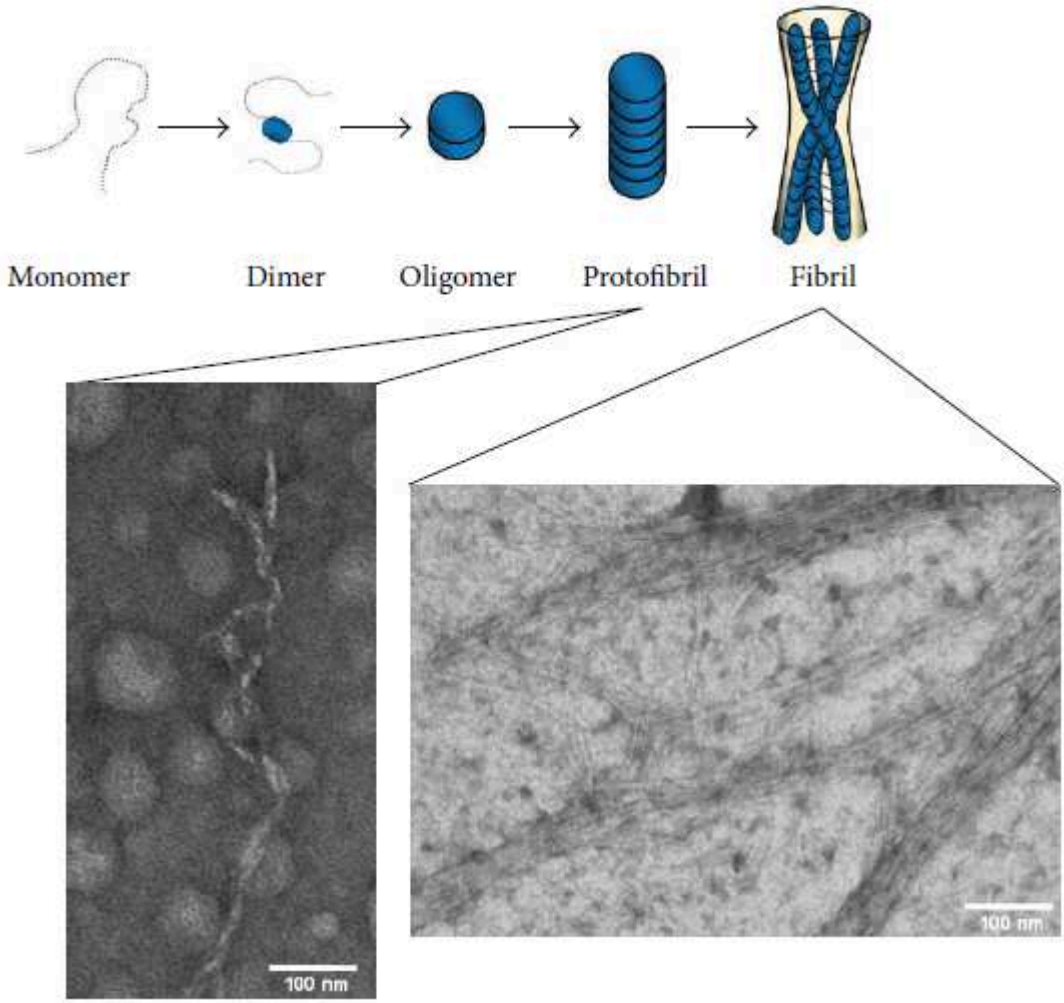

Figure 18 - Schematic process of Amylin forming nanoparticulate fibrils.

Analysis of amyloid fibrils has revealed that individual β-strands are orientated perpendicular to the long fiber axis and thus form β-sheets [169-172]. Research studies by Goldsbury *et al.* revealed that Amylin fibrils grow at both ends at a rate of approximately 1.1 nm per minute and that the width of fibrils ranged between 6 and 8 nm [168].

Previously there was general acceptance that the fibrillar form of Amylin is the toxic species [173-181]; however, the more recent consensus is that the soluble oligomeric structures exert the toxic effect [182-188]. Two noteworthy experiments for the latter hypothesis were conducted in 2006 and 2010 [188-189]. Meier *et al*. evaluated rifampicin as a potential inhibitor of type II diabetes and found that although it did prevent fibril formation, and toxicity of Amylin was still present, thus concluding that the soluble oligomers are the toxic species [189]. The second study showed that the fibrillar species of Amylin was positively correlated with longevity of transgenic mice, once again suggesting that the prefibrillar or oligomeric form is toxic [188]. Although there is currently a general consensus that the oligomeric form of Amylin is the toxic species, there are numerous theories regarding its mechanism of cytotoxicity.

The first mechanism of toxicity postulated is membrane disruption and subsequent disturbance of intracellular homeostasis. It was initially reported by Westermark *et al*. that Amylin disrupts cell membranes thereby causing cell death [156]. Thereafter, Lorenzo *et al*. exposed islet cells sandwiched between coverslips as well as unprotected cells to human Amylin aggregates and found using Nomarsky microscopy that Amylin interaction with cell membranes was crucial for toxicity [190]. Subsequent studies supported this theory by demonstrating that Amylin aggregates formed pores or channels in lipid bilayers [174,183,184,191]. Planar phospholipid bilayer membranes were used to demonstrate that nonselective ion voltage-dependent channels were formed in the presence of Amylin [174]. This will promote the influx of Ca^{2+} and Na^{+} and K^{+} efflux and thereby disrupt ionic homeostasis [174]. Kayed *et al*. also employed lipid bilayers and showed that there was increased conductance in the presence of Amylin oligomers and fibrils [184]. In addition, intracellular calcium levels were found to be elevated after exposure to Amylin, and it is noteworthy that destabilization of intracellular Ca^{2+} homeostasis was a mechanism used by other amyloidogenic peptides to induce toxicity [173,192].

Subsequent studies also demonstrated that fibril formation was increased in the presence of anionic lipid membranes [171,193], and it was suggested that electrostatic interactions between Amylin and the negatively charged lipids on membranes are responsible for Amylin association with the cell membrane [194]. In addition, Amylin was found to insert into membranes and incorporate membrane lipids into the growing amyloid fibril, thereby causing membrane disruption [194-197]. It seems that membrane disruption could be a leading cause of Amylin-mediated toxicity.

The second proposed mechanism of Amylin-mediated toxicity is generation of reactive oxygen species (ROS) such as hydrogen peroxide (H_2O_2),which results in cell death [173]. It was also shown that generation of ROS was a mechanism used by other amyloidogenic peptides for toxicity [173]. At the same time, Schubert *et al*. detected peroxides using 2',7'-dichlorofluorescein diacetate, and they also demonstrated that Amylin increased the accumulation of H_2O_2 in B12 cells [198].

The third hypothesis of Amylin-mediated toxicity is apoptosis. Lorenzo *et al*. showed that aurintricarboxylic acid, an endonuclease inhibitor that stops apoptosis, is able to reduce Amylin-mediated toxicity of islet cells [190].

Amylin increased expression of the p21 and p53 tumor suppressor genes, both of which encode for proteins that arrest cell proliferation, leading to apoptosis (**Fig. 19**) [199].

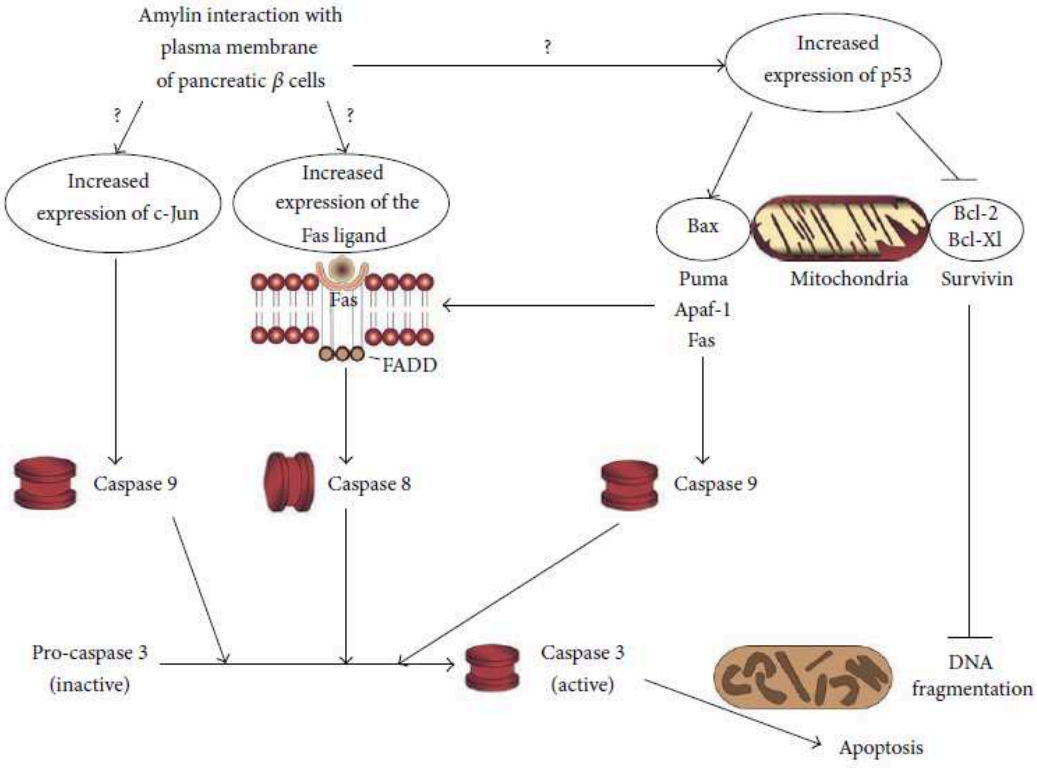

Figure 19 - The proposed roles of the c-Jun, Fas, and p53 proteins in apoptosis induced by human Amylin in pancreatic betas.

The theory that apoptosis is the mechanism by which Amylin causes cell death was further supported by the finding that Amylin increases the expression of c-Jun, a gene that is involved in the apoptotic pathway (**Fig. 19**), in RINm5F and the human insulinoma cell line (CM) [200]. Huang *et al*. later showed that Amylin could trigger endoplasmic reticulum stress-induced apoptosis [201]. In the presence of Amylin, levels of Fas/Fas ligand (FasL) and Fas-associated death domain (FADD), both of which are involved in apoptosis, were elevated (Figure 4) [202]. More recently, it was concluded that Amylin oligomers induced elevated cytosolic levels of Ca^{2+} in the rat insulinoma cell line INS 832/13 that resulted in hyperactivation of the protease calpain-2, leading to apoptosis [203].

The previously mentioned mechanisms could possibly work together to eventually result in cell death.

Gurlo *et al*. performed *in vivo* experiments with an oligomer-specific antibody and cryoimmunogold labeling and showed that the toxic oligomer is present in the secretory pathway and is able to disrupt membranes herein as well asmitochondrial membranes [204]. These events result in cellular dysfunction and apoptosis [204]. Lim *et al*. further supported the hypothesis that the mechanism of Amylin toxicity is membrane disruption by showing that mitochondrial proteins were deregulated when SH-SY5Y neuroblastoma cells were exposed to Amylin [205].

To circumvent the toxic effect of Amylin-generated ROS, a number of quinone derivatives that were known to scavenge free radicals were evaluated [175]. However, it was found that only rifampicin and its analogues p-benzoquinone and hydroquinone inhibited the toxic effect of Amylin whereas other antioxidants with scavenging ability did not exhibit any inhibitory effect on Amylin toxicity [175]. This study was the first to observe that an inhibitor (rifampicin) could bind to Amylin aggregates and prevent its attachment to the cell surface [175].

It was proposed that resveratrol reduces fibrillogenesis by preventing lateral growth of the Amylin β-sheet [206]. A recent review indicated that even though resveratrol could have an impact on diabetes by a multitude of mechanisms as evidence by *in vitro* testing, few clinical human trials have been conducted possibly due to its poor bioavailability [207].

Since analysis of the rat Amylin sequence implied that the unique presence of proline residues could be responsible for the lack of amyloid formation in rodents, the design of an inhibitor containing a proline substitution was encouraged. With this in mind, Abedini *et al*. synthesized full length Amylin but substituted the serine at position 26 with proline and found that this modified peptide could bind to Amylin and prevented fibril formation [208]. A possible explanation for this observation is that proline is known to induce β-turns in peptides [209]. Fibril growth requires β-sheet conformation of incoming Amylin chains, and a modified bent peptide binding to Amylin will therefore disrupt the free stacking of β-sheet Amylin molecules [216-217]. Although this modified form of Amylin inhibited Amylin-mediated cytotoxicity, another Amylin derivative that contains three substitutions with proline at residues 25, 28, and 29 was already undergoing clinical trials [210-215,218-223].

There are many different factors that allow the assumption to be made that the fibrillar transformation of the 37 amino acid residue, Amylin, into a mature amyloid fibril, which occurs in a process producing many oligomeric intermediates, can be linked at the biochemical level as part of the cause of β death that can lead to T2DM. Proof of such a statement has been shown through amyloid formation in transplanted pancreatic islet cells. Experimental islet cell transplantation was done, in which human islet cells, once they became available, were made diabetic by injection and were then used in studies testing the effects of hyperglycemia on human beta cell function.

With the human islets it was found that the alpha cells remained intact, while the beta cells decreased in number and amyloid fibrils were found densely packed intracellularly with their plasma IAPP levels being increased more than five times that of the baseline value. This data in human islets differed from rat islets, which showed only very sparse amyloid fibrillar formation, but that was to be expected due to the differences in the Amylin sequence that prevent fibril formation in the rodent IAPP amino acid sequence. The results of such studies of transplanting the pancreatic islet cells proved a firm connection between amyloid fibrils and the destruction of beta cells that can lead to type 2 diabetes.

T2DM is characterized by a slowly progressive degeneration of islet βs, resulting in a fall of insulin secretion and decreased insulin action on peripheral tissues [224]. This same study demonstrates the deposition of amyloid material as a major pathological factor in T2DM. The facts indicate that amyloid deposits are seen in over 95% of type

2 diabetics and that the severity of the disease positively correlates with the extent of islet amyloid deposits.

In a healthy individual, amyloid is not observed, in part because the fibril formation is typically inhibited by insulin. Insulin should be produced in 50-100 molar excess of IAPP, and this is a sufficientamount for it to suppress amyloid formation in healthy individuals [225].

Copper-mediated oxidation (and H_2O_2 generation) could be an important step in the processes leading to islet β degeneration and progression of T2DM [226].

CONNECTION BETWEEN Aβ AND AMYLIN

A rapidly ageing population and the modern sedentary lifestyle, combined with changes in diet, have to be blamed for the fact that both T2DM and AD are reaching epidemic proportions. World-wide numbers of patients with diabetes are projected to rise from ~171 million at the turn of this century to 366 million by 2030 [227]. For comparison, more than 26 million people are currently living with AD, a number that will quadruple to more than 106 million by 2050 unless strategies are put into place that slow down, cure or even prevent dementia altogether. Of all dementing disorders, AD is the most common form, comprising 50-70% of all cases [228].

In the AD brain, there are two key molecules that undergo a change in tertiary structure followed by self-association and deposition, the amyloid-β (Aβ) peptide and tau, amicrotubule-associated protein [229].

T2DM progression correlates well with Amylin deposition. Interestingly, Amylin, forms aggregates already in the pre-diabetic stage. In doing so it undergoes a change in tertiary structure, similar to what is known for a β and tau in AD, and the peptide is finally deposited in βs, becoming a characteristic histopathological hallmark lesion of T2DM [230-231].

Both T2DM and AD are characterized by insoluble protein aggregates with a fibrillar conformation. Amylin aggregation is associated with pancreatic β loss (although T2DM is believed to arise from insulin resistance in target organs),whereas Aβ and tangle formation is associated with neuronal cell loss. β loss leads to diabetes, nerve cell loss to dementia. Therefore, T2DM and AD are both conformational diseases.

Human Amylin shares many biophysical and physiological properties with Aβ. The two molecules are similar in size but have little similarities in their primary sequence

(**Fig. 20**). However, different from rat Amylin, they fold into similar secondary structures.

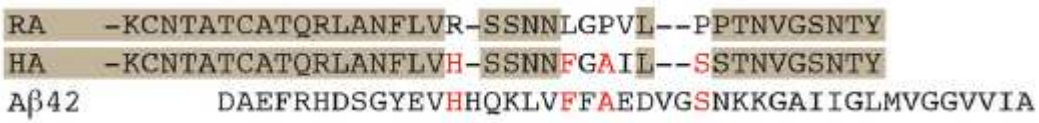

Figure 20 - Alignment of the sequences of human (hA) and rat Amylin (rA) and comparison to Aβ42. Shading shows similarities in the rat and human Amylin sequences while important similarities between hA and Aβ42 are shown in red.

In amyloidoses, the proteins in question are subjected to posttranslational modifications. Of the non-enzymatic posttranslational modifications, deamidation of asparagines and glutamine is the most common. Deamidation can influence the structure, stability, folding, and aggregation of proteins and has been proposed to play a role in amyloid formation inAD [232]. While the role deamidation has in AD in forming amyloid plaques is not fully understood, one hypothesis is that in the turn region of Aβ, the Asp23Asn mutation and subsequent deamidation to isoAsp23 might cause a structural change that subsequently initiates folding of Aβ into β-sheets [233]. By examining the effects of deamidation on the kinetics of amyloid formation by Amylin it was found that deamidation accelerates amyloid formation and that the deamidated material can seed amyloid formation of unmodified Amylin [234]. This is highly reminiscent of what has been reported for fibrillar tau that was found to recruit "normal" tau into aggregates [235], and interestingly, tau is also a deamidated protein [236].

For the two amyloidogenic molecules Amylin and Aβ, shared and separate modes of toxicity have been revealed, that are in part receptor-mediated, with the receptors, at least to some degree, being shared between the two molecules [229]. One of these receptors is the Amylin receptor that exists as a dimerized form of the calcitonin receptor (CTR) complexed with the Receptor activity modifying protein 3 (RAMP3), all of which are highly expressed in brain [237,238]. This trimeric constellation generates a receptor that binds Amylin with a significantly higher affinity than, for example, Calcitonin gene related peptide (CGRP) or adrenomedullin [239]. Aβ toxicity in rat cholinergic basal forebrain neurons can be blocked by the Amylin receptor antagonist AC187 [240]. Another receptor that is shared between Aβ and Amylin is APP, and both molecules induce APP expression in neuronal and astrocyte cultures [241]. The neurotoxicity of the two molecules is furthermore mediated by specific

integrin signaling pathways, and both can be inhibited with integrin-specific antibodies and cytochalasin D [242].

Human Amylin and Aβ deregulate identical mitochondrial proteins supporting the notion that both amyloidoses have common targets [243]. The human Amylin receptor mediates the biological effects of Aβ as shown by the team of Jhamandas *et al*. (2011), and in Aβ-forming transgenic mice, the receptor is up-regulated in brain regions with an elevated amyloid load [244]. Patch clamping of human foetal neurons showed that the electrophysiological effects of Aβ could be blocked with yet another Amylin receptora ntagonist, the highly selective 24 amino acid-long AC253 [244]. AC253 attenuated Aβ-mediated caspase-dependent and -independent apoptotic cell death in human foetal neurons (**Fig. 21**).

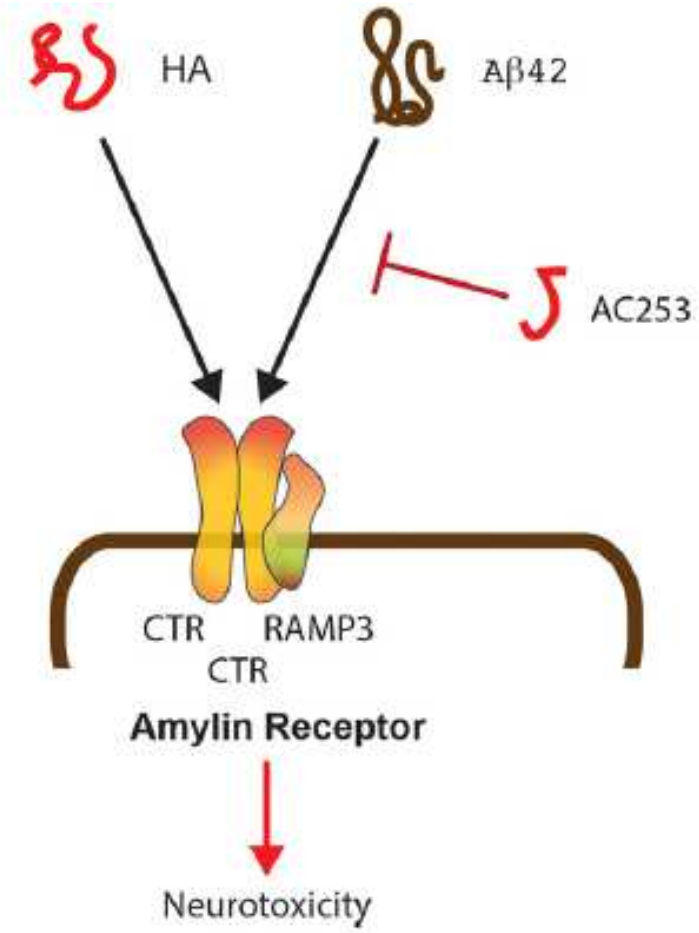

Figure 21 - hA and Aβ42 both bind to the Amylin receptor that is composed of two molecules of CTR and one molecule of RAMP3. The small hA-derived peptide AC253 abrogates toxicity of both hA and Aβ42 mediated via the Amylin receptor.

In Aβ-forming mice, both Amylin receptor subunits were found up-regulated in brain areas with a high amyloid burden, suggesting that the latter may be a signal for up-regulation.

Recent binding data indicate that Amylin has a high affinity for the AMY3 isoform of Amylin receptors [245]. However, the precise intracellular signal transduction pathways following AMY3 activation are not fully understood, and it is not known whether Aβ directly activates AMY3. Amylin receptors are heterodimerized by CTR and one of three RAMPs, thus generating multiple Amylin receptor subtypes, AMY1-3 (**Fig. 22**) [246].

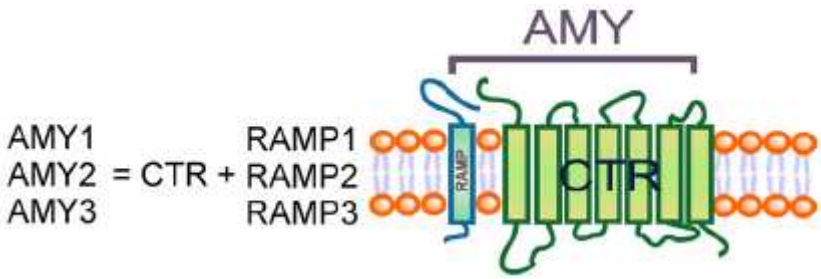

Figure 22 - AMY receptor structure.

The importance of receptor splice variation in AMY physiology remains to be elucidated. These Amylin receptor subtypes are pharmacologically distinct and demonstrate different binding affinities to members of the calcitonin peptide family.

Using HEK293 cells that stably express the Amylin receptor, both Aβ and human Amylin were found to induce cell death at low micromolar concentrations. hAmylin and Aβ1-42 induced cell death is dependent on AMY3 expression. In cells expressing other Amylin receptor subtypes (AMY1 or AMY2) or single components of AMY3 (CTR or RAMP3), hAmylin, and Aβ1-42 did not induce significant cell death. In the presence of human Amylin, however, the effect of Aβ42 was occluded, suggesting a shared mechanism of action between the two peptides. Moreover, the Amylin receptor antagonist AC253 blocked toxic responses including cell death, in response to an activation of the Amylin receptor by either human Amylin itself, Aβ42, or up on their co-application. This suggests that the Amylin receptor may represent a novel therapeutic target for the development of compounds in the treatment of neurodegenerative conditions such as AD.

Aβ1-42 directly activates AMY3 and triggers several intracellular signaling pathways, including cytosolic cAMP and Ca^{2+} rises. AMY3 likely regulates cellular functions by changing activity of PKA, ERK1/2, and Akt. The sustained activation of AMY3

triggers phosphorylation of ERK1/2 resulting in cell death. Putative uncontrolled elevations of cytosolic Ca^{2+} as a result of prolonged AMY3 activation may also perturb homeostasis of the endoplasmic reticulum, produce mitochondrial dysregulation and engagement of caspases that contribute to apoptosis [247].

The possible pathophysiological mechanisms whereby Aβ1-42 activates AMY3 and triggers multiple signaling pathways are illustrated in **Fig. 23**.

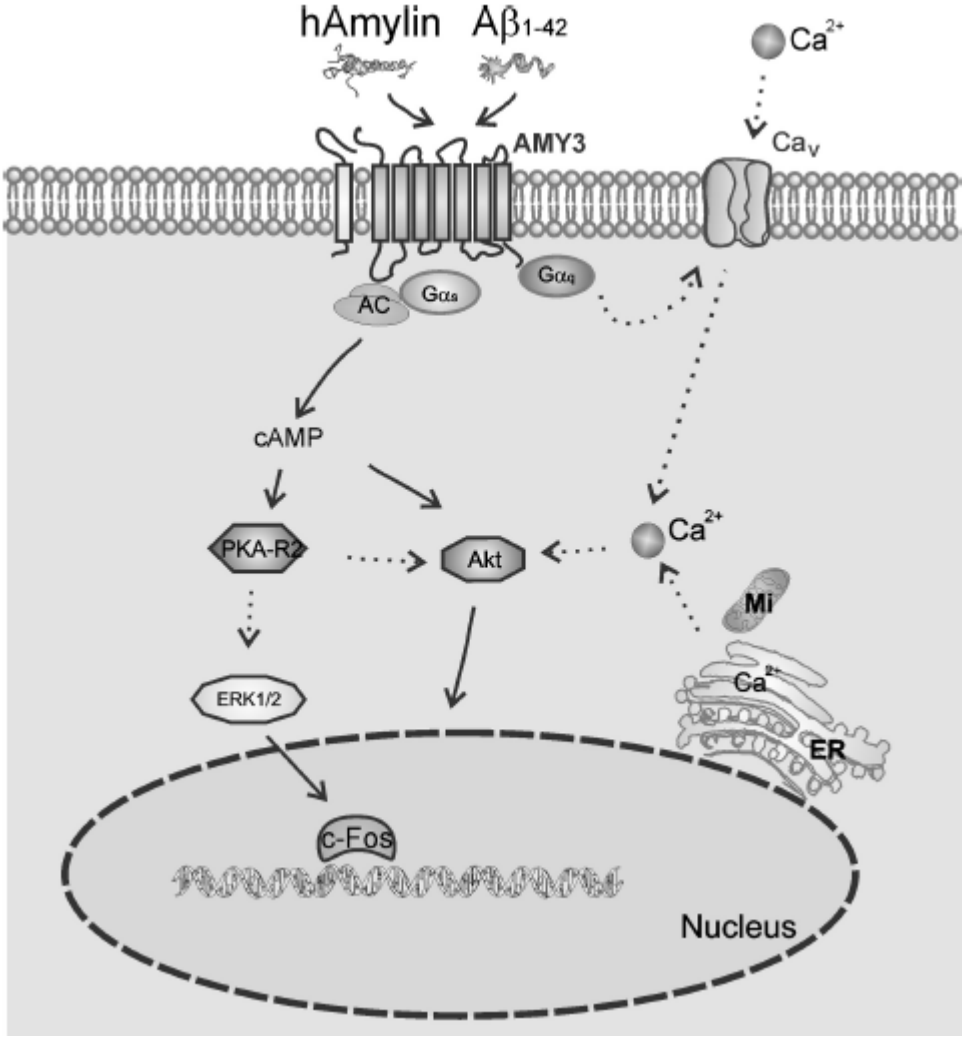

Figure 23 - Aβ1-42-activated cellular signaling pathways and AMY3 role in AD. AMY3 is a multimeric complex formed by CTR and RAMP3. Direct activation of AMY3 with hAmylin and Aβ1-42 results in $G\alpha_s$-mediated adenylate cyclase (AC) stimulation, with subsequent increase in cellular cAMP, stimulation of PKA R2, downstream activation of ERK1/2, and an increase transcription factor cFos expression. The observed cytosolic Ca^{2+} rise could be due to $G\alpha_q$ activation. Akt is also activated followed cAMP and PKA activation. The cytosolic Ca^{2+} changes could also contribute to Akt activation. Long term AMY3activation could trigger an ERK1/2 pathway that may cause Ca^{2+} imbalance and perturb homeostasis of the endoplasmic reticulum (ER), leading to cell death. MI, mitochondria.

Compelling evidence indicates that excess consumption of sugar- sweetened beverages and high fat diets play an important role in the epidemic of obesity, a major risk factor for T2DM, a disease that has been associated with a higher incidence of AD. When Aβ plaque-forming transgenic APP/PS1 mice were fed with 10% sucrose-sweetened water, compared with control mice fed with no sucrose added to the water, the sucrose group gained more body weight and developed glucose intolerance, hyperinsulinemia, and hypercholesterolemia. These metabolic changes were associated with an exacerbation of the memory impairment that characterizes the Aβ-plaque-forming model, and an up to 3-fold increase in insoluble Aβ levels and its deposition in the brain. Interestingly, steady-state levels of Insulin Degradating Enzyme (IDE) did not change, but there was a 2.5-fold increase in brain apolipoprotein E levels, a molecule with a central role in sporadic AD [248]. In a complementary study, diabetic BBZDR/Wor rats (T2DM model) were assessed for characteristic AD changes in their frontal cortices. While neuronal loss was also found in a model of T1DM (BB/Worrats), this loss was associated with a 9-fold increase of dystrophic neuritis in the T2DM model. In addition, different from the T1DM model, protein levels of APP, β-secretase and Aβ were all increased in the T2DM rats, as were levels of hyperphosphorylated forms of tau. Collectively, the data show that accumulation of Aβ and hyperphosphorylated tau occurs in experimental diabetes. Interestingly, the changes were more severe in the T2DM model and appeared to be associated with insulin resistance and possibly, hypercholesterolemia [249].

Levels of Aβ and Amylin are determined by the net effect of (1) their production, and (2) their degradation and clearance. Aβ-degrading peptidases *in vivo* are neprilysin (NEP) and IDE. For IDE, additional substrates were identified, such as Amylin or insulin [250]. Enhanced IDE activity correlates well with decreased Aβ levels in brains of IDE/APP double transgenic mice [251], and IDE shows a decreased degrading activity of Aβ in AD compared to control brains [251]. *In vivo*, IDE substrates compete with each other, and this imbalance may contribute to the pathogenesis of AD and T2DM [250]. Interestingly, mutations in *IDE* cause human T2DM-like symptoms [252].

Similar to Aβ, Amylin can induce apoptotic cell-death [253]. It was found that in 20 DIV (days *in vitro*) hippocampal cultures, non- aged Aβ42 was able to illicit toxicity at 5μM, and this effect was enhanced by aging of Aβ42, whereas aged preparations of

Aβ42 were already significantly toxic at 0.5μM, compared to the PBS control [254]. It was observed a similar dose-dependency in the human Amylin-treated cells, revealing enhanced neurotoxicity of aged compared to non-aged human Amylin preparation. Different from human Amylin and Aβ42, rat Amylin was no toxic to hippocampal neurons at either concentration tested. This suggestes that a specific receptor-peptide interaction may be involved in neurotoxicity. These data are consistent with studies in HeLaand βs in which human, but not non-amyloidogenic mouse Amylin induced an aggregation state-dependent apoptosis [255]. When cortical neurons were exposed to either Aβ42 or human Amylin, it was found that, different from hippocampal cultures, these were generally less susceptible. Similar to Aβ42, aging of human Amylin enhanced its neurotoxic properties to a degree similar to what was found for hippocampal cultures. Together, this suggests that hippocampal neurons are more susceptible to the neurotoxic effects of both human Amylin and Aβ42, indicating selective vulnerability. It was also found that rat Amylin, which does not form fibrils, while not being toxic to hippocampal neurons, surprisingly, it was to cortical neurons [254].

While it is still not fully clear to which cellular components Aβ binds in order to exert its toxicity it appears unlikely that there are just one or two cognate receptors, or that there are only one or two assembly forms of the peptide that can induce neuronal dysfunction; infact, Aβ is likely to bind to different components of neuronal and non-neuronal plasma membranes and there by induces complex patterns of synaptic dysfunction and network disorganization [256]. As far as Amylin is concerned,this molecule bind store ceptors (such as the Amylin receptor) but at the same tim ,it was found that the β- aggregates of Amylin can also bind directly on the surface of lipid bilayers, without penetrating into the bilayer structure [257].

At a proteomic level, T2DM and AD share a remarkably similar profile. This is impressively illustrated by ananalysis of pancreatic islets that identified several novel proteins that are also associated with AD pathogenesis [258]. Interestingly, in a proteomic study using Aβ-injected tau transgenic pR5 brains, it was identified a significant subset of “islet” proteins to be deregulated upon Aβ injection, such as GRP78, valosin-containing protein, calreticulin, the HSP family or peroxiredoxin [259]. Similarly, in the insoluble “formic acid” fraction of Aβ-treated P301L tau-transfected cells, it was identified Insulin-like growth factor binding protein 2 precursor

(IGFBP-2) as being up-regulated, again pointing at similarities between DM and AD. Together this implies that similar proteins and pathways are activated by Amylin and Aβ, respectively, in either pancreatic islets (T2DM) or neurons(AD).

CONDITIONED MEDIUM AND CELLULAR COMMUNICATION

Conditioned medium, occasionally referred to also as CFCS (cell-free culture supernatant), is spent media harvested from cultured cells. The medium is obtained by sterile filtration of used culture media and is added to fresh culture media for up to one third of the final volume. It contains metabolites, growth factors, and extracellular matrix proteins secreted into the medium by the cultured cells. Examples of each might include: metabolites such as glucose, amino acids, and nucleosides; growth factors such as interleukins, EGF (epidermal growth factor), and PDGF (platelet-derived growth factor); and matrix proteins such as collagen, fibronectin, and various proteoglycans [260].

Conditioned media are often used for the cultivation of particularly fastidious cells and cell lines because they contain many mediator substances that were secreted by the cells cultivated in this medium. These mediator substances contain growth factors and cytokines and may promote the growth of new cells and may help them to “take”. It may make a great difference if conditioned media are obtained from short-term or long-term cultures of cells, both of which may contain entirely different secreted factors.

Biological activities found in conditioned media obtained from cultures of different cell lines have been the first indication of the existence of soluble mediators now known under the collective term of cytokines. The analysis of the effects of conditioned media on different cell types and the biochemical analysis of the constituents responsible for a particular biological activity is still one of a number of ways pursued to detect novel secreted growth factors.

Astrocytes are the main producers of NGF in the central nervous system (CNS) [261], and thereby participate in the regulation of various neuronal activities. It has been proved that the medium conditioned by astrocytes protects neurons from death induced by ethanol [262], and increases neuronal survival in a model of ischemia *in vitro* [263,264]. It also reduces NO levels and the lactate dehydrogenase released, stabilizes the cell membrane, promotes cellular energy metabolism, and electrolyte balance [265]. Even for the normal functioning of the retina it is necessary that the retinal pigment

epithelium (RPE) contributes through the production of trophic and growth factors [266]. The secreted substances participate in the regulation of angiogenesis (VEGF and PEDF) [267,268], apoptosis (bFGF), cell differentiation (PDGF) [269], and act as trophic support to the photoreceptor cells (PEDF, BDNF, NT-3) [270].

The medium conditioned by endothelial cells contains a combination of factors (VEGF, bFGF, IGF and EGF) that promote the *in vitro* differentiation of stem cells in hematopoietic and endothelial cells [271].

Over the last number of years, many research groups have analysed conditioned media under well-defined experimental conditions to aid in their biomarker discovery investigations. Proteins released into conditioned media by cultured cells are a rich source of material for biomarker discovery experiments [272]. Certain proteins secreted from cells that enter the circulatory system can be exploited as molecules for screening for the presence of disease or monitoring therapeutic effectiveness. This technique provides a useful and less invasive alternative to direct clinical specimen analysis for the discovery of novel biomarkers. By using a cell culture model system in which the cells were grown in serum-free media, the identification of candidate biomarkers through the use of proteomic analysis is enhanced due to a lower dynamic range, spanning five or six orders of magnitude [273] and a smaller diversity of proteins. Large data sets of secreted or shed proteins have emerged as candidate biomarkers from studies of cell populations, and many of these have been initially validated in clinical samples achieving high levels of sensitivity and specificity [274-277].

Proteins identified in media conditioned by cell lines will exit the cells through a number of different pathways. During the classical secretory pathway, proteins containing an ER (endoplasmic reticulum) signal sequence, generally at the N-terminus, are secreted in an ER/Golgidependent manner [278]. During secretion through the non-classical pathway, no signal sequences are present and proteins are released by a variety of mechanisms, including shedding of plasma membrane microvesicles, direct efflux through plasma membrane transporters and exocytosis of secretory lysosomes/exosomes [279]. Exosomes are small (40-90 nm) membrane vesicles of endocytic origins that harbour components of the secretome including membrane and cytoplasmic proteins [280].

It is also likely that alternative pathways or mechanisms are present for proteins to exit cells that have yet to be discovered. (**Fig. 24**).

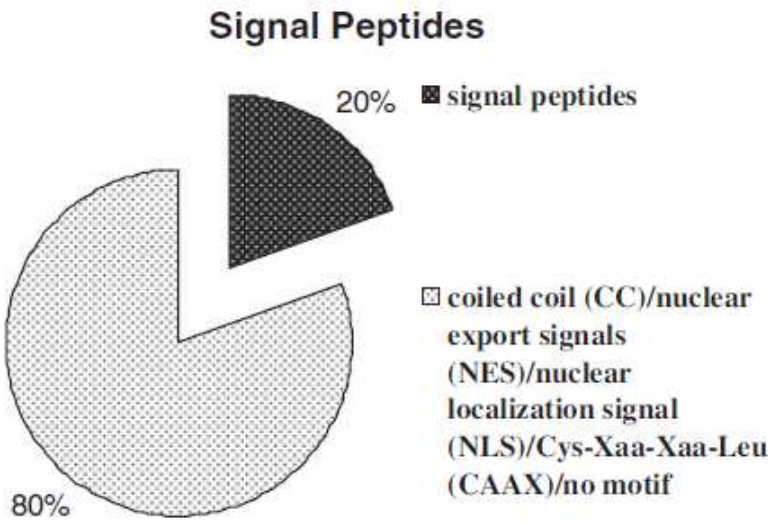

Figure 24 - Analysis of conditioned media from colon cancer cell lines. In-solution digestion and MS analysis of conditioned media from four colon cell lines – HCT116, HT-29, SW480 and WiDr demonstrated that 92 proteins were common to all four. Further analysis of these 92 proteins showed that 18 of them had a signalling peptide for processing through the classical secretory pathway. As shown in the pie chart, the majority of common proteins exited the cells by alternative pathways.

Analysis of conditioned media has many advantages over direct analysis of clinical specimens. These advantages include the non-invasive method of sample collection and the fact that a large number of cell lines representing various stages/histotypes are readily available [281].

NITRIC OXIDE

Since the discovery in 1986 that nitric oxide (NO) is the endothelium-derived relaxing factor, this molecule has been shown to have numerous other physiological functions, including platelet aggregation, bronchodilation, neurotransmission, and antimicrobial activity [282-285] Although NO is often described as highly toxic and reactive, it is not. Inhaling low concentrations of gaseous NO is approved by the Food and Drug Administration for the treatment of persistent pulmonary hypertension of the newborn [286-292]. In addition, NO can be produced for 80 years by neurons in human brain without overt toxicity. Neither superoxide nor NO is particularly toxic *in vivo* because there are efficient means to minimize their accumulation [293,294]. Superoxide is rapidly removed by high concentrations of scavenging enzymes called superoxide

dismutases (SOD) with distinct isoenzymes located in the mitochondria, cytoplasm, and extracellular compartments.

NO is rapidly removed by its rapid diffusion through tissues into red blood cell [295,296], where it is rapidly converted to nitrate by reaction with oxyhemoglobin (**Fig. 25**).

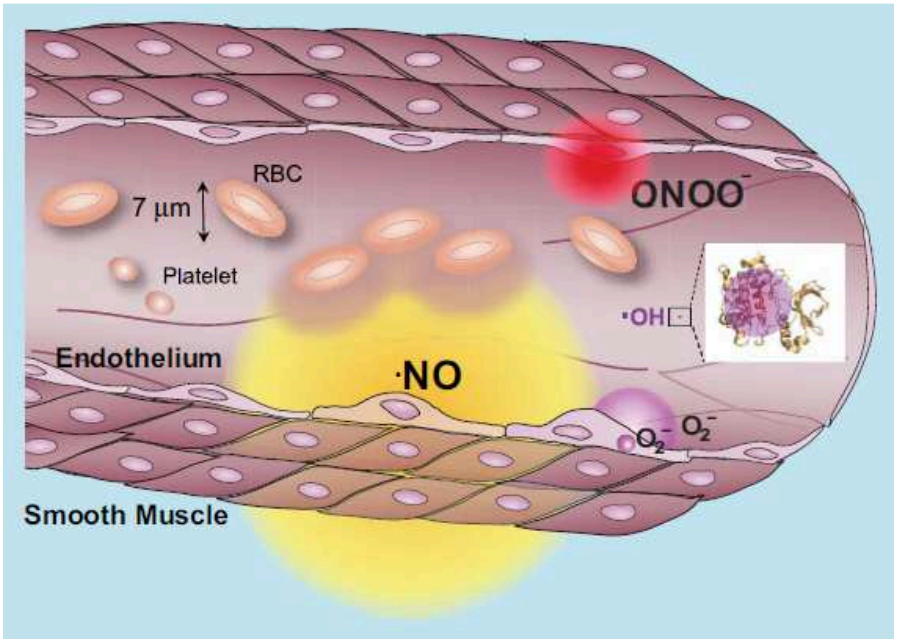

Figure 25 - Cellular diffusion of superoxide, peroxynitrite, and hydroxyl radical. These circles indicate the extent to where the concentration of each species from a point source would decrease by 50%. The diffusion of peroxynitrites accounts for its rapid reaction with carbon dioxide and with intracellular thiols. The diffusion distance for nitric oxide is calculated based on its half-life of 1 s *in vivo*, which results mostly from its diffusion into red blood cells.

NO is produced by a group of enzymes known as nitric oxide synthases, which generate NO through the conversion of L-arginine to L-citrulline (**Fig. 26**).

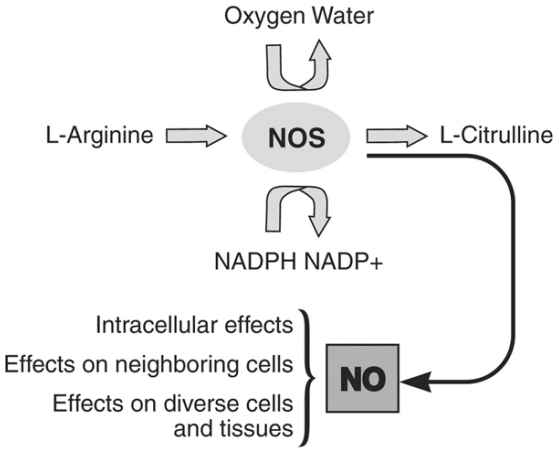

Figure 26 - Production of nitric oxide. NADPH, nicotinamide adenine dinucleotide phosphate; NO, nitric oxide; NOS, nitric oxide synthase.

Mammalian cells are endowed with three genes encoding distinct isoforms of NOS – NOS1, NOS2, and NOS3 – with 51-57% homology between isoforms and different localizations, regulation, catalytic properties, and inhibitor sensitivity (**Fig. 27**).

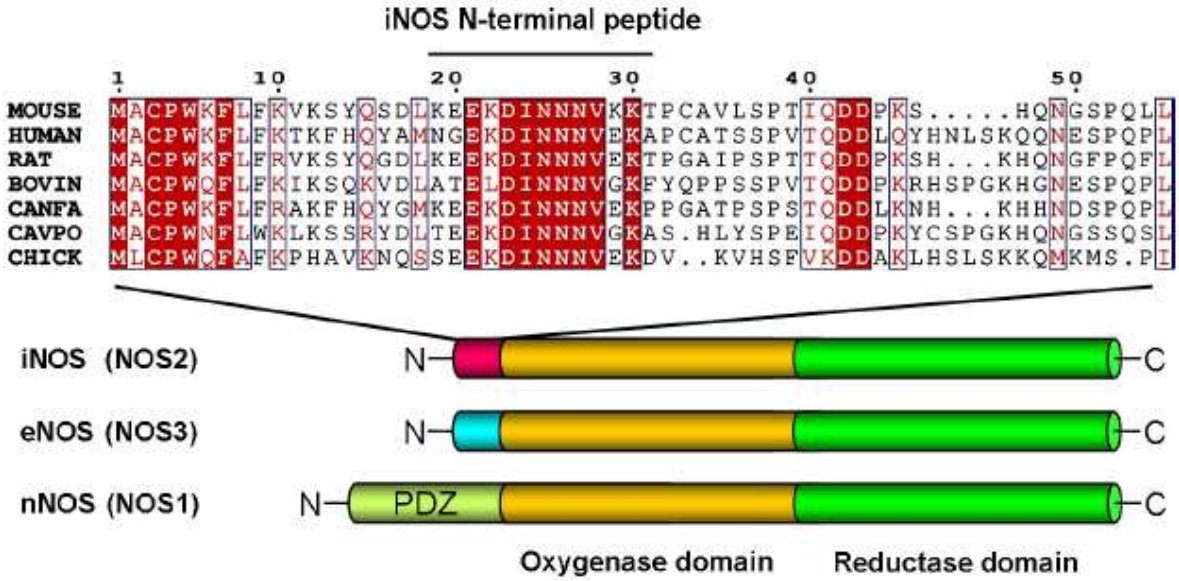

Figure 27 - Domain structure of NO synthases and amino acid sequence alignments of the N-terminal region of iNOS proteins. The EKDINNNVXK sequence is conserved in iNOS (NOS2) but is not present in either eNOS (NOS3) or nNOS (NOS1). The sequence of the mouse iNOS N-terminal peptide used in ITC and NMR experiments (iNOS19–31) is indicated. The amino acid numbering refers to the mouse protein (Swiss-Prot ID P29477). Outlining indicates regions of conserved amino acid sequence. Red lettering indicates amino acid similarity, and red shading indicates amino acid identity.

NOS1, also known as nNOS (isoform first purified and cloned from neuronal tissue), and NOS3 or eNOS (isoform first found in endothelial cells) are also termed as constitutive since they are expressed continuously in neurons and endothelial cells, respectively. They are also dependent on a rise in tissue calcium concentration for activity and therefore produce low, transient concentrations of NO. In contrast, NOS2 is an inducible, calcium-independent isoform, also called iNOS. Unlike NOS1 and NOS3, induction of NOS2 results in continuous production of NO [297]. It is inducible by immunological stimuli in virtually all nucleated mammalian cells. Once induced, the enzyme continues to produce much higher NO concentrations for many hours or even days. An important regulator of NOS2 is the tumor suppressor gene p53 which senses raised cellular NO and inhibits NOS2 by a negative feedback loop [298].

Under normal physiological conditions, cells produce small but significant amounts of NO which contribute to regulation of anti-inflammatory effects and its antioxidant properties [299,230]. However, in tissues with a high-output of NO, iNOS is upregulated and effects such as nitration (addition of NO_2), nitrosation (addition of NO^+), and oxidation will prevail [299]. Excessive NO production has been linked to

cancer, diabetes, and several neurodegenerative disorders, including Alzheimer's and Parkinson's diseases [301-304].

Interaction of NO with O_2 or O_2^- results in formation of reactive nitrogen species (RNS). The RNS, dinitrogen trioxide (N_2O_3) and peroxynitrite ($ONOO^-$), can induce two types of chemical stresses, nitrosative and oxidative [305]. N_2O_3 is a potent nitrosating agent which has been shown to N- and S- nitrosate a variety of biological targets to yield potentially carcinogenic nitrosamines and nitrosothiol derivatives. N-nitrosation may have important implications in the known association between chronic inflammation and malignant transformation [305,306]. $O_2^-$and NO may rapidly interact to produce the potent cytotoxic oxidants peroxynitrite ($ONOO^-$) and its conjugate acid ONOOH (**Fig. 28**).

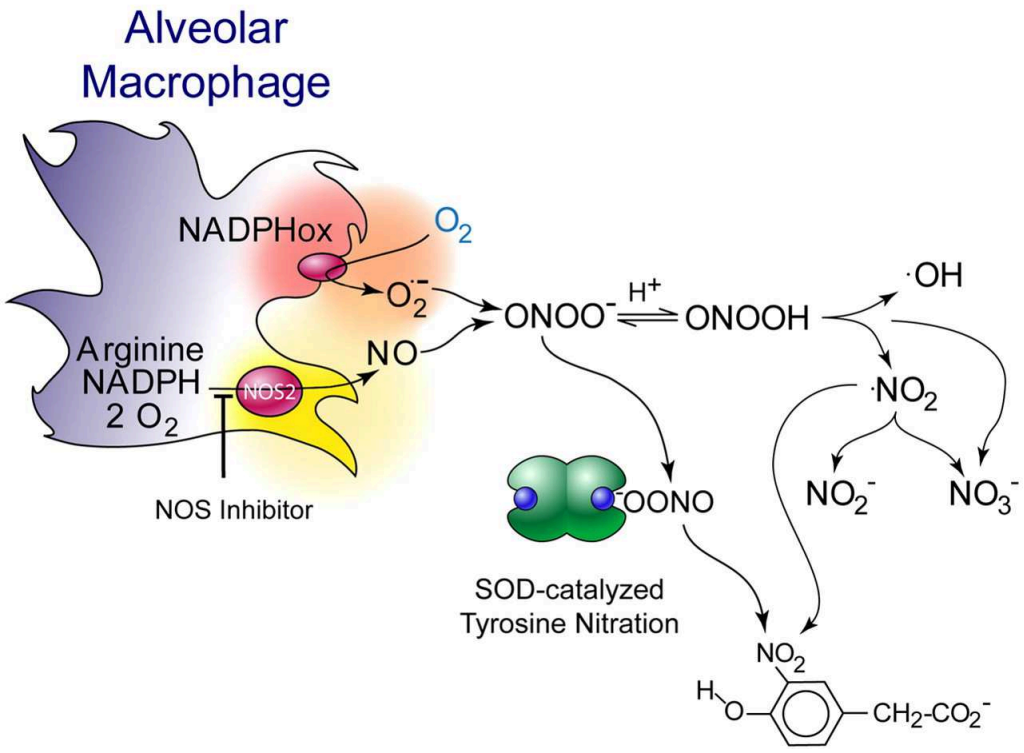

Figure 28 - Alveolar macrophages produce peroxynitrite. When alveolar macrophages are stimulated to produce both superoxide and nitric oxide, peroxynitrite is quantitatively produced as evidenced by the amount of nitric oxide and superoxide produced and the amount of oxygen consumed.

Several enzyme complexes, such as NADPH oxidases (NADPHox) and xanthine oxidase, can be activated in many cellular systems to actively produce large amounts of superoxide. Modestly increasing superoxide and NO each at a 10-fold greater rate will increase peroxynitrites formation by 100-fold. Under proinflammatory conditions, simultaneous production of superoxide and NO can be strongly activated to increase production 1000-fold, which will increase the formation of peroxynitrite by a

1000000-fold . Without superoxide, the formation of nitrogen dioxide by the reaction of NO with oxygen is miniscule by comparison. NO and superoxide do not even have to be produced within the same cell to form peroxynitrite, because NO can so readily move through membranes and between cells.

Once the level of cellular damage inflicted by peroxynitrites supercedes any possibility of repair, the cell eventually dies via one of the two main pathways of cell demise, necrosis or apoptosis. Necrosis is associated with loss of cellular ATP, leading to membrane disruption, release of noxious cellular debris, and the development of secondary inflammation. In contrast, apoptosis occurs in a well-choreographed sequence of morphological events characterized by nuclear and cytoplasmic condensation with blebbing of the plasma membrane. Apoptosis is orchestrated by the proteolytic activation of cysteine proteases known as caspases, that requires preserved ATP levels to proceed properly, and which may be triggered either by the activation of death receptors (extrinsic pathway) or by the permeabilization of the outer membrane of mitochondria (intrinsic pathway) [307,308]. The mechanisms of peroxynitrite-mediated apoptotic and necrotic cell death are presented in **Fig. 29**.

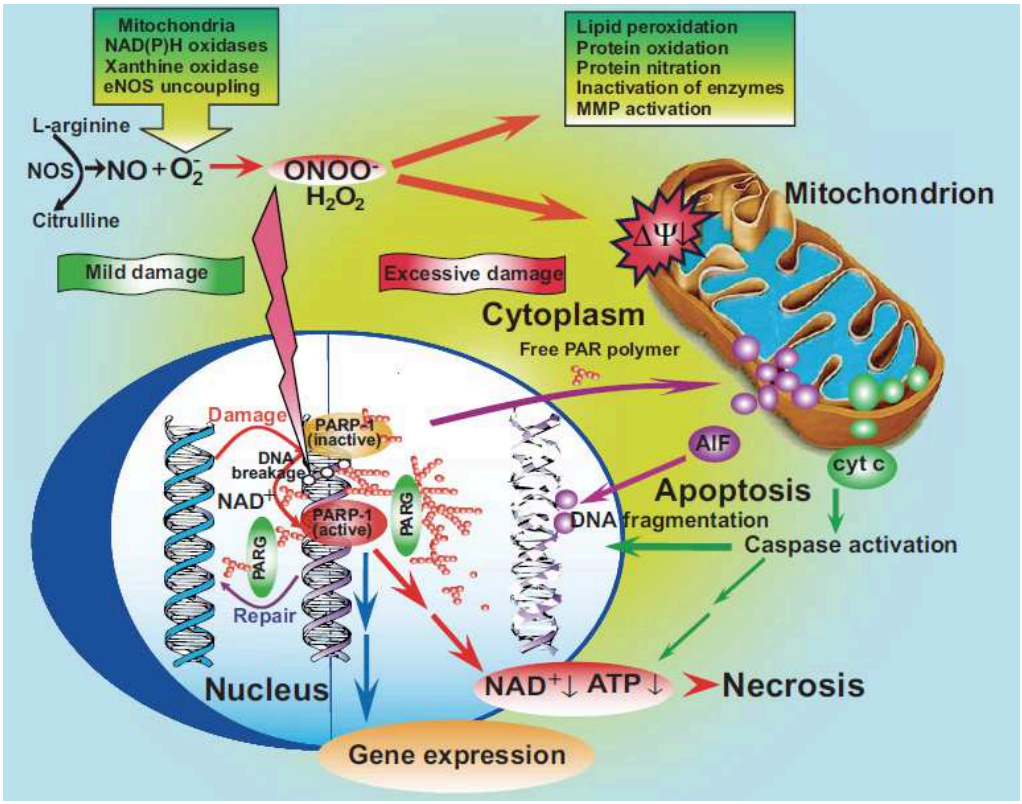

Figure 29 - Molecular mechanisms of peroxynitrite-mediated cell death. NO sources are restricted to the activity of the various NO synthases, whereas $\bullet O_2^-$ arises from multiple sources, including electron leak from the mitochondria, NADPH oxidase, xanthine oxidase, and uncoupling of NO synthases. Once a flux of NO and $\bullet O_2^-$ is produced simultaeously in close proximity, the generation of peroxynitrite is considerably enhanced.

NO is often considered to be just another signaling molecule. But it is important to consider how NO communicates information to understand why NO has so many physiological roles *in vivo*. The production of cGMP by guanylate cyclase is the major signal transduction mechanism of NO. Soluble guanylate cyclase contains the same heme protoporphyrin IX as hemoglobin with iron in the ferrous form that binds NO with great affinity. Deoxyhemoglobin binds NO with a 10,000-fold greater affinity than molecular oxygen [309,310]. Only 5-10 nM NO is necessary to activate guanylate cyclase. NO can diffuse from where it is synthesized into surrounding cells where it will activate soluble guanylate cyclase in the target tissue to produce cGMP. In turn, cGMP activates cGMPdependent kinases in the target tissue that modulates intracellular calcium levels to modulate many diverse activities in the target tissues.

NO is a small hydrophobic molecule that crosses cell membranes without channels or receptors as readily as molecular oxygen and carbon dioxide. The diffusion coefficient of NO in water at 37°C is slightly faster than oxygen and carbon dioxide [311], which is ideal for quickly transmitting information over short distances. Because NO is freely permeable to membranes, NO will repeatedly diffuse in as well as out of a cell over the time span of a second.

The hydrophobicity of NO will allow slightly faster diffusion in a lipid membrane than in water so that membranes provide effectively no barrier to NO.

Red blood cells provide a drain for NO that creates a sharp diffusion gradient leading to the vasculature [295,312,313]. The addition of a red blood cell outside of a cell will capture much of the NO produced inside of this cell, because the hemoglobin will greatly reduce the reentry of NO into the cell [314].

Although the biological half-life of NO is only a scant few seconds *in vivo*, a second is long compared with a simple neural reflex or to the time needed to contract a muscle. A sprinter can run ~10 m within the reported half-life of NO (far shorter than the total distance covered of a molecule of NO as it bounces around inside and between cells in the same time). The relatively short overall distance that NO can diffuse limits its action to only a few cells near the source of production. Thus NO produced in the gut, for example, will not influence its actions in the central nervous system (CNS). On the other hand, the intermediate lifetime of NO coupled with its rapid diffusion through most tissues allows NO to integrate and modulate complex physiological processes [315].

The nNOS is particularly well suited to produce NO in a manner that facilitates synaptic plasticity [316,317]. The amino terminus of NOS1 contains an additional sequence lacking on NOS2 and NOS3 that anchors the enzyme to the cytoskeleton in postsynaptic boutons beneath the *N*-methyl-D-aspartate (NMDA) receptor [318]. The NMDA receptor has been implicated in learning and development as well as in many forms of excitotoxic neurodegeneration [319] The NMDA receptor only activates when a neuron has been partially depolarized, as occurs when a neuron has been firing frequently. In addition, the receptor must bind glutamate and glycine to the extracellular surface for thechannel to open. A local group of neurons that are firing repeatedly for a few milliseconds is sufficient to cause local increase in NO. The synthesis of NO is initiated by extracellular calcium entering the neuron through the NMDA receptor. NO plays an important role in long-term potentiation, the most widely studied neuronal equivalent of learning *in vitro* [320,321].

Local neuronal activity can be temporally integrated because NO will only be synthesized by localized groups of neurons that had been depolarized through repeated activation that is necessary to open NMDA receptors [322]. NO can help enhance the synaptic efficiency of surrounding axonal arbors of neurons that have been active, whereas the axonal arbors from neurons that have not been activated will be weakened. The ability to modulate local groups of neurons on a moderate time scale is one in the reasons why the CNS is a major source of NOS and why it undergoes radical changes in expression throughout development [323-325].

Due to its transient nature, the amount of NO present in biological samples such as serum, blood, or microdialysis samples is most commonly estimated through measurement of the more stable major NO oxidation products, nitrite and nitrate [326,327]. In addition, the ratio of arginine to citrulline has also been employed [328,329]. Hetrick *et al*. have reviewed spectroscopic and electrochemical methods for the detection of NO. There are several commercially available molecular probes that react with a partially oxidized species of NO (N_2O_3) to produce fluorescent triazole derivatives [330-332]. The most popular probes are based on diaminofluorescein (DAF) and have been extensively employed for imaging NO production in live cells with microscopic techniques [333]. One drawback of DAF probes is that they can react with dehydroascorbate (DHA) to produce fluorescent derivatives that interfere with NO analysis [334-335]. Therefore, for accurate quantitation of NO in single cells or bulk

cell lysates, the separation of the reaction products of the dye with NO from those with dehydroascorbate is desirable. For this reason, Sweedler's group employed capillary electrophoresis and fluorescence detection to quantitate NO production in the neurons of Aplysia californica [334-335].

NO production by macrophages in culture was explored by Goto *et al*. using a microfluidic device incorporating on-line reduction of nitrate by nitrate reductase, followed by reaction with the Griess reagent and thermal lens detection [336].

BLOOD-BRAIN BARRIER (BBB) AND DYNORPHIN A (1-17)

The blood-brain barrier (BBB) is a unique biological interface that maintains brain homeostasis by preventing and regulating the permeation of endogenous substances, ions, and xenobiotics (toxins, pollutants, and drugs, for example) into the extracellular space of the brain [337-339]. Although beneficial for neurobiological purposes, this interface is also themajor obstacle in the development of drugs for treatment of central nervous system (CNS) disorders and brain cancers [340-342].

The major component of the BBB is the brain microvessel endothelial cell (BMVEC). Specialized proteins, such as claudin, occludin, and cadherins, hold the endothelial cells together to produce tight junctions (TJs), areas where adjacent endothelial cells are physically held together, making passive transcellular transport of small hydrophilic molecules extremely difficult. The "tightness" of these junctions can be evaluated bymeasuring the transendothelial electrical resistance (TEER). The cells that make up the BBB exhibit TEER values that are almost three orders of magnitude higher than those in peripheral capillaries. In fact, the resistance across these endothelial cells is so great that even the movement of small hydrated ions, such as Na^+ and Cl^-, is significantly restricted. The surface of BMVECs is also strongly anionic and creates an electrostatic barrier for the transport of negatively charged compounds. In addition to the physical and electrostatic barriers to transport, these cells also create a metabolic barrier. There are a number of intracellular and extracellular enzymes, including peptidases, nucleotidases, monoamine oxidase, and cytochrome P450, that convert substrates into less permeable or less toxic compounds. Additionally, the BBB is an immunological barrier that prevents bacteria and viruses from entering the brain.

The endothelial cells that make up the BBB are part of the larger neurovascular unit (NVU) that also contains pericytes, astrocytes, microglia, and neurons [337-339]. All

the cells in the NVU play a role in the maintenance of the BBB as well as in blood-brain signaling in both directions [343]. The endothelial cells are surrounded by a basement membrane that is shared with pericytes, generally undifferentiated cells that differentiate into support cells in the brain vasculature (e.g., vascular smooth muscle cells). Known functions of the pericytes include helping to build and maintain the basement membrane at the BBB. Astrocytes are connected to the endothelial cells via their end feet and provide growth factors and nutrients to both endothelial cells and local neurons [338,339]. The cells that make up the blood-brain barrier and the neurovascular unit are presented in **Fig. 30**.

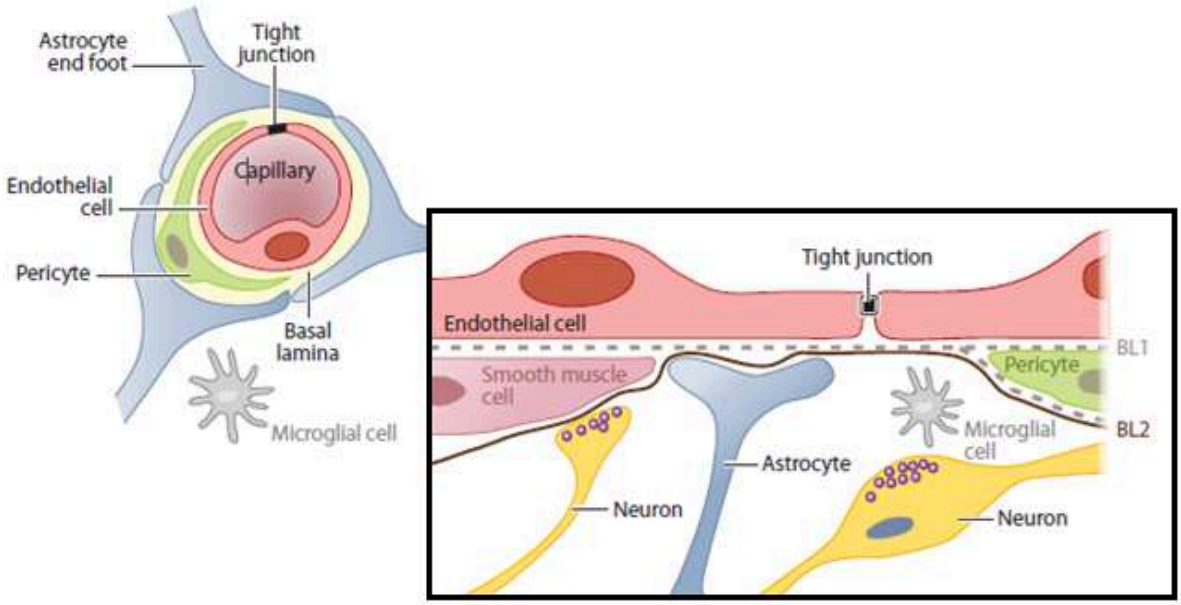

Figure 30 - The cells that make up the blood-brain barrier and the neurovascular unit.

These cells, therefore, play an important role in blood-to-brain communication. Microglia are also a part of the NVU and are involved in the immune response [344]. Normally, these cells are in a resting state, but they quickly become activated if there is a disturbance in the homeostasis of the brain such as during ischemia, infection, or an influx of albumin from the blood.

As mentioned above, the primary role of the BBB is to maintain the homeostasis of the brain by inhibiting the uncontrolled influx of molecules from the blood into the brain. There are many natural substances that, if allowed into the brain, would severely disrupt neuronal activity or cause brain damage (e.g., glutamate). A complementary second role of the BBB is to supply nutrients to the brain in a regulated manner. This task is accomplished using specific transport systems for molecules needed to maintain the cells in the brain [345]. Examples of such transport systems include transporters for

glucose, insulin, amino acids, and neurotransmitter precursors. A third role of the BBB is to protect the brain against toxins present in the blood. Examples include poisons, pollutants, and drugs, as well as endogenous metabolites or proteins. Specialized transport proteins, expressed on the apical (blood) side of BBB endothelial cells, are responsible for the efflux of undesirable compounds, such as lipophilic toxins, that may otherwise cross the cell membrane.

The BBB is also an important participant in the brain's immune system, and it can direct inflammatory cells to act quickly in response to changes in the neurovascular space. For example, if albumin crosses the BBB (owing to head trauma or stroke), an inflammatory reaction in the brain, microglia cellular activation, and programmed cell death may result [346]. Lastly, the BBB serves as an important chemical messaging system between the CNS and the PNS. Substances released in the periphery can be transported to the brain and generate a neuronal response. Likewise, substances that are released from the brain into the periphery can generate a physiological response in a remote tissue. In particular, cytokines and neuropeptides are important mediators of such signaling. This transport/messaging system can be involved in a variety of disorders, including depression, drug addiction, Alzheimer's, and Parkinson's [342]. The endothelial cells that make up the BBB have TJs that allow very few small hydrophilic molecules, such as ethanol or mannitol, to pass into the brain. The membrane is also highly negatively charged, so anionic compounds are generally excluded. Owing to these restrictions, most molecules are transported across the BBB by one of the following mechanisms [347] (**Fig. 31**).

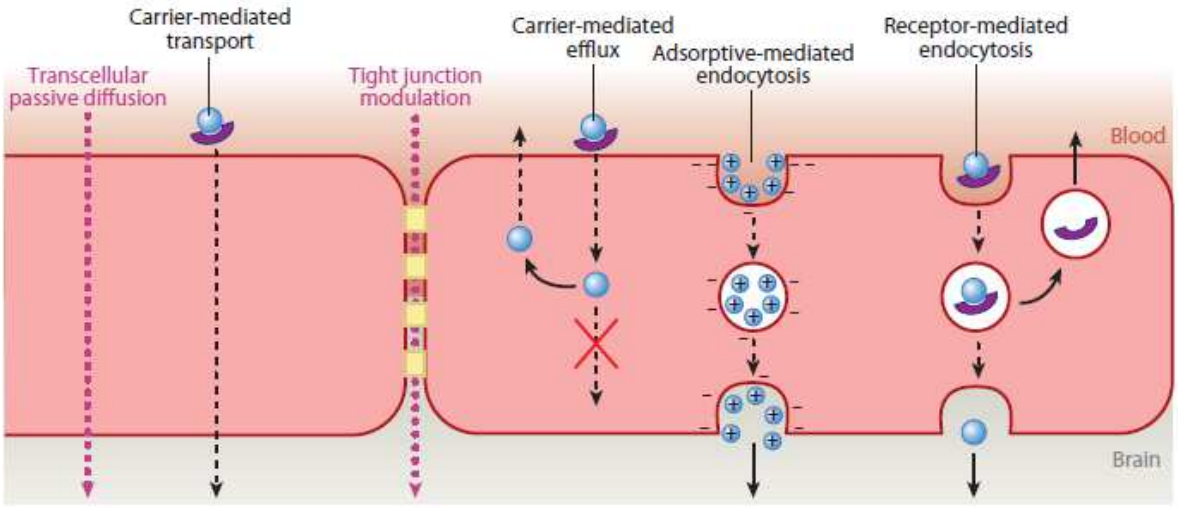

Figure 31 - Mechanisms of transport across the blood-brain barrier.

1. Transcellular passive diffusion: Small lipophilic compounds can passively diffuse across the endothelial membrane. In general, the more lipophilic a molecule is, the greater its ability to permeate. Examples of compounds that are transported by this mechanism include acetaminophen and fluoxetine.
2. Carrier-mediated transport: Various transporters are used to bring essential polar molecules into the brain. For example, there are specific amino acid, nucleoside, peptide, vitamin, and glucose transporters. Neurotransmitters such as dopamine and serotonin do not cross the BBB; however, their precursors, levodopa and tryptophan, are transported through this mechanism.
3. Receptor-mediated endocytosis: This is a common method of transport for large peptides and proteins and is facilitated by binding to a receptor on the membrane surfaces followed by endocytosis. Examples of molecules transported by this approach include insulin, transferrin, cytokines, and other large peptides.
4. Adsorptive-mediated endocytosis: Due to the highly anionic character of the BBB, cationic molecules adsorb nonspecifically to the membrane and undergo endocytosis. This mode of transport has a lower affinity and a higher capacity than receptor-mediated endocytosis. Highly positively charged molecules such as histones, cationized albumin, and arginine containing peptides are examples of molecules transported by this approach.
5. TJ modulation: Typically, the TJs between the BMVECs restrict the passage of even very hydrophilic compounds from crossing the BBB via paracellular diffusion; however, if the TJs are disrupted, nonspecific passage into the brain of molecules that would normally be excluded can occur. Changes in the resistance of the TJs are usually due to a disease or administration of a drug that disrupts the proteins that make up the TJs. Experimentally, this can be accomplished through the administration of hyperosmolar solutions such as 25% mannitol. The high ionic strength causes the endothelial cells to shrink, opening the TJs. Clinically, this is employed for the treatment of brain tumors. Additionally, leukocytes and other immune cells can modify TJs or cross the BBB via transcellular mechanisms. Changes in the TJs can also occur during ischemia or brain trauma.

Along with these transport mechanisms of substances from the blood to the brain, efflux mechanisms also shuttle substances out of the endothelial cells and back into the blood before they have a chance to enter the brain. These carrier-mediated efflux

mechanisms pose a significant challenge to pharmaceutical scientists attempting to deliver drugs into the brain. Examples of carrier-mediated efflux systems that are present at the BBB include the multidrug-resistance proteins such as P-glycoprotein. Understanding the BBB and the NVU is important for several reasons. If the integrity of the BBB is compromised due to diseases such as AIDS, undesired substances could leak into the brain, generating an immune or inflammatory response [348]. Conversely, if drugs are unable to pass through the BBB, they will be ineffective for the treatment of neurological and psychiatric disorders, including depression, schizophrenia, Alzheimer's, and Parkinson's. Likewise, anticancer drugs must be able to enter the brain to treat brain tumors. In addition, the BBB plays an important role as a chemical messaging system between the CNS and the PNS. Peptides and other substances can be released in the brain or periphery, traverse the BBB, be transformed by a separate set of enzymes, and trigger a neurological or physical response at a remote location.

Investigating the transport and metabolism of endogenous substances at the BBB is important for determining their potential role in neurodegenerative diseases. In particular, the metabolism and transport of neuropeptides at the BBB can provide insight into their role in CNS disorders.

Dynorphin A 1-17 (Dyn A 1-17) is an endogenous neuropeptide known to act at the kappa opioid receptor. Dyn A 1-17 is a major posttranslational product of the preprodynorphin gene [349-352]. The primary amino acid sequence of dynorphin A (YGGFLRRIRPKLKWDNQ) is highly conserved and is identical in human, rat and mouse, bovine, and porcine species [349,350,352].The structures of dynorphin and its major metabolites are shown in **Fig. 32**.

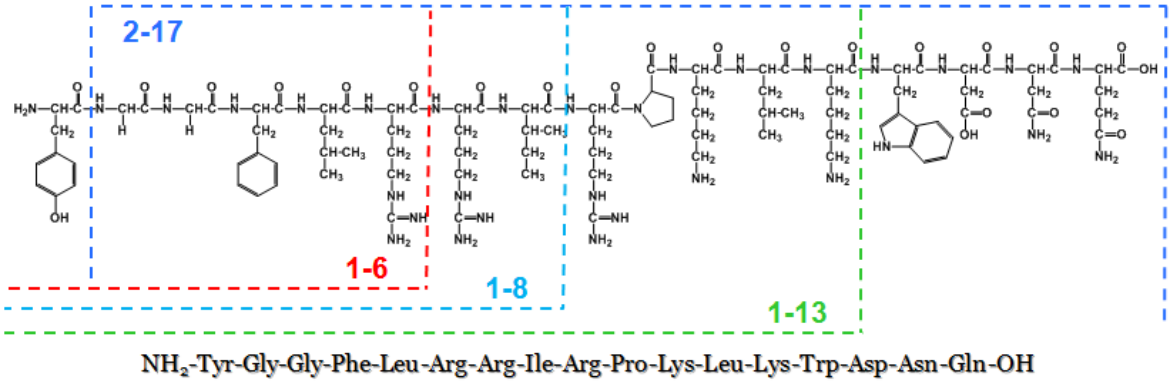

Figure 32 - Structure of Dynorphin A 1-17 with metabolites of interest (1-6, 1-8, 1-13, 2-17) indicated by dotted lines.

Once released into the extracellular space, neuropeptides undergo enzymatic degradation (**Fig. 33**) and, therefore, investigating Dyn A 1-17 metabolism at the BBB is important since the metabolites exhibit unique biological functions compared to the parent compound.

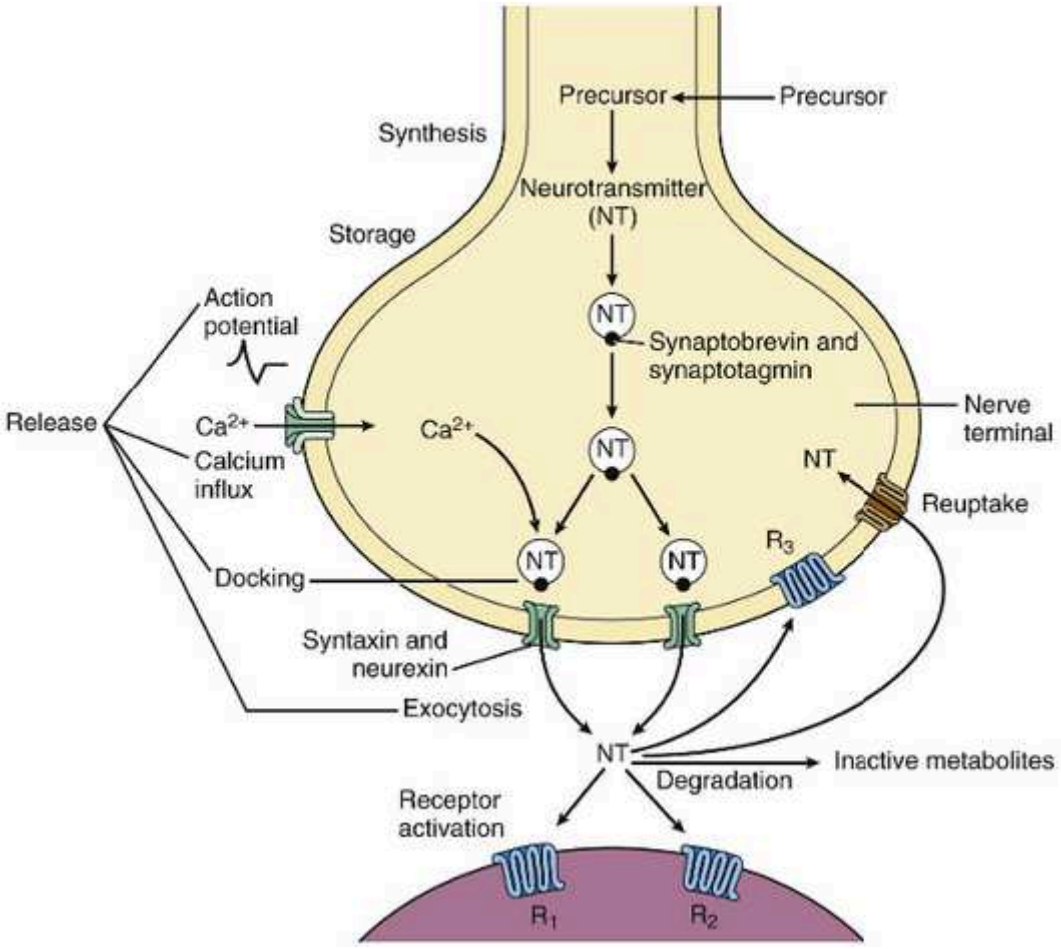

Figure 33 - Central nervous system (CNS) neurotransmission and sites of drug action. After exocytosis, the neuropeptides may activate presynaptic and postsynaptic receptors. A neurotransmitter's action is then terminated either by its reuptake into the presynaptic neuron or by its degradation to inactive compounds, with degradation catalyzed by enzymes located on presynaptic and postsynaptic neuronal membranes or within the cytoplasm.

It is possible that a metabolite, rather than the parent peptide, may be responsible for some of the reported neurotoxic effects of dynorphin.

Up-regulation of Dyn A 1-17 synthesis has been implicated in a variety of neurological disorders, including Alzheimer's [353], Parkinson's [354], neuropathic pain [355], stress [356], and depression [357] and, at elevated concentrations, has been shown to be neurotoxic [358-360].

The deleterious effects of dynorphin A seen with secondary neuronal injury are mediated largely through nonopioid mechanisms. Many of the negative consequences of dynorphin A cannot be blocked by opioid antagonists [361-370]. Intrathecal

administration of low dosages of dynorphin A (1-13) causes opioid analgesia in tail-flick and hotplate assays that can be prevented by opioid antagonists.

In contrast, high dosages or sustained exposure to dynorphin A (1-13) induces hyperalgesia, allodynia, and even hind-limb paralysis. Because the deleterious effects of dynorphin can be prevented by the *N*-methyl-D-aspartate (NMDA) receptor antagonist MK-801, but are largely unaffected by opioid antagonists, suggests that NMDA receptors mediate the maladaptive effects of dynorphin [366,369,371-374].

Data from Kurt *et al*. support the tenet that dynorphin toxicity is mediated through NMDA receptors by showing that dynorphin A fragments [e.g., dynorphin A (2-13)], which retain NMDA receptor activity but lack kappa opioid receptor activity are highly neurotoxic, while those fragments that possess opioid activity alone, such as dynorphin A (1-5) (Leu-enkephalin), are not toxic (**Fig. 34**).

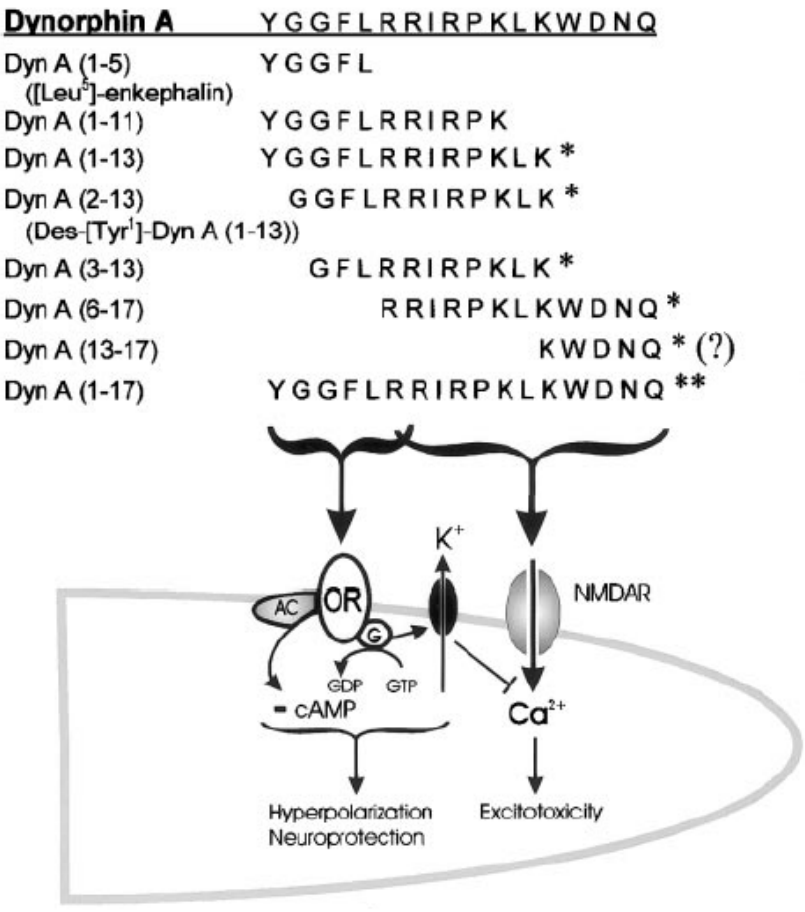

Figure 34 - Hypothetical structure-activity-based model, suggesting the relationship between dynorphin A-derived peptides, opioid (OR), and NMDA receptors (NMDAR). Evidence suggests that dynorphin A has dual actions - opioid and nonopioid - that reside within distinct domains of the parent peptide. *toxic, **very toxic, guanosine triphosphate (GTP), and guanosine diphosphate (GDP), GTP-binding proteins (G).

The neurotoxicity of individual dynorphin peptide fragments can differ significantly from one another, which has been previously noted *in vivo*. This suggests that dynorphin toxicity is mediated by complex interactions between dynorphin A, its metabolites and excitatory amino acid receptors. Pathophysiologic changes in dynorphin A biosynthesis, release and/or metabolism during spinal cord injury may influence neurotoxic outcome. Presumably, the differential toxicity results from unique pharmacodynamic interactions of each of these peptides with NMDA receptors and/or particular NMDA receptor subtypes.

Dynorphin has long-been suspected of having dual actions at both opioid and NMDA receptors [368,369,373,375-383]. A nonopioid action for dynorphin is supported by findings that dynorphin A-derived peptide fragments, which lack the N-terminal tyrosine necessary for opioid receptor activity, retain toxicity through actions at nonopioid glutamatergic receptors [368,369,373,376,378,379,384-388]. It was found found that the toxic effects of dynorphin A reside in the C-terminal portion of the peptide [373,389,390]. Dynorphin A (3-13), (3-13), (6-17), and (13-17) were toxic, while dynorphin A (1-5) and (1-11) were nontoxic.

Interestingly, all the toxic fragments shared a lysine residue at position 13. Kurt *et al*. results suggest that both the carboxyl and amino terminal sequences flanking lysine-13 are toxic – perhaps through independent mechanisms.

Single channel- and whole cell-patch clamp studies suggest that dynorphin A interacts directly with NMDA receptors [362,363,391,392].

Dyn A 1-6, the N-terminal fragment of Dyn A 1-17, has been identified as a major metabolite of the parent peptide Dyn A 1-17,in both the central nervous system (brain and spinal cord) [354,393,394] and peripheral tissues (blood and plasma) [393,395-397].

Dyn A 1-11 amide analogs can be used to treat peripheral pain and cocaine addiction. Dyn A-(1-11) analogs have shown blood-brain barrier penetration in the *in vitro* bovine brain microvessel endothelial cell (BBMEC) model [398].

MATERIALS AND METHODS

HUMAN NEUROBLASTOMA CELL LINE (SH-SY5Y)

SH-SY5Y cells (ATCC® CRL-2266™) were cultured in DMEM/F12 medium (1:1) supplemented with 10% (v/v) fetal bovine serum (FBS), penicillin (50 U/ml) and streptomycin (50 μg/ml). The cells were maintained in a humidified environment at 37°C and 5% CO_2 and cultured in 75 cm^2 culture flasks. The medium was changed twice a week and cells were splitted at about 80% confluence. The day prior to treatment cells were harvested and seeded in 48-well plates at a density of 25000 cells/well. The cells were treated as soon as it was reached appropriate confluence.

In order to evaluate the cytotoxicity produced by the amyloidogenic peptides, neuroblastoma cells were treated for 24-48 hours with different preparations of Aβ25-35 and hA17-29. In order to determine the contribution of some specific receptors on Aβ- and hA-induced toxicity, cells were pre-treated for 2 hours with antibodies and then treated with the peptides.

RAT BRAIN ENDOTHELIAL CELL LINE (RBE4)

RBE4 cells were graciously donated by Dr. Cardile's laboratory at the University of Catania. These cells were cultured in Ham's F10 medium supplemented with 20% (v/v) plasma-derived serum (PDS), 2 mM L-glutamine, penicillin (50 U/ml) and streptomycin (50 μg/ml), 0,5% of endothelial cell growth supplement (ECGS), and 2% of heparin. The cells were maintained in a humidified environment at 37°C and 5% CO_2 and cultured in 25 cm^2 culture flasks that were pre-coated with collagen. The medium was changed twice a week and cells were splitted at about 90-95% confluence. The day prior to collecting conditioned medium, cells were harvested and seeded in 6-well plates at a density of 300000 cells/well. The cells were treated as soon as it was reached appropriate confluence. Conditioned medium for 24 hours was obtained from both treated and untreated RBE4 cells.

hA17-29 AND Aβ25-35 PEPTIDES PREPARATION

The synthesis of the hA17-29 peptide was carried out in our laboratories. The peptide was assembled on a polyethylene glycol-polystyrene resin (PALPEG-PS) by using an

Applied Biosystems Pioneer peptide synthesiser. Purification of the peptide was carried out by preparative RP-HPLC using a Vydac C-18 with a linear gradient of acetonitrile/water containing 0.1% TFA. The identity and purity of the peptide were confirmed by electrospray ionisation mass spectrometry (ESI-MS) and analytical RP-HPLC, respectively.

The Aβ25-35 peptides used in the experiments were purchased by Bachem.

For both peptide the protocol of monomerization consists of a first dissolution in 1,1,1,3,3,3-hexafluoro-2-propanol (HFIP), that acts as a solvent to eliminate any secondary structures present. The peptide dissolved in HFIP at the final concentration (C_f) of 1 mM was divided into aliquots and the HFIP left to evaporate under chemical hood; the dried peptide can be used immediately or stored at -80°C. Before the aggregation process, peptides previously treated with HFIP were dissolved in dimetilsulfoxid (DMSO) to C_f of 5 mM and subsequently diluted to the concentration of aggregation (100 μM) with PBS 0.01 M, pH 7.4, and then incubated at 37°C, alone or in presence of metals in a 1:1 ratio.

ANALYSIS OF AGGREGATION BY THIOFLAVIN T (Th-T) ASSAY

Thioflavin T is a dye which generates a fluorescent signal in case of link with β-sheet structures. In aqueous solution this pigment has a fluorescence emission peak at 430 nm when excited at 342 nm; in presence of fibrils, emission spectrum moves towards the red with a peak at 482 nm when excited at 450 nm [399]. For measures with the Th-T we used the ratio of Th-T 3μM and 5μg/ml of peptide according to LeVine III. Before reading, different preparation of the peptides were incubated for 10 minutes with the Th-T, then fluorescence at 450/482 ex/em was measured to determine the presence or absence of aggregates with β-sheet structures.

ANALYSIS OF AGGREGATION BY ATOMIC FORCE MICROSCOPY (AFM)

Atomic force microscopy (AFM) or scanning force microscopy (SFM) is a very high-resolution type of scanning probe microscopy, with demonstrated resolution on the order of fractions of a nm; it is one of the principal tools for imaging, measuring, and manipulating matter at the nanoscale. The information is gathered by scanning the

surface with a mechanical probe, such as piezoelectric elements that facilitate precise movements. The AFM consists of a cantilever with a sharp tip (probe) at its end that is used to scan the surface (**Fig. 35**).

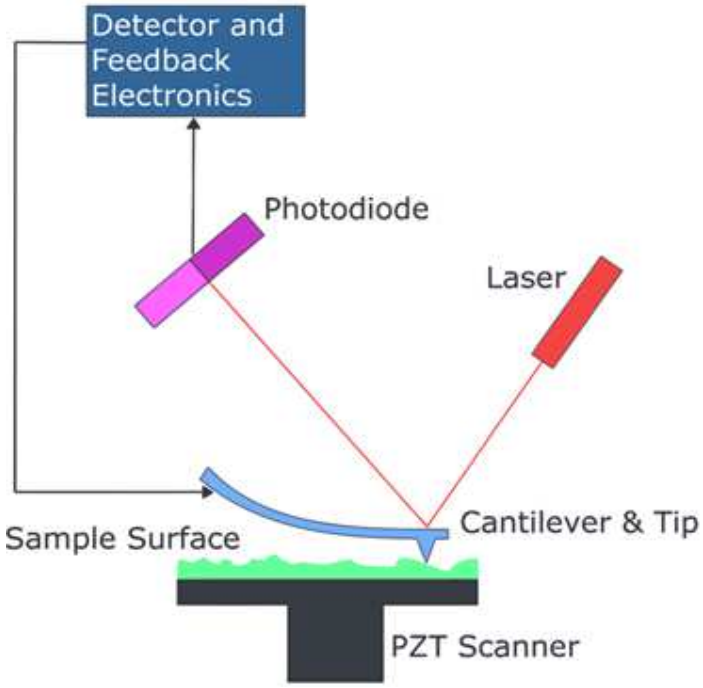

Figure 35 - Block diagram of atomic force microscope using beam deflection detection.

The cantilever is typically silicon or silicon nitride with a tip radius of curvature on the order of nanometer. When the tip is brought into proximity of a sample surface, forces between the tip and the sample lead to a deflection of the cantilever. Depending on the situation, forces that are measured in AFM include mechanical contact force, Van der Waals forces, capillary forces, chemical bonding, electrostatic forces, magnetic forces, etc.. Typically, the deflection is measured using a laser spot reflected from the top surface of the cantilever into an array of photodiodes.

AFM is an ideal tool for follow the early events of fibril assembly because it is capable of directly detecting and measuring the dimensions of small species that are adsorbed from aqueous media.

For AFM analysis, the sample (10 μL) was adsorbed onto a mica and analyzed directly by sensing the adsorbed material with a microfabricated silicon tip attached to a sensitive cantilever. The resulting relief map was subsequently converted into a visual image.

ELISA ASSAY

The presence of oligomeric species in peptide preparations was determined by ELISA assay with A11 antibody (Invitrogen), directed specifically against oligomeric species of amyloidogenic polypeptides. ELISA (Enzyme-Linked Immunosorbent Assay) is an immunoenzymatic assay useful to detect the presence of an antigen, immobilized on a solid support, with a specific antibody further applied over the surface; this antibody is linked to an enzyme and, in the final step, a substance containing the enzyme substrate is added. The subsequent reaction produces a detectable signal, most commonly a colour change in the substrate.

A little amount (5 ng) of peptide, freshly prepared or incubated at 37°C (100 μM in PBS), was immobilized on a microtiter plate; after treatment with primary antibody A11 (1 μg/ml), a HRP-conjugated antibody and then a substrate for HRP (TMB), absorbance at 450 nm was measured with a microtiter plate reader**.**

In order to detect the αB-crystallin release in conditioned medium by endothelial cell cultures (RBE4) treated with Aβ25-35, the medium was analyzed by αB-Crystallin Immunoset.

MTT ASSAY

The toxicity of the peptides was measured through the determination of cell viability in the treated cells compared to control (untreated cells), by MTT [3-(4,5-dimethylthiazol-2-yl)-2,5-diphenyltetrazolium bromide] assay. The test is based on the ability of the mitochondrial enzyme, cytochrome c oxidase and succinate dehydrogenase, to reduce yellow tetrazole into purple formazan that, being unable to cross the plasma membrane, will accumulate within the living cells. Solubilization of formazan with an appropriate detergent will yield purple colour in proportion to the amount of formazan produced and consequently to the viability of cells. After treatment with the peptides, cell cultures were incubated for 2 hours at 37°C with a MTT solution (1mg/ml in PBS); the formed crystals were melted with DMSO. After the solubilization of the formazan crystals, a part of the supernatant (200 μL) was used to read the absorbance at 590 nm using a microplate reader.

MICROCHIP ELECTROPHORESIS (MCE) COUPLED TO LIF (LASER INDUCED FLUORESCENCE) DETECTION

Microfluidic devices have many advantages for the analysis of cells, including the ability to grow and manipulate single or multiple cells on chip as well as the possibility to integrate on-line sample preparation and analysis.

MCE employs what is called a "gated" injection to deliver sample into the separation channel. Injections occur for about 200 milliseconds to 1 second (500 milliseconds in our case) and inject about a couple picoliters. First, voltage is applied to two leads (2400-2200) and a gate is established. Next, the buffer voltage floats to 0 and sample fills all the channels. Then gating is re-established and the result is a sample plug migrating down the channel while the analytes within it are separated.

After separation, the analytes are detected using LIF. LIF uses a high-powered laser to shoot a beam of light (in our case, 488 nm wavelength) through the channel at a point close to the end. As fluorescent compounds pass over it, they fluoresce at a slightly different wavelength (in our case 515 nm for DAF-FM, and 517 nm for 6-CF) and a photomultiplier tube (PMT) detects this light and converts it to a voltage reading.

JURKAT CLONE E6-1 CELL LINE

Jurkat clone E6-1 cell line (ATCC® TIB-152™) were cultured in RPMI 1640 medium supplemented with 10% (v/v) fetal bovine serum (FBS), 2 mM L-glutamine, penicillin (100 μg/mL), and streptomycin (100 μg/mL). The cells were maintained in a humidified environment at 37°C and 5% CO_2 and cultured in 25 cm^2 culture flasks. Cells were passaged every 2-3 days to avoid overgrowth.

Stimulation of NO production in cells was accomplished using purified LPS from the *Escherichia coli* line 0111:B4. 7.5 μL of a 1 mg/mL LPS stock solution was added to 5 mL of healthy Jurkat cells in a cell culture flask and then incubated for 3-5 h. Unstimulated (native) Jurkat cells from the same population were incubated under identical conditions and used as a control for each stimulation experiment.

Bulk cell analysis

Jurkat cells suspended in their original medium were labeled with DAF-FMDA and 6-CFDA under dark conditions prior to bulk cell lysis and analysis. DAF-FMDA is fluorogenic and membrane permeable. Once inside the cell, DAF-FMDA is hydrolyzed

by non-specific cytosolic esterases to form 4-amino-5-methylamino-2',7'-difluorofluorescein (DAF-FM). The hydrolyzed ye further reacts with a partially oxidized species of NO (N_2O_3) to form a triazole (DAF-FM T), which has a high fluorescence yield. 6-CFDA is also fluorogenic and membrane permeable and is hydrolyzed by esterases to yield a charged fluorescent moiety that is membrane impermeable. We used 6-CFDA as an internal 1 standard to correct for differences in fluorescence intensity when using different devices. Stock dye solutions were prepared in 99% DMSO. The dyes were loaded in a stepwise manner into the cell suspension. 10 µL of a 5 mM DAF-FM DA solution in DMSO were aliquoted into the culture flask and allowed to react for 15 min. Then 10 µL of 1 mM 6-CFDA was diluted in 990 mL of ultrapure water, added to the culture flasks, and reacted for an additional 20 min. Between the additions of the fluorescent probes, the flasks were returned to the incubator. After dye loading, the Jurkat cell suspension was centrifuged at 3500 rpm for 3 min and supernatant was removed. Cells were resuspended in RPMI medium and centrifuged again to remove residual dye not sequestered by cells. The cell pellet was then lysed in 250 mL of electrophoresis buffer (10 mM boric acid, 7.5 mM SDS, pH 9.2). The lysate was filtered using a 3 kDa molecular weight cut-off centrifugal filter to eliminate particles that could cause blockage of the microchip channels. The filtered lysate was then loaded into the sample reservoir of the microchip.

Single cell analysis

Stock solutions of DAF-FMDA and 6-CFDA were prepared daily for each new set of experiments using 99.9% DMSO. The dye solution was prepared by adding appropriate volumes 6 of the two stock solutions to enough sterile PBS to make a 2 µM DAF-FMDA and 2 µM 6- CFDA solution. 1 mL of the cell suspension was centrifuged at 2000 rpm for 1 min and the supernatant was discarded. The cells were then re-suspended in the dye solution and incubated for 20 min at 37ºC on a heat block. Another centrifugation was performed under the same conditions to remove the dye solution, and the labeled cells were re-suspended in RPMI medium containing 2% (w/v) BSA prior to experiments.

MICROCHIP FABRICATION

Bulk cell analysis

The fabrication of hybrid PDMS-glass microfluidic devices has been described previously by our group [400]. In these experiments, SU-8 10 negative photoresist was spin-coated onto a 4-in diameter silicon wafer with a resulting thickness of 15±1 mm using a Cee 100 spin coater. The photoresist-coated wafer was then transferred to a hotplate for a soft bake at 65°C for 2 min and then 95°C for 5 min. Microfluidic channel designs were produced using AutoCad LT 2004 and printed onto a transparency film at a resolution of 50000 dpi. The coated wafer was covered with the transparency film mask and exposed to UV light (344 mJ cm^{-2}) for 16 s using an i-line UV flood source. Following the UV exposure, the wafer was post-baked at 65°C for 2 min and 95°C for 10 min. The wafer was then developed in SU-8 developer, rinsed with 2-propanol (IPA), and dried under nitrogen. A "hard bake" was performed at 200°C for 2 h. The thickness of the raised photoresist, corresponding to the depth of the PDMS channels, was confirmed with a profilometer. PDMS channels were made by pouring a 10:1 mixture of PDMS elastomer and curing agent, respectively, onto the SU-8 patterned silicon wafer. The PDMS-covered wafer was then placed in an oven at 70°C overnight to harden the PDMS. The microchip design for all cell analysis experiments was a simple "T" design. This design consisted of a 5 cm separation channel and 0.75 cm side arms as shown in **Fig. 36**.

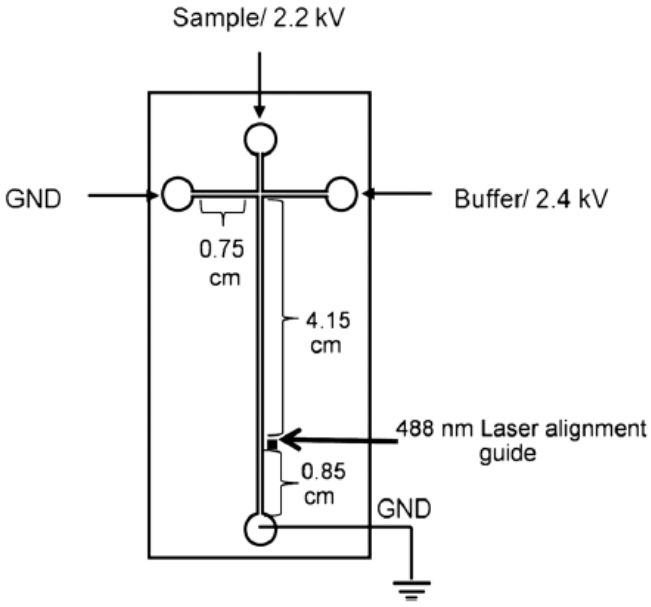

Figure 36 - A schematic of a simple ''T'' 5 cm microchip design with channel dimensions and applied voltages.

An additional square guide 8.5 mm from the outlet reservoir of the separation channel was added to aid in laser alignment. The width and depth of the channels were 50 mm and 14 mm, respectively. Holes for the reservoirs were created in the PDMS using a 4 mm biopsy punch. The PDMS layer containing the embedded channels was reversibly sealed to a borofloat glass plate to complete the hybrid device.

Single cell analysis

The microfluidic device (**Fig. 37 A**) was fabricated using established soft lithography procedures [401].

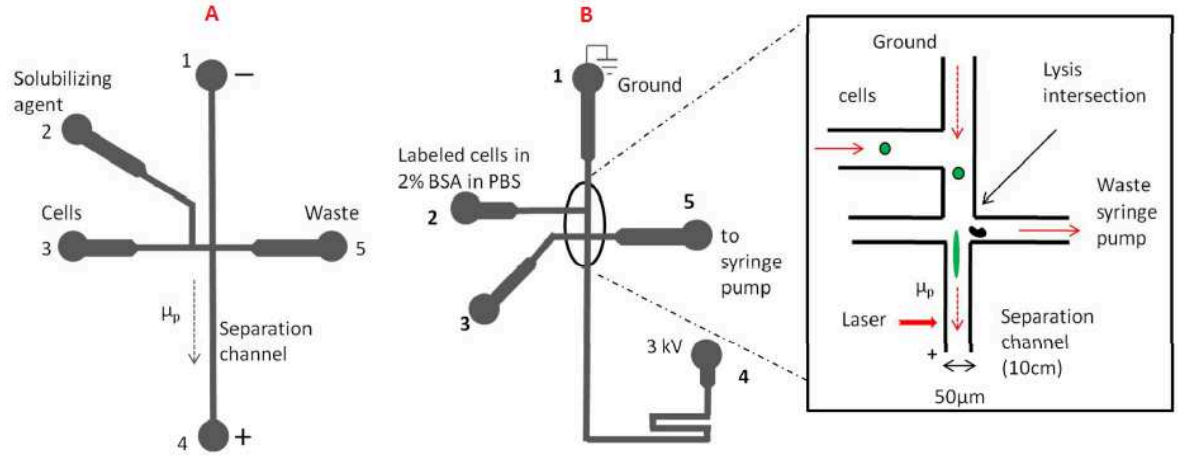

Figure 37 - A is the initial chip design. **B** is a schematic of improved microfluidic chip used for single cell lysis experiments. The lysis intersection of the microchip is shown in the inset. The solid arrows indicate the direction of bulk fluid flow while the broken arrows show the direction of electrophoretic migration (μ_p).

Briefly, SU-8 2010 negative photoresist was spun to a thickness of ~20 µm on a 4 in silicon wafer using a spin coater. The coated mask was then placed on a 65 ºC hot plate for a 2-min soft bake followed by a 4-min hard bake on a 95ºC hot plate. A mask containing the microfluidic channel pattern, created using AutoCAD LT 2006, was placed on the wafer that was then exposed to ultraviolet light. The unpolymerized photoresist was washed off using SU-8 developer, rinsed with isopropyl alcohol, and blown dry with nitrogen. A 10:1 w/w mixture of PDMS prepolymer and curing agent was then poured over the mold and cured for at least 50 min at 80ºC. Access holes to the channels were drilled on a 75×50 mm glass slide using a 2 mm diamond-tipped drill bit and fitted with glass reservoirs using epoxy resin. A Nanoport assembly placed on reservoir 5 (**Fig. 37 B**), a micro-splitter valve, threaded adapters, and PEEK tubing, all from Upchurch Scientific, were used to connect the microfluidic device to the syringe pump. The cured PDMS was peeled off the mold and placed over the glass slide with the ends of the channels aligned with the access holes on the glass slide. Another glass

slide was placed on top and the excess PDMS was trimmed off. The channel dimensions 1 were determined by measuring the height and width of the features on the silicon wafer mold using a profilometer. The channels were 19 μm deep, corresponding to the height of the features on the mold. The narrow sections of the channels were 50 μm wide. The wide sections of the channel from reservoirs 1, 2, 3 and 4 were 160 μm while that from reservoir 5 was 500 μm (**Fig. 37 B**).

MICROCHIP OPERATION

Bulk cell analysis

Prior to loading a bulk cell lysate sample onto the microchip, three conditioning flushes were performed. Using vacuum, the channels were filled with IPA and the excess IPA was then removed from the reservoirs. The IPA prevented the formation of gas bubbles in the separation and sample channels. The channels were then flushed with 0.1 M NaOH followed by separation buffer prior to use. The separation buffer consisted of 10 mM boric acid and 7.5 mM SDS, pH 9.2. Fluorescence detection was carried out using a Nikon Eclipse Ti-U inverted microscope with a 488 nm laser for excitation, and a photomultiplier was used for detection. The signal was amplified using a SR570 low noise current preamplifier at 1 mA V^{-1}.

Sample was introduced using a 0.5 s gated injection. Separations were performed in the positive polarity mode using a 30 kV high voltage power supply For all separations, voltages of 2400 V (separation) and 2200 V (sampling) were used. An in-house written LabVIEW program was used for data acquisition as well as for control of the high voltage power supply. Origin 8.1 software was employed for data analysis.

Single cell analysis

The separation buffer consisted of 25 mM sodium borate, 20% v/v acetonitrile, 2% w/v BSA, 0.6% w/v Tween-20, and 2 mM SDS. Initially, all the reservoirs were filled with the separation buffer by applying reverse pressure facilitated by a vacuum pump. Reservoir 2 **(Fig. 37 B)** was evacuated and replaced with a suspension of the fluorescently labeled cells. The waste reservoir was threaded to provide the connection, via PEEK tubing, to a 1000 μL glass syringe on a syringe pump. Cell transport and fluid flow in the channel manifold were achieved by setting the syringe pump at

withdrawal mode at a flow rate of 0.25 µL/min and adjusting the flow splitter until the cells were traveling at a rate at which most of the lysate from the cells was injected into the separation channel.

Cell lysis and subsequent electrophoretic injection and separation were achieved by applying 3 kV using a high voltage supply across reservoirs 1 and 4 **(Fig. 37 B)**.

A multi-line argon-ion laser was used as the excitation source. The 488 nm beam was selected using a dispersive prism and then reflected off a series of mirrors and directed into a Nikon eclipse TS100 microscope through the rear port and via a 20× objective to the microscope stage. The beam was focused onto a small spot in the separation channel, 5 mm below the lysis intersection. The fluorescence emission from the dyes was detected by a photomultiplier tube attached to the trinocular port of the microscope. The signal was amplified using a low noise current preamplifier at 1 µA/V with 100 Hz low-pass filter and sampled at 100 Hz using a PC1-6036E I/O card. The program controlling the high voltage power supply and data acquisition was written in-house using LabVIEW. Data analysis was performed using Igor Pro. Video images of the experiment were collected using a digital color video camera mounted on the side port of a Nikon TE-2000-U inverted microscope. Frame grabs retrieved in Image J were used to calculate the flow rate of the analytes down the separation channel.

PREPARATION OF STANDARDS

An overview of the DEA/NO preparation protocol is presented in **Fig. 38**.

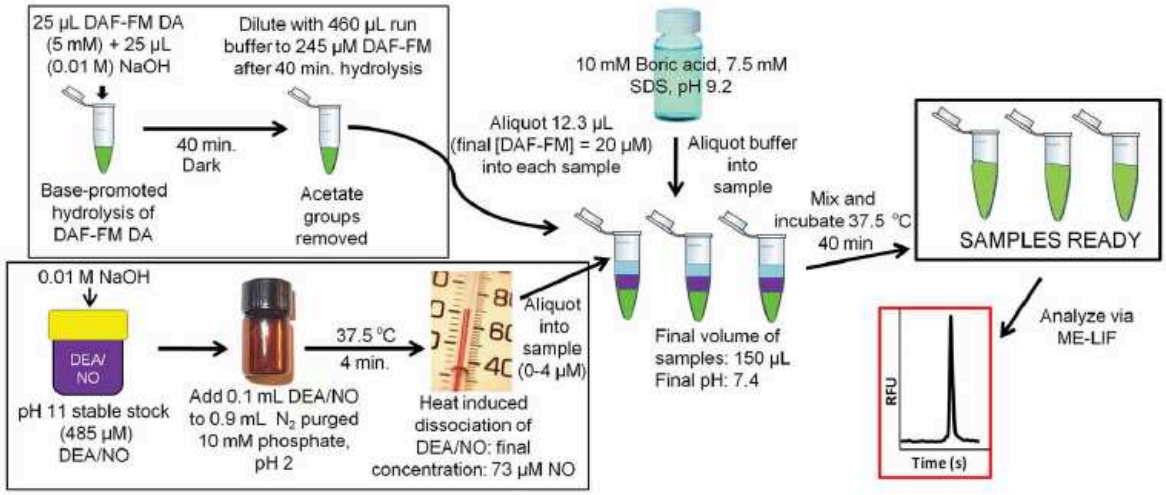

Figure 38 - The protocol used for preparation of DEA/NO sample preparation.

Briefly, stable stock solutions of NO donor DEA/NO were prepared in 0.01 M NaOH just prior to use. NO release was facilitated by placing aliquots of the stock DEA/NO solution into deoxygenated 0.01M phosphate buffer (pH 2, 37.5°C) for 4 min. In a separate reaction, DAF-FM DA was incubated in 0.01 M NaOH for 40 min for the base-promoted hydrolysis of both acetate groups [402]. This served as a substitute for the esterase activity that is responsible for cleaving the acetate groups *in vivo*. Following hydrolysis in NaOH, equal concentrations of the resulting 4-amino-5-methylamino-20,70-difluorofluorescein (DAF-FM) were aliquoted into solutions containing 0-4 mM NO, reacted for 40 min at 37.5°C to produce the benzotriazole derivative of DAF-FM (DAF-FM T), and analyzed via microchip electrophoresis.

The dehydroascorbate derivative of DAF-FM (DAF-FM DHA) was prepared by combining DAF-FM prepared as described above with a 70-fold excess of ascorbic acid in run buffer. The synthesis of DAF-FM DHA was accomplished using following procedure: ascorbic acid (AA) was oxidized to DHA in a high pH solution (9.2) by dissolved oxygen. The DAF-FM (20 μM) was then reacted with the oxidized AA (1.45 mM) solution for about 10 min to generate DAF-FM DHA.

RAW 264.7 CELL LINE

RAW 264.7 cells (ATCC® TIB-71™) were cultured in DMEM supplemented with 10% (v/v) fetal bovine serum (FBS), penicillin (100 μg/mL), and streptomycin (100 μg/mL). The cells were maintained in a humidified environment at 37°C and 5% CO_2 and cultured in 25 cm^2 culture flasks. Cells were passaged every 1-2 days to avoid overgrowth.

Stimulation of NO production in cells was accomplished using purified LPS (from the *Escherichia coli* line 0111:B4) alone or in combination with recombinant IFN-γ.

In order to determine the contribution of iNOS in NO production, cells were pre-treated for 1 hour with different iNOS inhibitors and then treated with LPS or LPS in combination with IFN-γ. The influence on NO production of other molecules has also been investigated.

GRIESS ASSAY

The Griess assay allows to measure the amount of nitrite (NO_2^-), which indirectly reflects the amount of NO produced by cells. This assay is based on the formation of a

diazonium salt for reaction of NO_2^- in the medium with sulfanilammide. The diazonium salt reacting with N-(1-naphthyl) ethylenediamine forms an azo-derivative spectrophotometrically monitorable (**Fig. 39**).

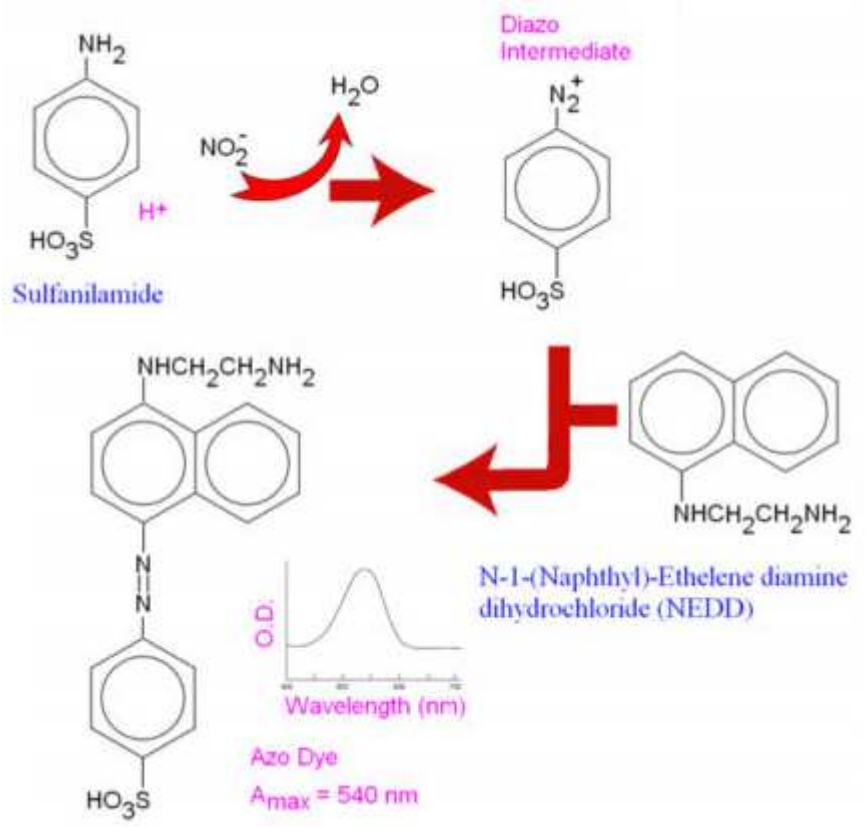

Figure 39 - Nitrite detection using the Griess assay.

In our experiments to investigate NO production Griess assay was carried out both outside and inside the cells.

- Outside: 100 µL of supernatant were taken from each well or flask, added to 100 µL of Griess reagent, left to react for 15 minutes, and then the absorbance at 540 nm was read using a plate reader.
- Inside: cells were harvested and centrifuged at 3500 rpm for 2 minutes. After centrifugation, supernatant was removed and the pellet was lysed with 500 µL of buffer containing 10 mM boric acid, 7.5 mM SDS, pH 9.2. The lysate was filtered using a 3 kDa molecular weight cut-off centrifugal filter. Finally, 100 µL of filtered lysate was added to 100 µL of Griess reagent, left to react for 15 minutes, and then the absorbance at 540 nm was read using a plate reader.

A nitrite standard reference curve was prepared for each assay for accurate quantitation of NO_2^- levels in experimental samples.

METABOLISM STUDIES IN CENTRAL NERVOUS SYSTEM TISSUES

The brains and spinal cords of male Wistar rats (350-400 grams) were removed on the day of the study and kept in ice cold mPBSA (modified PBSA)prior to experiments. Animals that could no longer be used for microdialysis studies were graciously donated by Dr. Craig Lunte's laboratory at the University of Kansas. Tissue slices were prepared with a sterile razor blade in a Petri dish on a bed of ice. For the metabolism studies, the tissue slices were exposed to dynorphin at room temperature (instead of 37 °C) to slow enzyme activity. For brain tissue slices, a 5 mm by 5 mm section was bathed in mPBSA spiked with 25 μM Dyn A 1-17. Aliquots (50 μL) were collected at various time points over a 4 hour period, mixed with 50 μL of ice-cold aqueous 0.1% formic acid solution, and centrifuged on a table-top centrifuge for 2.5 min. Following centrifugation a 60 μL aliquot was removed and further diluted with 48 μL H2O with 0.1% formic acid. Prior to analysis by LC-MS/MS, 12 μL of a 10 μM bradykinin solution was added to serve as an internal standard for quantitation. Similarly, a 5 mm length of spinal cord (width approximately 2 mm) was prepared and bathed in mPBSA spiked with 25 μM Dyn A 1-17. Following the metabolism study, the brain and spinal cord slices were homogenized in PBSA and analyzed for total protein content by the Pierce BCA assay. Metabolism results are expressed as μM dynorphin peptides per mg of protein.

ISOLATION AND MAINTENANCE OF BOVINE BRAIN MICROVESSEL ENDOTHELIAL PRIMARY CULTURES (BBMEC)

Microvessel endothelial cells were isolated from the cortical grey matter of bovine brains by enzymatic digestion and centrifugation as described by Audus and Borchardt in 1986 [403]. Briefly, bovine brains were obtained from a slaughter house in DeSoto, KS and transported to the laboratory in ice cold minimum essential medium (MEM), pH 7.4. Collagenase and dispase digestions in conjunction with centrifugation steps and both dextran and percoll gradients were used to isolate the endothelial cells from red blood cells and lipids. Following isolation the bovine brain microvessel endothelial cells were stored at -80 °C for up to 6 weeks in complete culture medium supplemented with 12% horse serum and 10% DMSO. BBMECs were thawed and then seeded, at a

density of approximately 50,000 cells/cm^2, on polycarbonate culture plates or 0.4 μm polycarbonate membranes that were pre-coated with rat tail collagen and fibronectin.
The plating medium consisted of 50% Minimum Essential Medium (MEM) and 50% Ham's F12 supplemented with 100 μg/mL streptomycin, 100 μg/mL penicillin G, 13 mM sodium bicarbonate, 10 mM HEPES, 10% platelet poor horse serum, 150 μg/mL heparin, and 50 μg/mL polymixin B. Seventy two hours after plating, the media was changed. The changing medium consisted of 50% Minimum Essential Medium (MEM) and 50% Ham's F12 supplemented with 100 μg/mL streptomycin, 100 μg/mL penicillin G, 13 mM sodium bicarbonate, 10 mM HEPES, 10% platelet poor horse serum, 100 μg/mL heparin, and 0.5% endothelial cell growth supplement (ECGs). The changing medium was then replaced every 48 hours. The cells were grown to confluency (12-14 days after seeding) at 37 °C in an atmosphere of 5% CO2 and 95% relative humidity.

METABOLISM STUDIES IN THE PRESENCE OF BBMECs

BBMECs were seeded onto 12-well polycarbonate cell culture plates at a density of approximately 50,000 cells/cm^2. Cells were grown until a confluent monolayer formed (typically 12 to 14 days after seeding) as determined by light microscopy. Metabolism studies were performed in modified phosphate-buffered saline supplemented with $CaCl_2$, $MgCl_2$, glucose and ascorbic acid, pH 7.4 (mPBSA). Before beginning each metabolism study, the growth medium was aspirated off and the cells were rinsed three times with pre-warmed (37°C) mPBSA. The 12-well plate was kept in a benchtop incubator, maintained at 37 °C and stirred continuously by a shaker. Cells were incubated with Dyn A 1-17 at varying concentrations and 60 μL aliquots were removed at various timepoints over the span of four hours. Aliquots were placed directly into autosampler vials containing 48 μL H_2O with 0.1% formic acid and were frozen (-20°C) until analyzed.
Prior to analysis, the samples were thawed, vortexed, and 12 μL internal standard (10 μM bradykinin) was added and analysis was performed via LC-MS/MS.

BBMEC PERMEABILITY STUDIES

BBMECs were grown on 0.4 μm polycarbonate membranes in a Petri dish at a density of approximately 50,000 cells/cm^2. Cells were grown until a confluent monolayer formed (typically 12 to 14 days after seeding) as determined by light microscopy. Transport studies were performed in modified phosphate-buffered saline supplemented with $CaCl_2$, $MgCl_2$, glucose and ascorbic acid, pH 7.4 (mPBSA). Before beginning each study, the growth medium was aspirated off and the cells were then rinsed three times with pre-warmed (37°C) mPBSA. The membranes were then removed and mounted in Side-by-SideTM diffusion chambers (**Fig. 40**).

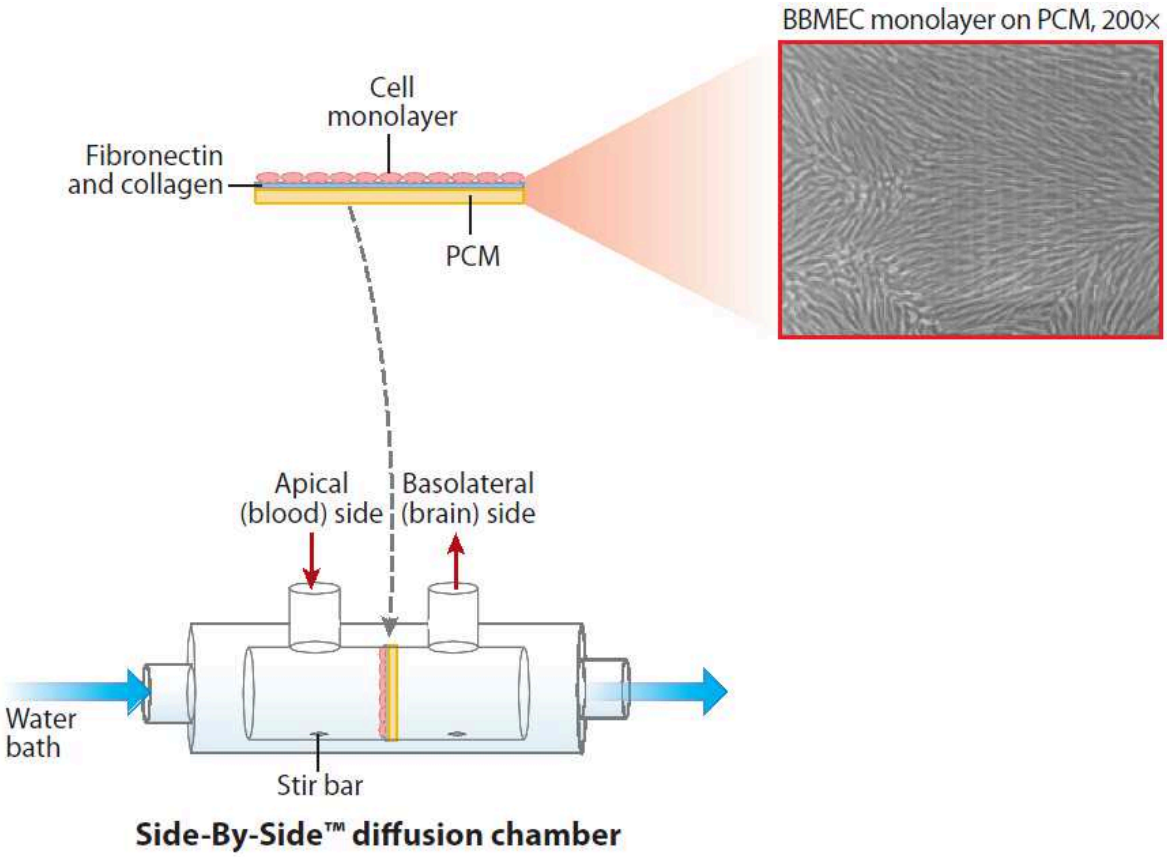

Figure 40 - Systems used for monitoring *in vitro* transport across the blood-brain barrier. In the Side-by-Side^{TM} diffusion chamber, cells are grown on polycarbonate membranes (PCMs) that are subsequently mounted between two water-jacketed, thermally controlled chambers. Abbreviation: BBMEC, bovine brain microvessel endothelial cell.

Prior to studies, the diffusion chambers were silanized with Sigmacote to prevent peptide adsorption to the chamber walls during the study.

Chambers were then pre-warmed (37°C) and rinsed three times with mPBSA. Following membrane placement, one side of the diffusion chamber was filled with 3 mL of mPBSA and examined for leaks. If the membrane was mounted correctly and no

leaks were present, the other side of the chamber was filled with 3 mL of mPBSA as well. The chamber temperature was maintained for the duration of the study by external circulating water baths (at either 37°C or 4°C depending on the experiment) and each chamber was stirred constantly at 600 rpm by Teflon coated magnetic stir bars driven by an external console. The donor side was then spiked with the peptide of interest and 60 µL aliquots were removed from the receiver side at various time points and then replaced with an equal volume of mPBSA to prevent changes in volume that could affect flux. Studies typically lasted 2-4 hours. Samples were collected directly into autosampler vials pre-filled with 48 µL H_2O with 0.1% formic acid and then stored at -20°C until use. Upon thawing, samples were vortexed and 12 µL internal standard (10 µM bradykinin) was added and analysis was performed using an LC-MS/MS.

Upon completion of the transport study, fluorescein or [^{14}C]-sucrose were added to the apical side of the monolayer and utilized to test the monolayer integrity. These low permeability markers do not readily cross the blood brain barrier and are an indicator of monlayer integrity. Fluorescein samples were placed directly into a 96-well plate and analyzed by a fluorescence microplate spectrophotometer at excitation and emission wavelengths of 490 and 520 nm respectively. Sucrose samples were mixed with 10 mL of scintillation fluid and analyzed by liquid scintillation counting.

For studies determining the permeability of fluorescein without Dyn A 1-6 pre-treatment, chambers were filled with the modified media (mPBSA), and the cells were allowed to equilibrate for 5 minutes. After the equilibration period, fluorescein was added to the apical side of the cell membranes such that the final concentration was 10 µM. Immediately a 100 µL aliquot was removed from the donor chamber and collected into a 96 well plate. Additional 100 µL aliquots were taken from the receiver chamber (t=10, 20, 30, and 60), and a final sample was taken from the donor chamber after 60 minutes as well. These fluorescence values were determined on a microplate spectrophotometer. The permeability of fluorescein was then determined using the following equation:

$$P_{app} = (ÄQ/Ät)/ A \times C_0$$

Where, ÄQ/Ät is the linear appearance of fluorescein in the receiver chamber, A is the cross sectional area of the cell monolayer (0.636 cm^2), and C_0 is the initial concentration in the donor chamber at t=0 (in this case, 10 µM).

In the Dyn A 1-6 transport studies, 20 µL of mPBSA was removed from the donor chamber and replaced with 20 µL of a Dyn A 1-6 stock solution, resulting in 18.6 µM peptide in the chamber. Bi-directional studies were performed by adding Dyn A 1-6 to either the apical (blood) or basolateral (brain) side of the mounted monolayers at 37°C. Aliquots (60 µL) were taken from the receiver chamber at various time points over a 4 hour period. Studies done at 4°C were carried out in the apical to basolateral direction over a 2 hour period at the same concentration. All samples were collected into autosampler vials containing H_2O with formic acid. Mass balance samples were collected from the receiver chamber at the start and finish of each experiment. Quantitation was performed via LC-MS/MS. Peptide permeability was calculated with the same equation described above for fluorescein.

ANALYSIS OF METABOLISM AND PERMEABILITY STUDIES BY LIQUID CHROMATOGRAPHY-TANDEM MASS SPECTROMETRY (LC-MS/MS)

Transport samples were analyzed by the LC-MS/MS protocol. Briefly, 60 µL aliquots were diluted with 48 µL H_2O with 0.1% formic, and prior to analysis 12 µL of a 10 µM bradykinin solution was added to serve as an internal standard for quantitation. Sample de-salting and separation were achieved using a 1.0x50 mm C18 analytical column with 5 µm particles and the corresponding guard column, 1.0x10 mm. The mobile phase was diverted to waste for the first 5 minutes of the LC run, then to the mass spectrometer from 5 to 12 minutes and again back to waste for the remainder of the run. The LC gradient program was as follows: initial conditions of 97% A, 3% B from 0 to 5 minutes, a linear ramp from 3 to 30% B from 5 to 6 minutes, holding at 30% B from 6 to 15 minutes, a linear return to initial conditions from 15 to 16 minutes, and column equilibration from 15 to 22 minutes holding at 3% B. Mobile phase A consisted of 100% H_2O with 0.1% formic acid. Mobile phase B consisted of 100% ACN with 0.1% formic acid.

RESULTS

AGGREGATION ANALYSIS OF Aβ25-35 THROUGH Th-T ASSAY

In order to evaluate the aggregation state and the influence of micro-environmental factor such as metals in the kinetics of fibrillogenesis, different preparations of Aβ25-35, freshly prepared and incubated at 37°C with or without copper, were analyzed by Th-T assay, a useful method to detect the presence of β-sheet structures.

In our experimental conditions it was found an increase in the fluorescence signal produced by the incubated peptide, without metal, compared to the freshly preparation that we used such as control. After incubation at 37°C the peptide forms soluble (Th-T-positive) aggregates which lose their solubility as the time of incubation increases, and fluorescence values return to levels similar to control; the presence of copper during incubation promotes the formation of insoluble (Th-T-negative) aggregates or the disintegration of the ones spontaneously formed (**Fig. 41**).

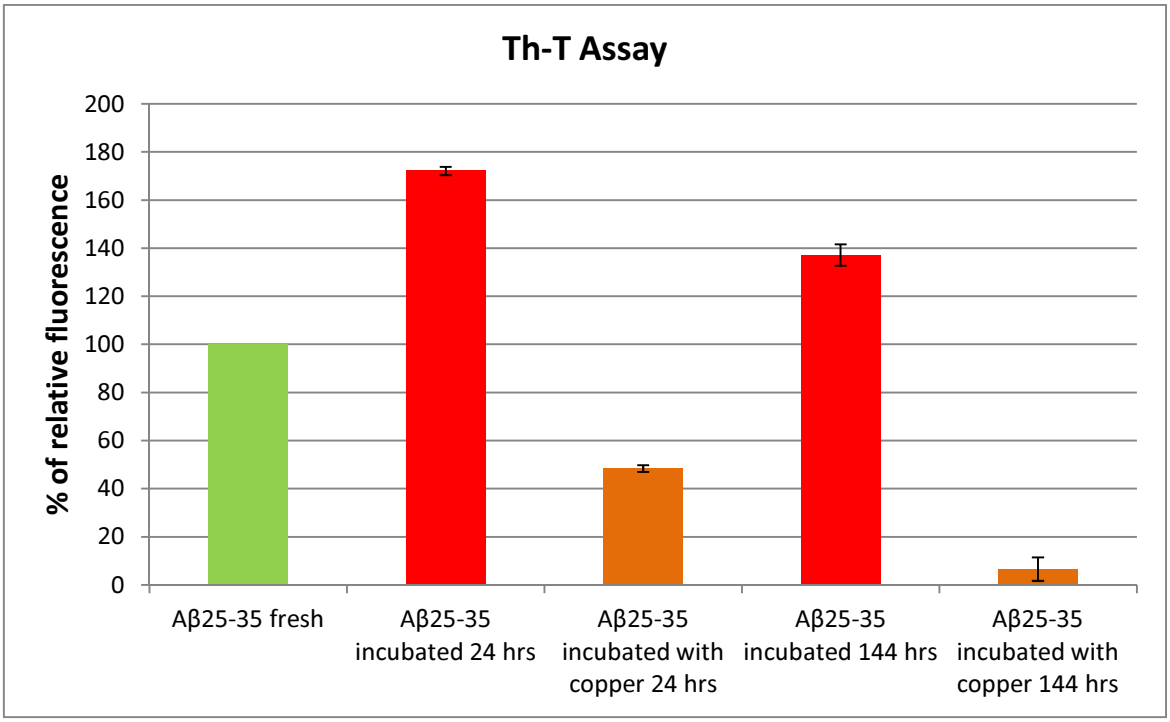

Figure 41 - Thioflavin T (Th-T) assay on different preparations of Aβ25-35. The peptide, immediately after being taken from the freezer (-80°C), was dissolved in DMSO and led to the concentration of aggregation (100 µM) in PBS 0.01 M. The sample "fresh" was prepared immediately before being analyzed. The incubated samples were kept in the temperature controlled (37°C) with [CO_2] of 5% and examined after 48 hours. In the sample containing $CuSO_4$, the ratio Cu^{2+}/peptide is equal to 1:1. Th-T 3 µM was incubated with Aβ25-35 (5 µg/ml) for 10 min. Fluorescence emission were measured at 450/482 ex/em. Data are means ± S.D. (n=4) of 3 independent experiments.

TOXICITY ANALYSIS OF Aβ25-35 THROUGH MTT ASSAY

In order to evaluate the relationship between aggregation state and toxicity, SH-SY5Y cells were treated with different preparations of Aβ25-35.

Data obtained after treatment of SH-SY5Y show a decrease in the viability of cells treated with the freshly prepared peptide and, in greater extent, in cells treated with the peptide incubated for 24 hours with copper in a 1:1 ratio; instead, incubated alone peptide does not influence cellular viability in a particular way. After a longer incubation time (144 hours) toxicity decreases for both peptide incubated with copper and peptide incubated without copper (**Fig. 42**).

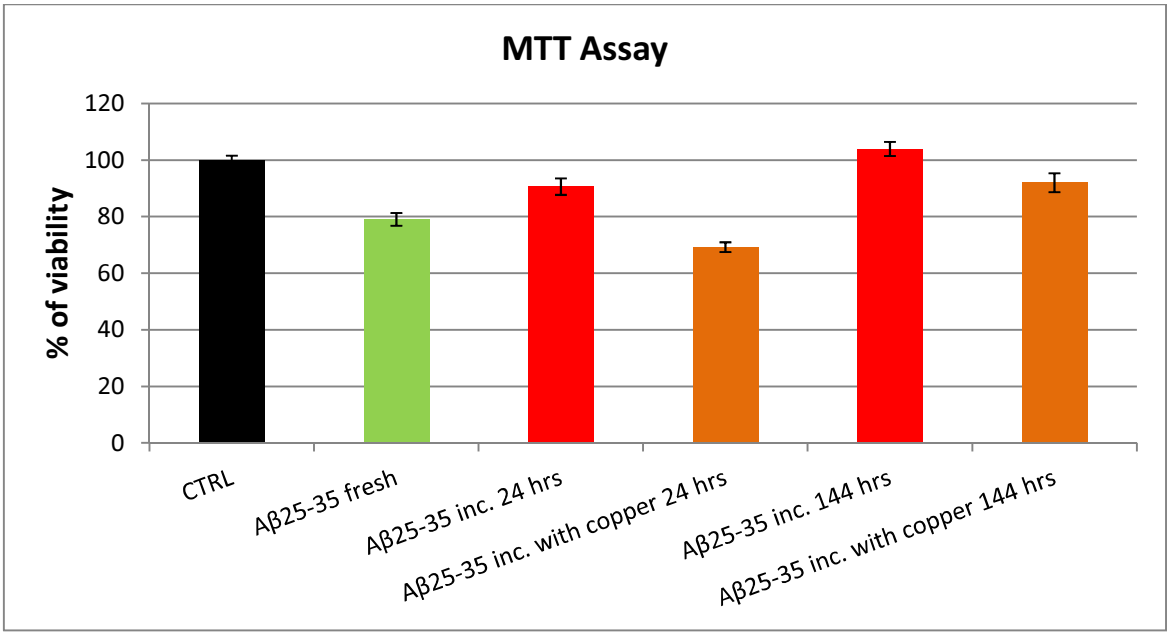

Figure 42 - MTT assay after 48 hrs of treatment with different Aβ25-35 (3 µM) preparations on SH-SY5Y cells. In the sample containing $CuSO_4$, the ratio Cu^{2+}/peptide is equal to 1:1. Data are means ± S.D. (n=4) of 3 independent experiments. Inc. is incubated.

These data are in agreement with the ones seen with Th-T assay; it is conceivable an evolution of the aggregation process, which finishes with the formation of not toxic structures. This process is influenced by the presence of metals which, altering the aggregates structure, cause a slowdown in the evolution to not toxic structures. Particularly, metal-incubated peptide toxicity is strongly evident within 24 hours of incubation before cells treatment; vice versa, the peptide incubated without copper quickly loses this toxic effect. This hypothesis is sustained by the observation that after a longer incubation period the peptide reaches not toxic aggregation states, even in presence of metals. Cellular viability is negatively influenced even by the freshly

prepared peptide, because of the presence of soluble toxic oligomers, which spontaneously form during the cells treatment time at 37°C.

ANALYSIS OF THE EFFECTS OF Aβ25-35 AND CONDITIONED MEDIUM ON CELL VIABILITY

A growing numbers of studies carried out in the past years show the vascular system plays a more and more critical roles in physio-pathological processes of the nervous system. Endothelial cells are in fact an essential element in the study of neurovascular unit. In order to understand if the endothelial cells, subjected to stressors, are able to release factors into the culture medium which may carry out a protective action against the neurons, endothelial cells (RBE4) were treated for 48 hours with Aβ25-35. Both conditioned medium from treated and untreated endothelial cells were then used for treating neuroblastoma cells (SH-SY5Y) (**Fig. 43**).

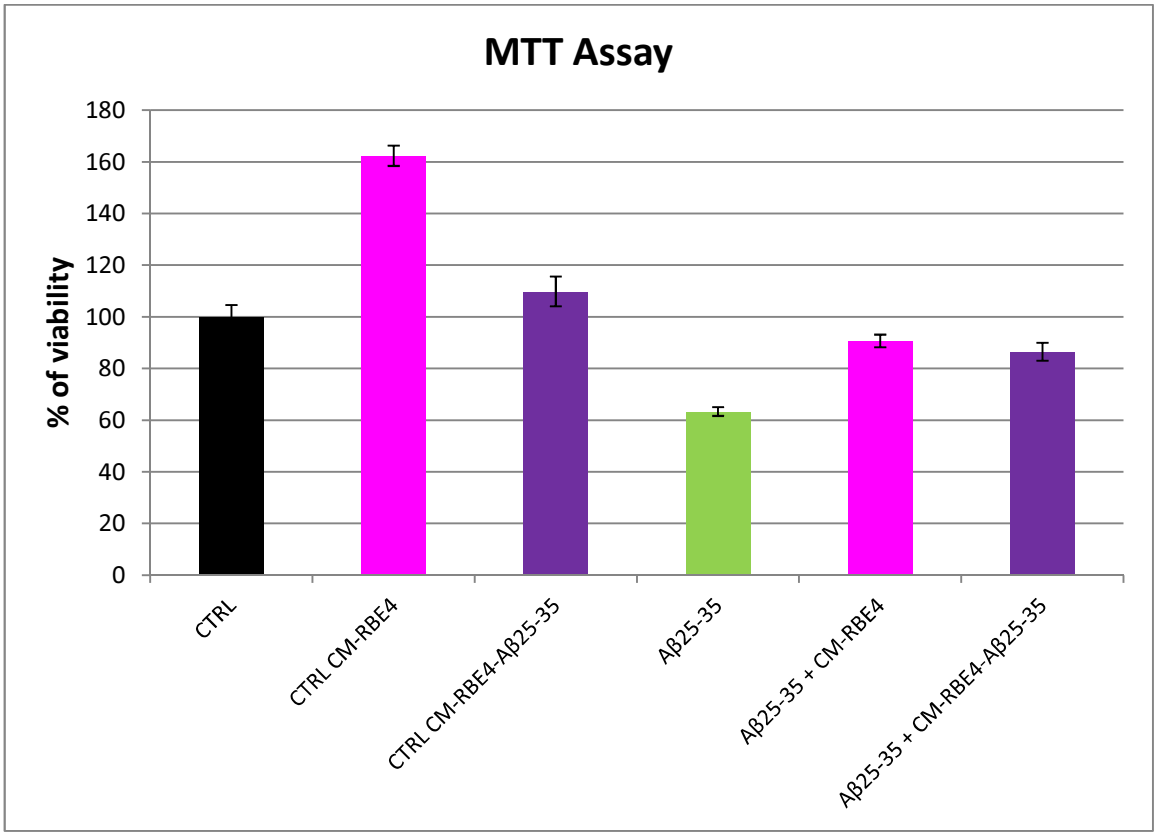

Figure 43 - MTT assay after 48 hrs of treatment with Aβ25-35 fresh (20 µM) on SH-SY5Y cells. The conditioned medium (CM) was obtained from endothelial cells (RBE4) treated for 48 hours with the same peptide at a concentration of 5 µM. Data are means ± S.D. (n=4) of 3 independent experiments.

The data obtained after treatment of SH-SY5Y cells show a higher cell viability for cells treated with the conditioned medium from untreated RBE4 cells compared to control (untreated cells). This suggests that the production of "beneficial" factors in

respect of SH-SY5Y cells does not depend on cellular stress. Even the cells treated with conditioned medium from RBE4 cells treated with Aβ25-35 show a greater vitality, but much less pronounced. It could explained as follows: 1) decrease in the number of cells secreting factors, following mortality Aβ25-35-induced; 2) ability of Aβ25-35 to obstruct/block the mechanism that leads to the production of the protective factors.

The SH-SY5Y cells treated with Aβ25-35 show a lowering of vitality of about 40% compared to control. The cells treated simultaneously with the conditioned medium from RBE4 cells (both treated and untreated) and Aβ25-35 show a significantly higher viability compared with cells treated with only the Aβ25-35, clearly demonstrating the beneficial effects of the factors produced by endothelial cells. Instead, there were no significant differences between SH-SY5Y cells treated with different conditioned media (from treated and untreated RBE4 cells) and Aβ25-35, although in the absence of the stressor their effect on viability was very different, even though still "positive". Future experiments will be aimed for understanding this phenomenon.

In order to identify the possible release of αB-crystalline, a heat shock protein (HSP), into the culture medium, the medium of RBE4 cells treated with Aβ25-35 was analyzed by αB-Crystalline Immuneset (**Fig. 44**).

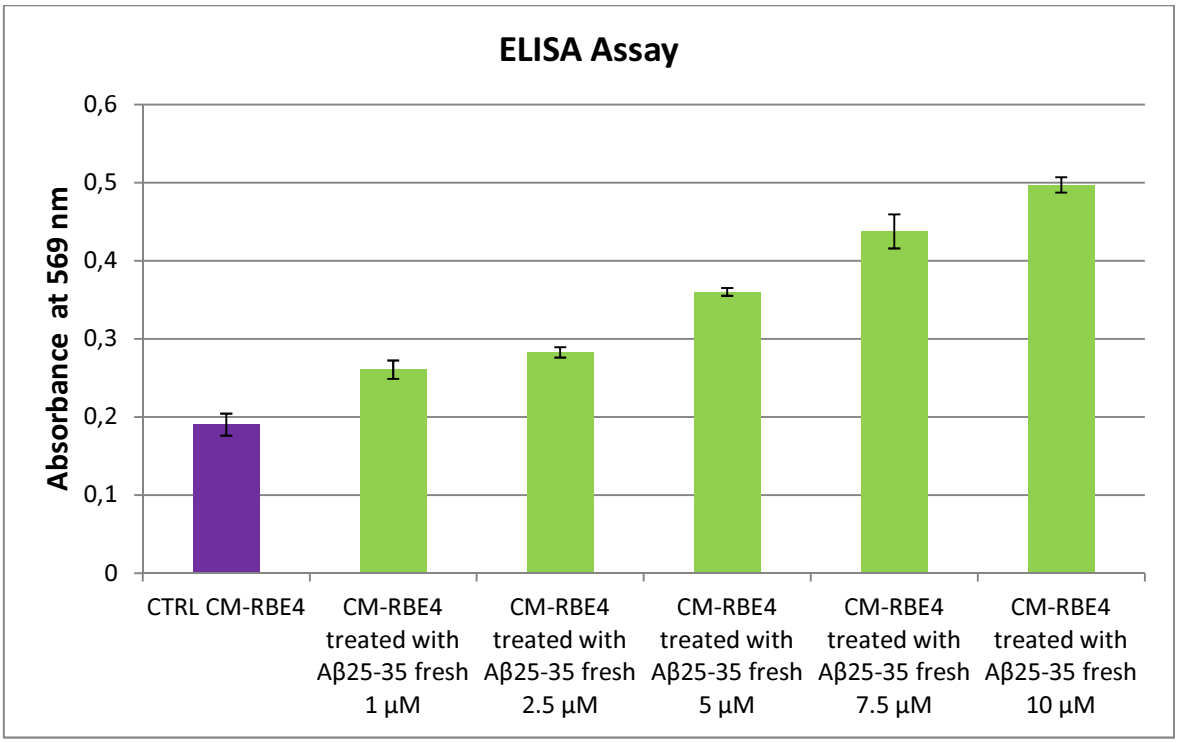

Fig. 44 - ELISA with αB-crystalline Immuneset of conditioned medium from endothelial cells (RBE4) treated with $A\beta_{25-35}$ fresh (1 to 10 µM for 48 hrs). Data are means ± S.D. (n=3) of 3 independent experiments. CM is conditioned medium.

It was found a roughly linear relationship between the concentration of Aβ25-35 used to treat the cells and the release of αB-crystalline in the culture medium. This is in agreement with literature data in which increased production of HSPs (in our case αB-crystallin), necessary for both the proper folding of proteins and the cell protection, is connected to events of cellular stress.

Using a standard curve it was calculated that the concentration of αB-crystalline in the medium conditioned from Aβ25-35-RBE4 cells was about 5 ng/mL.

AGGREGATION ANALYSIS OF hA17-29 THROUGH Th-T ASSAY

The ability of different preparations of hA17-29 to form β-sheet structures was analyzed by Tioflavin T (Th-T) assay. Both incubated samples (alone and in the presence of $CuSO_4$) have given a fluorescence signal greater than the fresh sample (control), showing that the incubation favors the formation of β-sheet structures by the peptide fragment (**Fig. 45**).

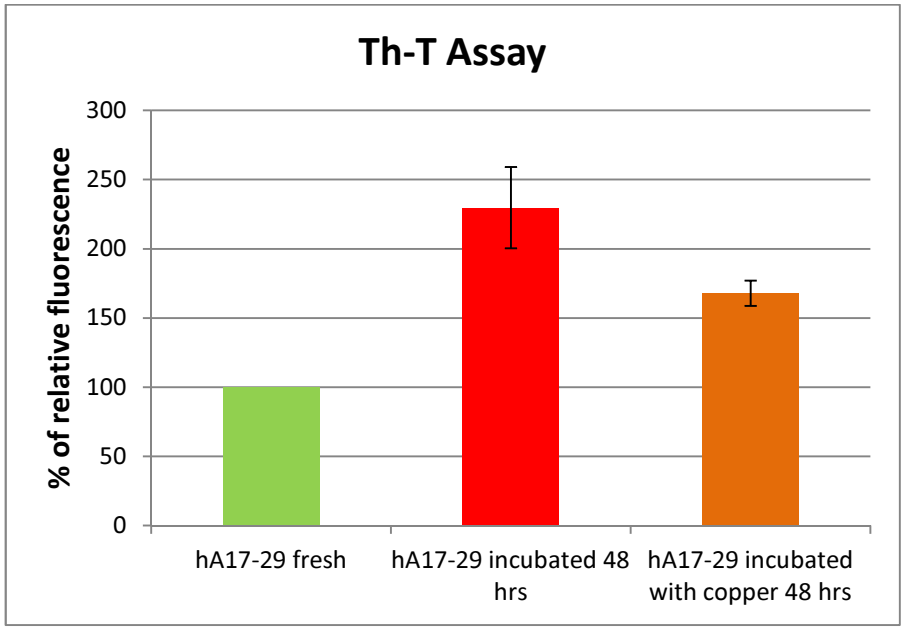

Fig. 45 - Thioflavin T (Th-T) assay on three different preparations of hA17-29. The peptide, immediately after being taken from the freezer (-80°C), was dissolved in DMSO and led to the concentration of aggregation (100 µM) in PBS 0,01 M. The sample "fresh" was prepared immediately before being analyzed. The incubated samples were kept in the temperature controlled (37°C) with [CO_2] of 5% and examined after 48 hours. In the sample containing $CuSO_4$, the ratio Cu^{2+}/peptide is equal to 1:1. In time course experiments 48 hrs of incubation produced the higher Th-T value. Th-T 3 µM was incubated with hA17-29 (5 µg/ml) for 10 min. Fluorescence emission were measured at 450/482 ex/em.

The highest fluorescence value has been supplied from the sample incubated in the absence of $CuSO_4$. This suggests that the presence of the metal cation (Cu^{2+}) may counter/destabilize the formation of Th-T positive structures.

To understand how the incubation period can influence the formation of β-sheet structures by hA17-29, the process was followed over time (0-72 hours) (**Fig. 46**).

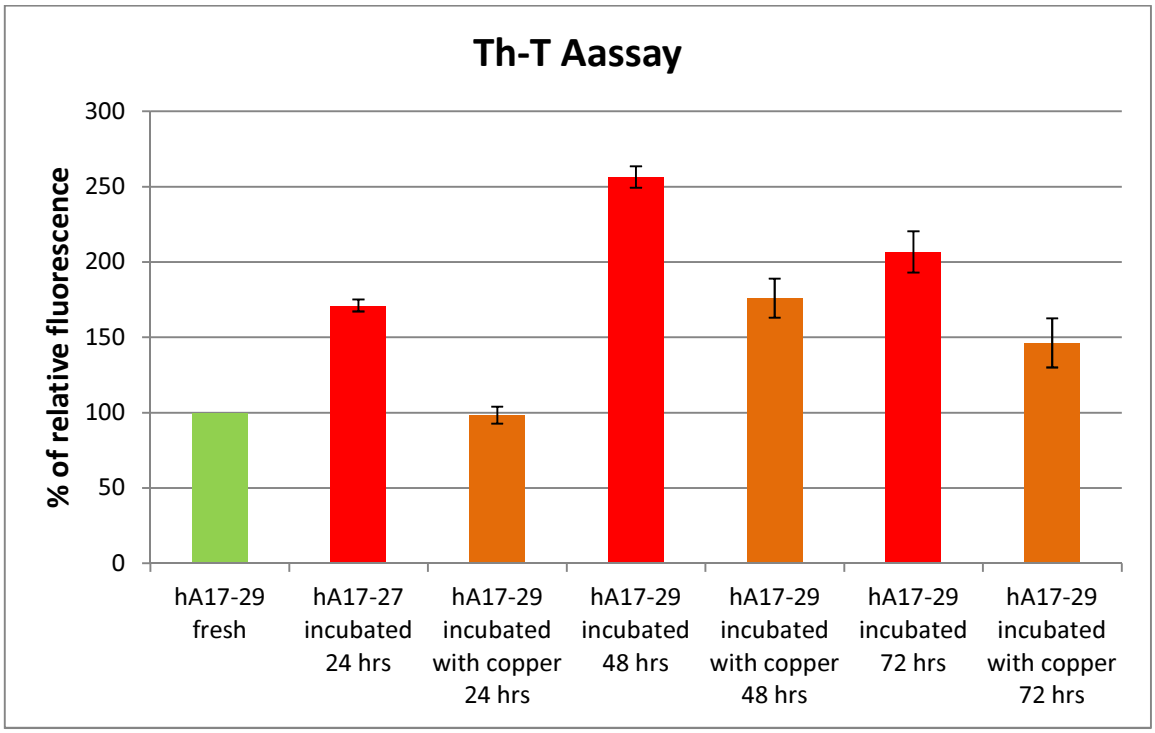

Fig. 46 - Thioflavin T (Th-T) assay on different preparations of hA17-29. The peptide, immediately after being taken from the freezer (-80°C), was dissolved in DMSO and led to the concentration of aggregation (100 μM) in PBS 0.01 M. The sample "fresh" was prepared immediately before being analyzed. The incubated samples were kept in the temperature controlled (37°C) with [CO_2] of 5% and examined every 24 hours (24-48-72 hours). In the sample containing $CuSO_4$, the ratio Cu^{2+}/peptide is equal to 1:1.

All samples incubated in the time interval considered have given a fluorescence signal greater than the fresh sample (control), showing that the incubation favors the formation of β-sheet structures by the peptide fragment. The state of aggregation changes as a function of incubation time. The highest fluorescence value has been supplied from the sample incubated in the absence of $CuSO_4$ for 48 hours. For longer periods of incubation the β-sheet structures appear to decrease, probably favoring the formation of Th-T negative precipitable macrostructures. The presence of $CuSO_4$ shown a general inhibitory effect on β-sheet formation (Th-T positive structures).

AGGREGATION ANALYSIS OF hA17-29 THROUGH AFM

In order to obtain some information about the structure of the aggregates related to changes in micro-environment, peptide samples incubated in presence of three major elements present within the cells, such as copper, zinc and ribose, were analyzed by AFM after 48 hours of incubation at 37°C (**Figg. 47-50**).

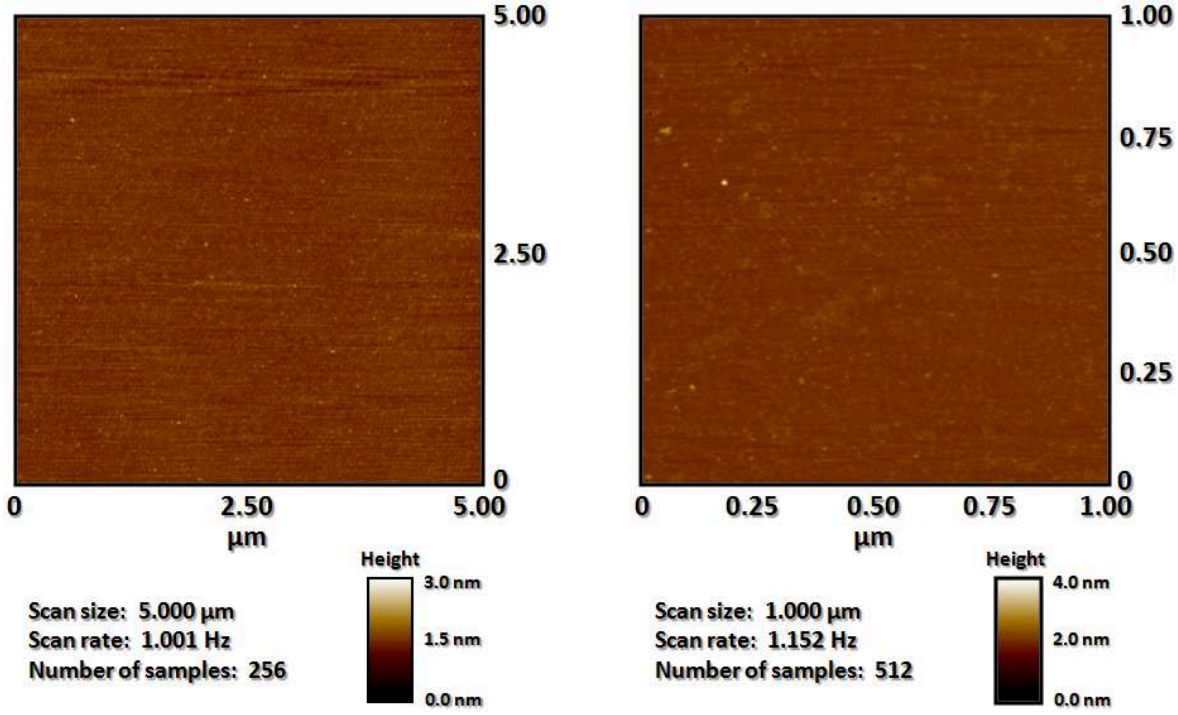

Fig. 47 - AFM images of hA17-29 100 µM fresh. This sample was prepared immediately before being analyzed.

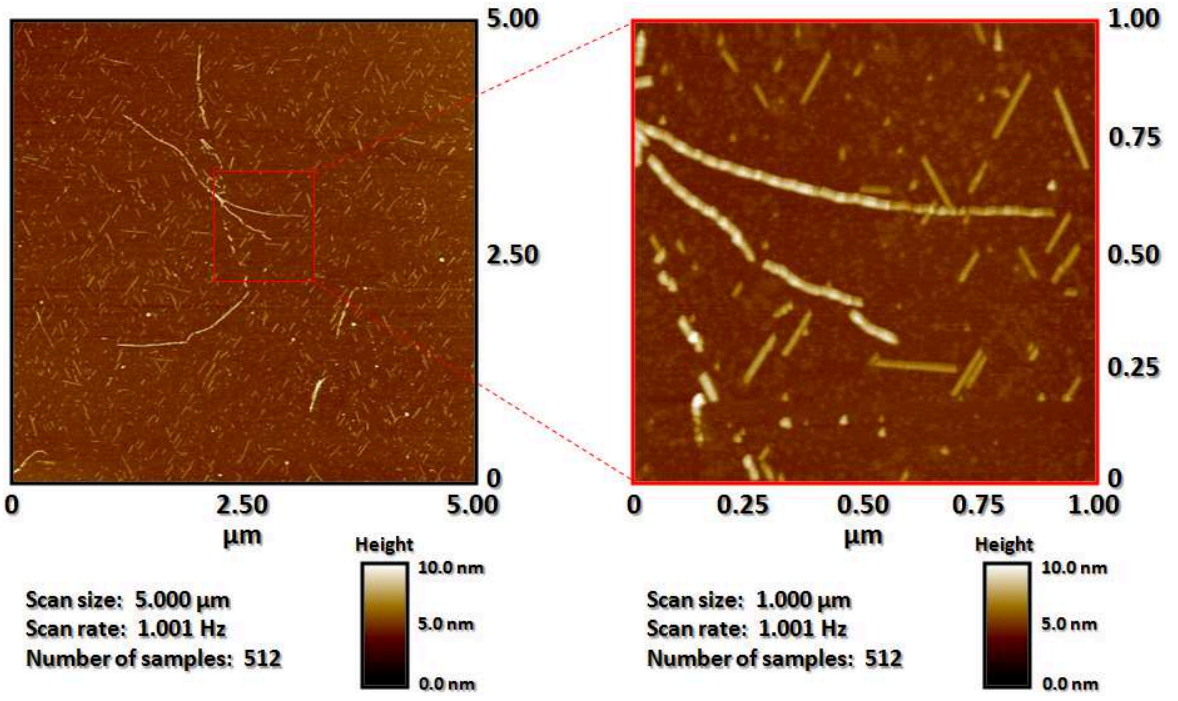

Fig. 48 - AFM images of hA17-29 100 µM incubated with copper for 48 hrs at 37°C. The ratio Cu^{2+}/peptide is equal to 1:1.

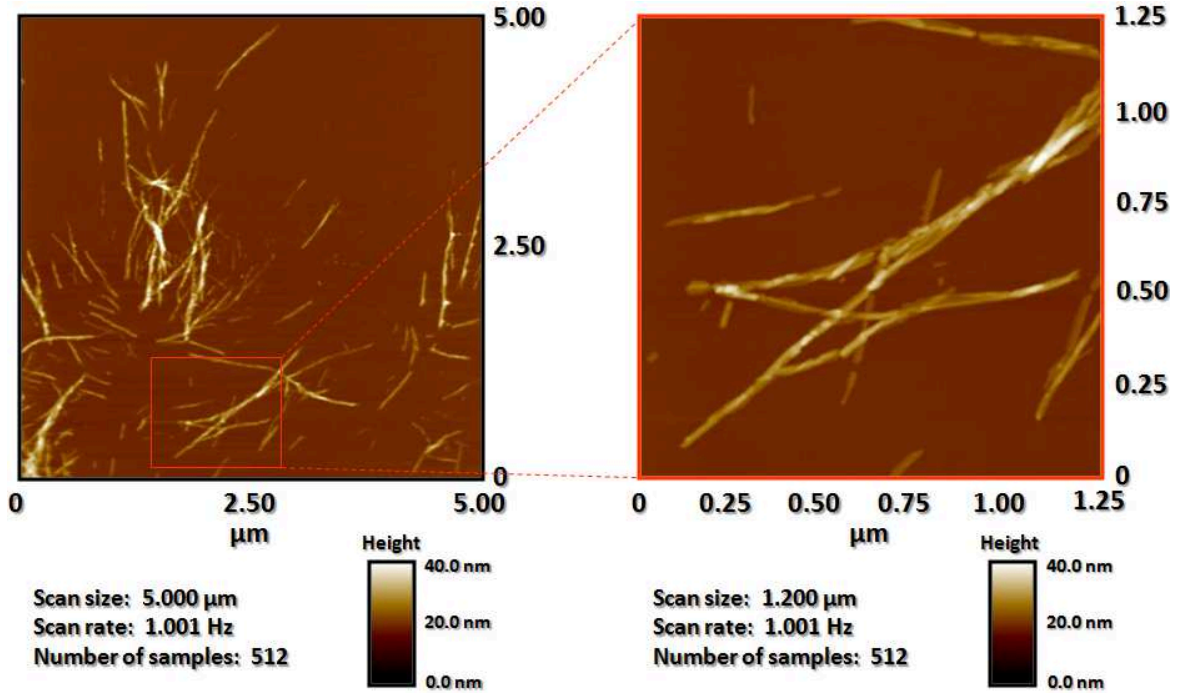

Fig. 49 - AFM images of hA17-29 100 µM incubated with zinc for 48 hrs at 37°C. The ratio Zn^{2+}/peptide is equal to 1:1.

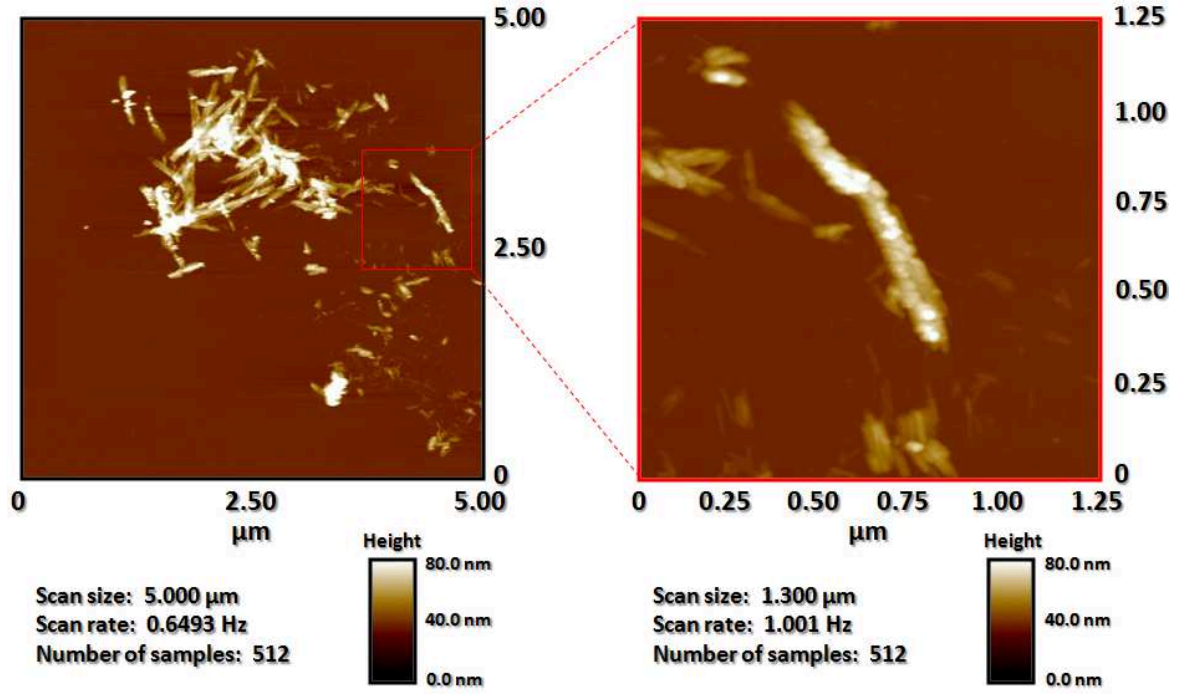

Fig. 50 - AFM images of hA17-29 100 µM incubated with zinc for 48 hrs at 37°C. The ratio ribose/peptide is equal to 10:1.

The fresh sample (**Fig. 47**) does not present any kind of aggregates. The incubation time, as shown previously in experiments with Thioflavin-T, favors the formation of aggregated structures. **Fig. 48** shows how the copper destabilize these structures, favoring the formation of oligomers.

Fibrillary aggregates of varying length, thin and unbranched, are visible in the sample incubated with Zn^{2+} (**Fig. 49**).

At last, the presence of ribose favors the formation of large aggregates (**Fig. 50**).

TOXICITY ANALYSIS OF hA17-29 THROUGH MTT ASSAY

In order to evaluate the relationship between aggregation state and toxicity**,** SH-SY5Y cells were treated for 48 hours with different preparations of hA17-29. The data obtained showed a decreased ability to reduce MTT, then less vitality, compared to control (**Fig. 51**), for all the samples hA17-29-treated.

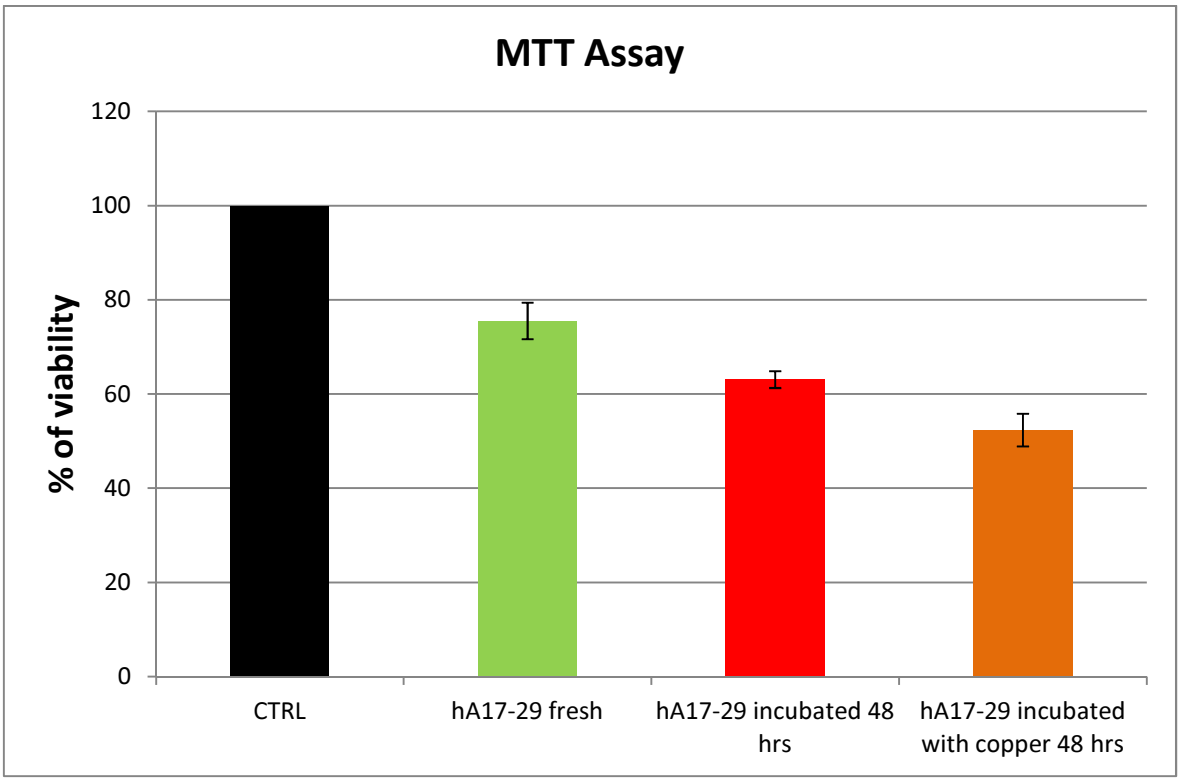

Fig. 51 - MTT assay after 48 hrs of treatment with different hA17-29 (25µM) preparations on SH-SY5Y cells. In the sample containing $CuSO_4$, the ratio Cu^{2+}/peptide is equal to 1:1. Data are means ± S.D. (n=4) of 3 independent experiments.

It can not be excluded any further changes in the status of aggregation during cell culture treatment, thus explaining the toxicity of freshly prepared peptide. The viability decreases in relation to time of incubation of the peptide. The pre-incubation in the presence of $CuSO_4$ further increases the toxicity of the peptide in fact the stronger decrease in cell viability was detected for the treatment with the peptide incubated in the presence of $CuSO_4$. This decrease of viability could also depend on the formation of toxic free radical species produced as a result of Fenton reactions.

Preliminary experiments were performed to analyze both the effect of the conditioned medium from endothelial cells (RBE4) and the possible biochemical pathways linked to it. The following antibodies were used during pretreatment: Anti-Flk1 (VEGFR-2) and Anti-p75 (NGFR).

The data obtained after treatment of SH-SY5Y cells showed a higher cell viability for cells treated with the conditioned medium from RBE4 cells compared to control (**Fig. 52**). This confirms our previous data. The SH-SY5Y cells treated with hA17-29 showed a lowering of vitality of about 20% compared to control. The cells treated simultaneously with the conditioned medium from RBE4 cells and hA17-29 showed a significantly higher viability compared with cells treated with hA17-29 only, clearly demonstrating the beneficial effects of the factors produced by endothelial cells.

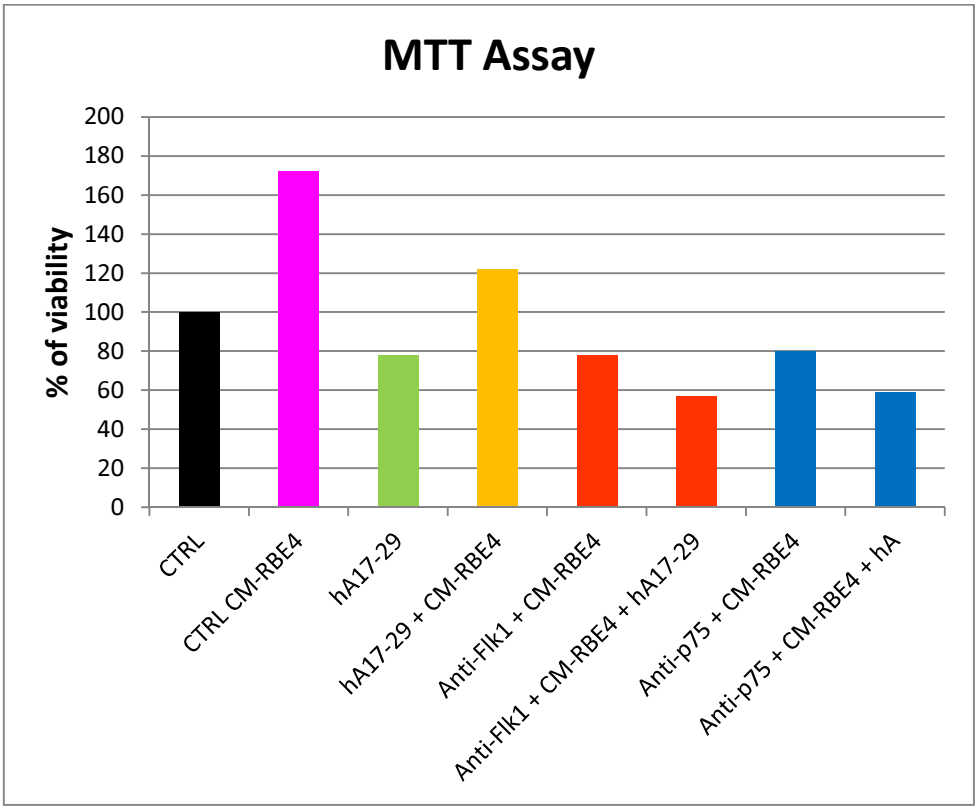

Figure 52 - MTT assay after 48 hrs of treatment with hA17-29 (20 µM) fresh, after a 2 hours pre-treatment with antibodies (2.5 µg/ml), on SH-SY5Y cells. The conditioned medium (CM) was obtained from endothelial cells (RBE4) cultured for 48 hours.

It is of great interest hot the cells pre-treated with antibodies have provided a result almost superimposable. In both cases they have reversed the effect of the conditioned medium, lowering the viability to about 80%. The cells treated with antibodies and hA17-29 showed a lowering of viability of about 40% compared to control. The value of low viability may depend on whether the cells are differentiated and therefore have

stopped dividing early. This idea comes from the observation by phase contrast microscope of the cells after 48 hours of treatment (**Fig. 53**).

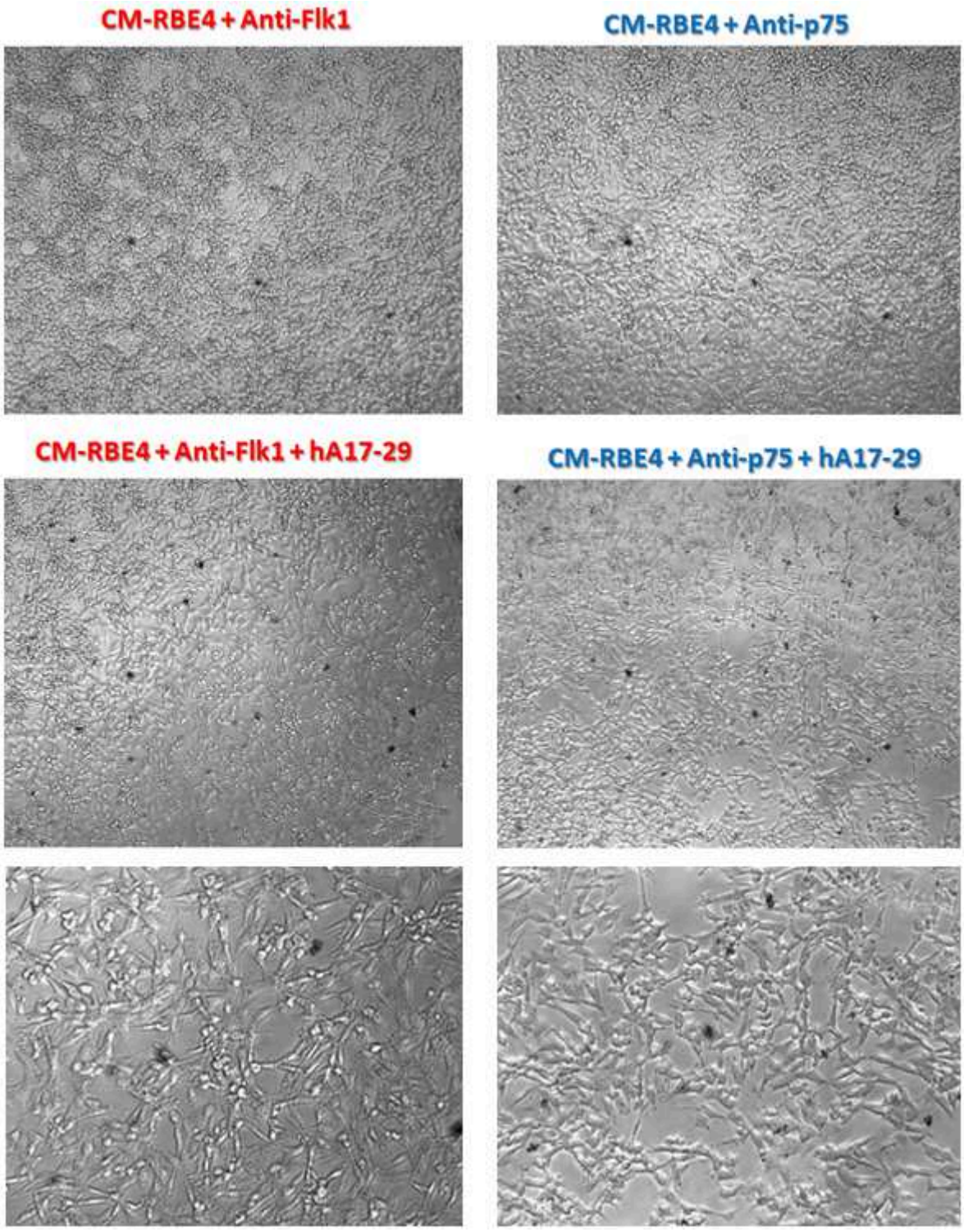

Figure 53 - Photos obtained with phase contrast microscope showing the possible cell differentiation in response to synergistic action between antibodies and hA17-29..

Future experiments will be aimed for understanding this phenomenon.

MONITORING INTRACELLULAR NITRIC OXIDE PRODUCTION USING MCE AND LIF DETECTION

Bulk cell analysis

NO production in the cells was measured using DAF-FMDA. Cells were co-labelled with 6-CFDA that was used as an internal standard to account for differences in cell viability, esterase activity, and volume.

Although DAF-FM is very selective for NO, Sweedler's group has shown that it reacts with DHA to produce derivatives (DAF-FM DHAs) with a fluorescence profile similar to that of DAF-FM T. Therefore, they employed capillary electrophoresis with LIF detection to separate DAF-FM T from DAF-FM DHA interference.

The migration time for the DAF-FM DHA peak using ME was therefore investigated. The DAF-FM DHA was separated from DAF-FM T and 6-carboxyfluorescein (6-CF) as shown in **Fig. 54**.

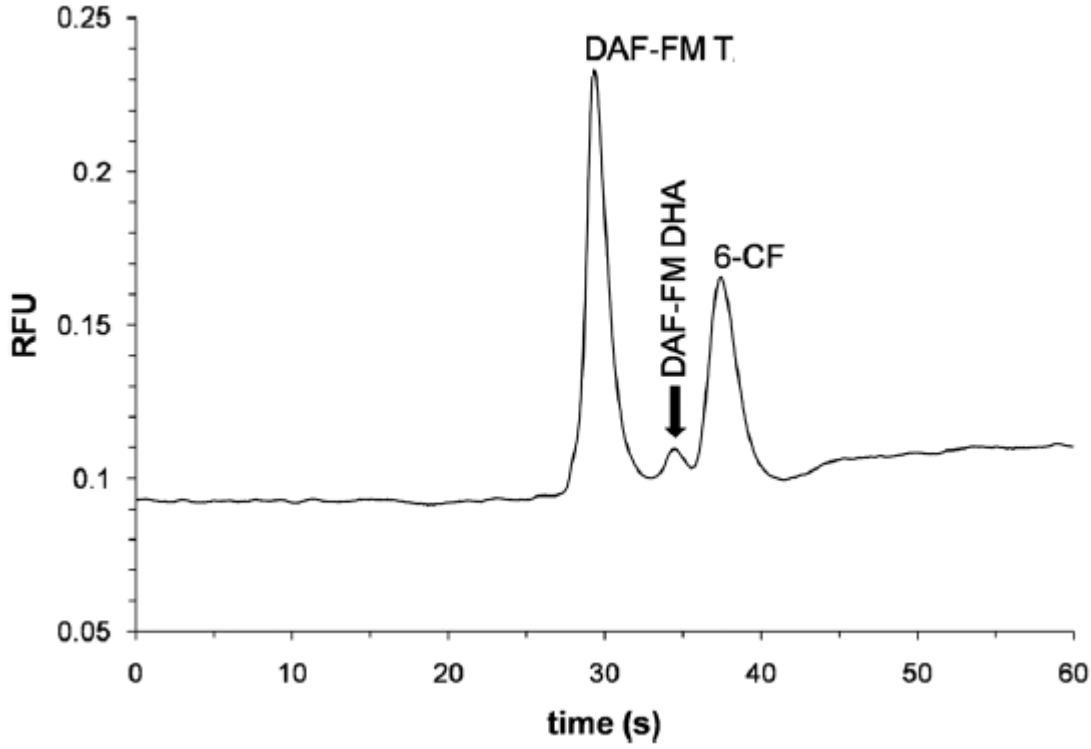

Figure 54 - Separation of DAF-FM T, DAF-FM DHA, and 6-CF using microchip electrophoresis with laser-induced fluorescence detection. Separation voltage was 2400 V (separation) and 2200 V (sampling). Run buffer consisted of 10 mM boric acid, 7.5 mM SDS, pH 9.2. Separation channel length was 5 cm. The final concentration of 6-CF was 0.024 μM. The DAF-FM DHA peak corresponds to a cellular concentration of ascorbate of 1.45 mM and the DAF-FM T signal corresponds to 200 nM NO.

Jurkat cell line has been shown to express inducible nitric oxide synthase (iNOS) following stimulation with LPS. Cells of the same passage number were divided into

two groups. One group was subjected to LPS stimulation and the other group was maintained under the native conditions. **Fig. 55** show typical electropherograms obtained for stimulated and native cells, respectively.

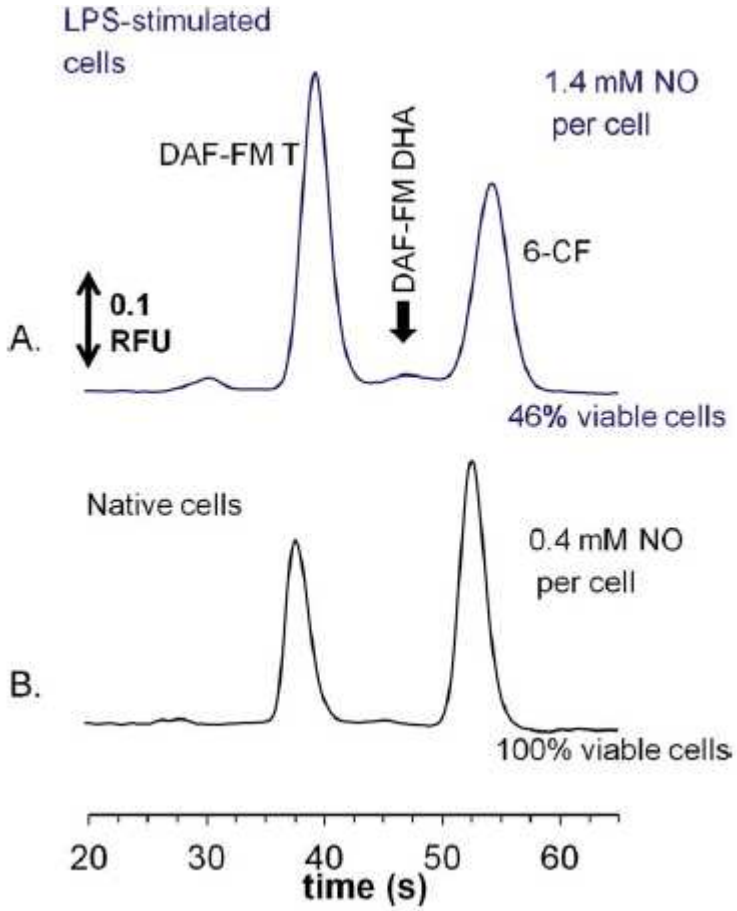

Figure 55 - Comparison of (A) LPS-stimulated and (B) native cell lysate. Separation conditions were the same as those in Fig. 52.

The first large peak is DAF-FM T and the second distinct peak corresponds to 6-CF. Peak identification was confirmed by incubating cells individually with either DAF-FMDA or 6-CFDA. The migration times for DAF-FM T and 6-CFDA in stimulated cells were 38.1 $\pm$ 0.3 s, and 53.1 $\pm$ 0.2 s, respectively. In native cell lysate, the migration times were 36.8 $\pm$ 0.3 s, and 51.5 $\pm$ 0.6 s. Slight shifts in migration times between runs is expected with PDMS substrates. Peak height reproducibility for DAF-FM T and 6-CFDA was between 2-13% in these studies. Under our separation conditions, DAF-FM T and DAF-FM migrate in the same position; however, DAF-FM is weakly fluorescent. Since DAF-FM has been reported to be photo-oxidized to generate a fluorescent product, DAF-FM solutions were protected from light during all experiments.

A negligible amount of fluorescence due to DAF-FM was observed in the blank electropherogram (**Fig. 56**).

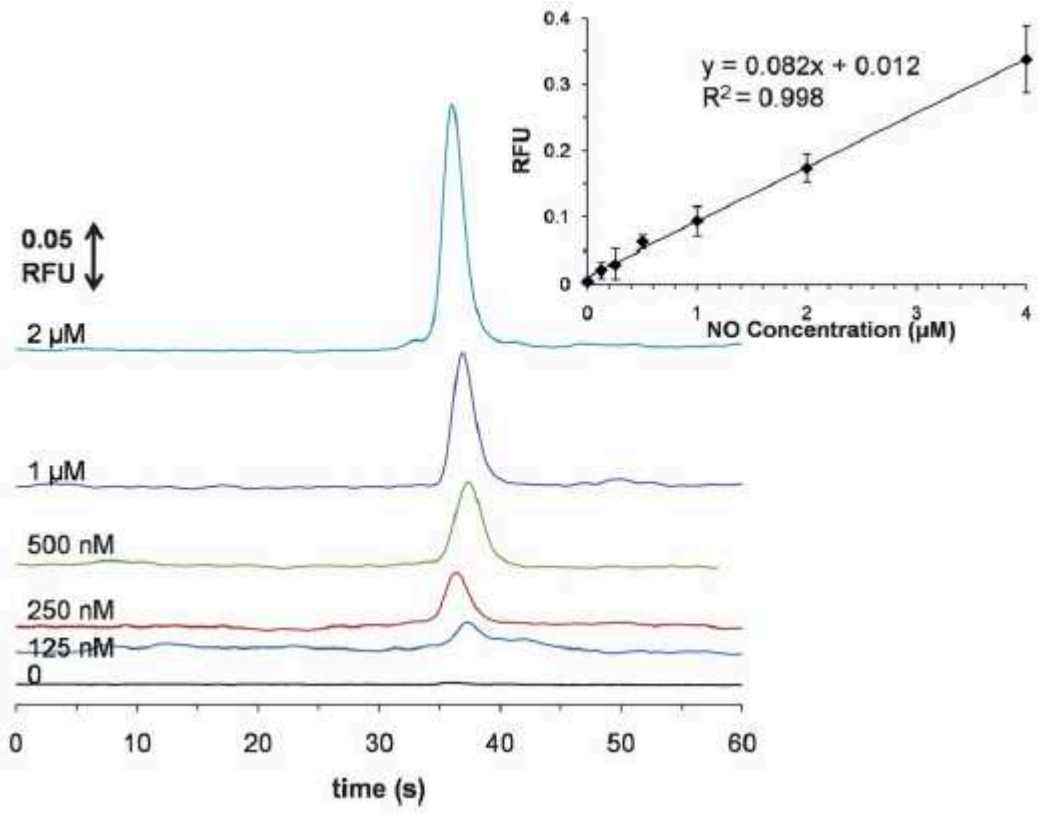

Figure 56 - Electropherograms of DAF-FM T prepared using different concentrations of NO and NO calibration curve. Separation conditions were the same as those in Fig. 54.

A small peak corresponding to DAF-FM DHA was also observed in the cell lysates samples as shown in Fig. 53. The Jurkat cells used in these studies were cultured in ascorbate-free medium. It has been reported that, under these conditions, the intracellular concentration of ascorbate should be close to zero. In a separate study using microchip electrophoresis with electrochemical detection, ascorbate was undetectable in the (underivatized) cell lysate (data not showed).

The DAF-FM T/6-CF peak height ratio can be used to estimate the relative concentrations of NO produced by the cells. This ratio showed that there was a 120% increase in NO production in LPS-stimulated cells compared to native cells. The percent increase was calculated based on the peak height ratios for DAF-FM T and 6-CF, and was calculated as follows:

$$\left(\frac{\left[\frac{\text{DAF-FM T}}{\text{6-CF}}\right]_{\text{stimulated}} - \left[\frac{\text{DAF-FM T}}{\text{6-CF}}\right]_{\text{native}}}{\left[\frac{\text{DAF-FM T}}{\text{6-CF}}\right]_{\text{native}}} \right) \times 100\%$$

During these experiments, it was noted that the cell pellets obtained from the stimulated cells were consistently smaller than those obtained for native cells, indicating that the excessive NO produced during stimulation could be causing cell apoptosis. Infact, Jurkat cells have been used as a model for the evaluation of the treatment of leukemic cancer cells by NO-generating drugs. Realizing that the concentration of NO measured by ME-LIF for the bulk cell lysates is very likely influenced by the large amount of cell death, the number of viable cells before and after each timulation (just prior to lysis) was measured using the Trypan blue exclusion assay. While native Jurkat cells (control experiment) typically increase their population by ~12-30% during a 3-h period, we determined that cells treated with 1.5 mg mL^{-1} LPS have a mortality rate of up to 69% during the same time frame. This substantial amount of cell death is associated with cytotoxic concentrations of NO produced by iNOS during stimulation, which greatly reduces the number of cells analysed in bulk. This can be seen in **Fig. 55 A**. The electropherograms corresponding to the LPS-stimulated cell lysate do not show a dramatic increase of overall fluorescence response for the DAF-FM T peak compared to the native cells. However, only 46% of the cells survived after LPS stimulation; thus, the concentration of NO detected per stimulated cell was, in fact, much greater than in native cells. In addition, the comparison of the DAF-FM T/6-CF peak height ratios obtained for native and LPS-stimulated cells clearly showed increased NO production in LPS-stimulated cell lysates. The average ratio for DAF-FM T/6-CF for native lysates was 0.69, while that for LPS-stimulated cells was 1.61 in the electropherograms shown in **Fig. 55**. The higher ratio in stimulated cells is due to an increase in NO production, resulting in a DAF-FM T peak of greater intensity. For three different sets of LPS-stimulated and native cell lysates, there was 120% increase or 2.2 $\pm$ 0.2 times higher NO production in LPS-stimulated cells.

To estimate the intracellular concentrations of NO in a single cell, a calibration curve for NO, using DEA/NO as an NO donor, was constructed. The NO standards were reacted with DAF-FM under conditions similar to the cell experiments (pH 7.4 and 37°C). A calibration curve was constructed by reacting appropriate concentrations of NO released by DEA/NO with DAF-FM and monitoring the response using the microchip electrophoresis device (**Fig. 56**). A linear response was observed from 0.125

to 4 μM with a correlation coefficient of 0.998. The limit of detection was estimated to be 40 nM at S/N=3 (based on a 125 nM NO standard solution at a S/N of 9 in **Fig. 56**). Using the cell counts obtained for each set of native and stimulated cells (the same three LPS-stimulated and native cell lysate data sets used for DAF-FM T/6-CF ratio calculations were used), the concentration of NO produced per cell could be estimated. **Fig. 57** shows bar graphs for the average intracellular concentration of NO in native versus LPS-stimulated cells.

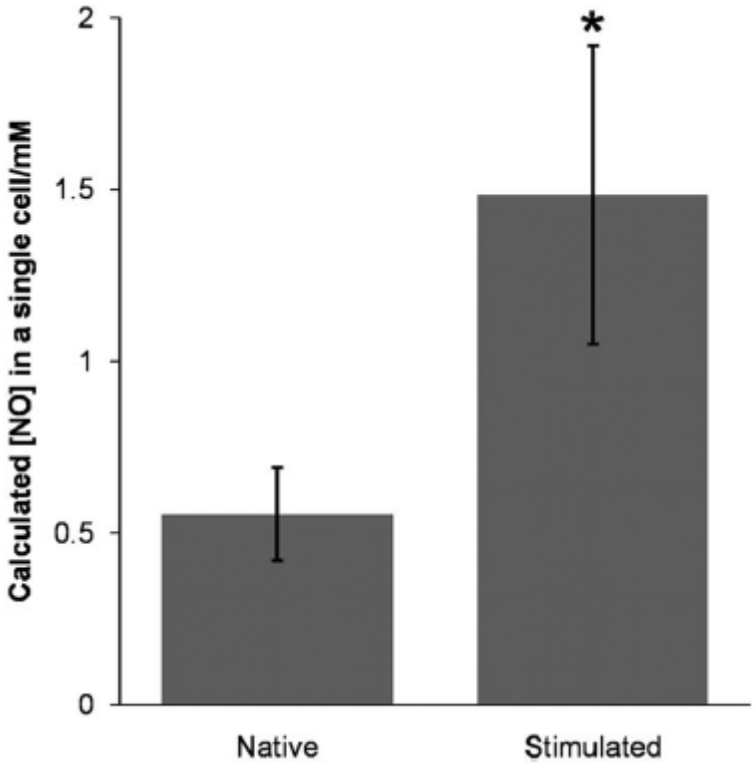

Figure 57 - Comparison of calculated average NO concentration in a single LPS-stimulated and a native Jurkat cell (n=3, p<0.05). For these calculations, the volume of a Jurkat cell was assumed to be 0.5 pL.

As can be seen in **Fig. 57**, there was an approximately 2.5-fold increase in NO production in a single LPS-stimulated cell 1.5±0.4 mM versus native cell 0.6±0.1 mM. The calculated NO concentration in a LPS-stimulated cell is statistically significant compared to the calculated NO concentration in a native cell (paired t-test, $p<0.05$). These values for NO production are very similar to those reported by Goto *et al*. for macrophages stimulated with LPS. These results confirmed our previous observations of elevated concentrations of NO in LPS-stimulated cells along with an increased mortality rate.

Single cell analysis

The initial experiments employed a previously published design shown in **Fig. 37 A**, previously shown in materials and methods.

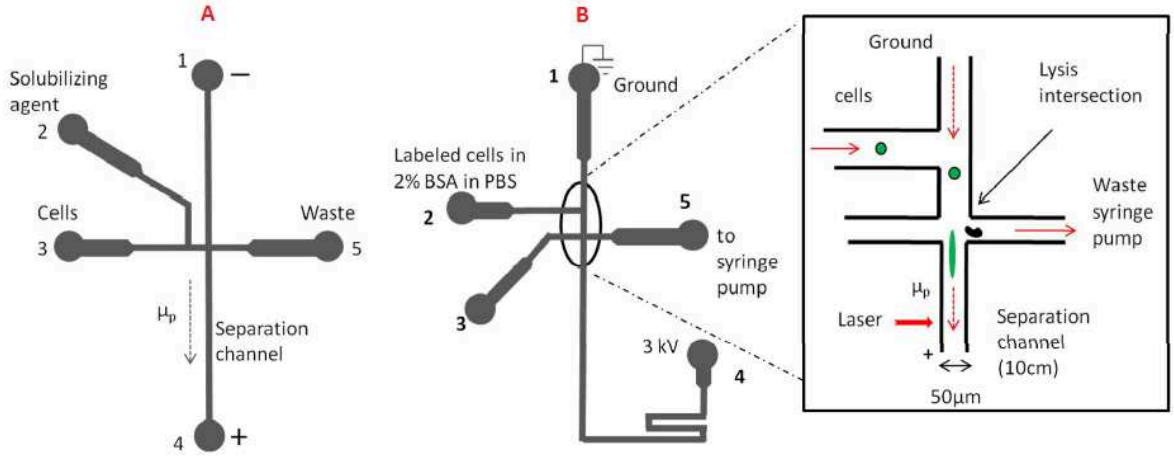

Figure 37 - A is the initial chip design. **B** is a schematic of improved microfluidic chip used for single cell lysis experiments. The lysis intersection of the microchip is shown in the inset. The solid arrows indicate the direction of bulk fluid flow while the broken arrows show the direction of electrophoretic migration (μ_p).

In this design, cells are loaded into reservoir 3 and flowed through the intersection to waste (reservoir 5). However, we found that reproducible injection of the cell lysate was difficult to realize with this design due to difficulty in precisely controlling the volumetric flow rates in the channel manifold using an external syringe pump. The flow rates on these devices are in the low nL/min range, and the flows from all of the channels at the lysis intersection must be carefully balanced in order to generate reproducible and complete injection of the lysate from the cell into the separation channel. Unpredictable changes in flow resistances over the course of a run due to partial obstructions in the various channels and small changes from device to device in terms of flow resistance make it difficult to reliably adjust the flow. In addition, there is a lag time in terms of when the flow rate is changed on the external pumping device and when this change is seen at the lysis intersection.

To improve the ruggedness and overall operation of the microfluidic device, therefore, we altered the manner in which the cells were transported into the channel intersection of the chip (region marked by black circle in **Fig. 37 B**). In the new design, cells are placed in reservoir 2 and are transported to the lysis area of the chip using the hydrodynamic flow generated by a syringe pump in withdrawal mode at reservoir 5. In this configuration, the cells make a 90° turn into the main channel where they encounter a DC electric field sufficient to lyse the cells. The lysate is then

electrophoretically injected into the separation channel while the cell debris is hydrodynamically shunted to a waste channel.

Fig. 58 shows consecutive image frames grabbed from a video demonstrating the lysis of individual Jurkat cells loaded with Oregon Green using this device.

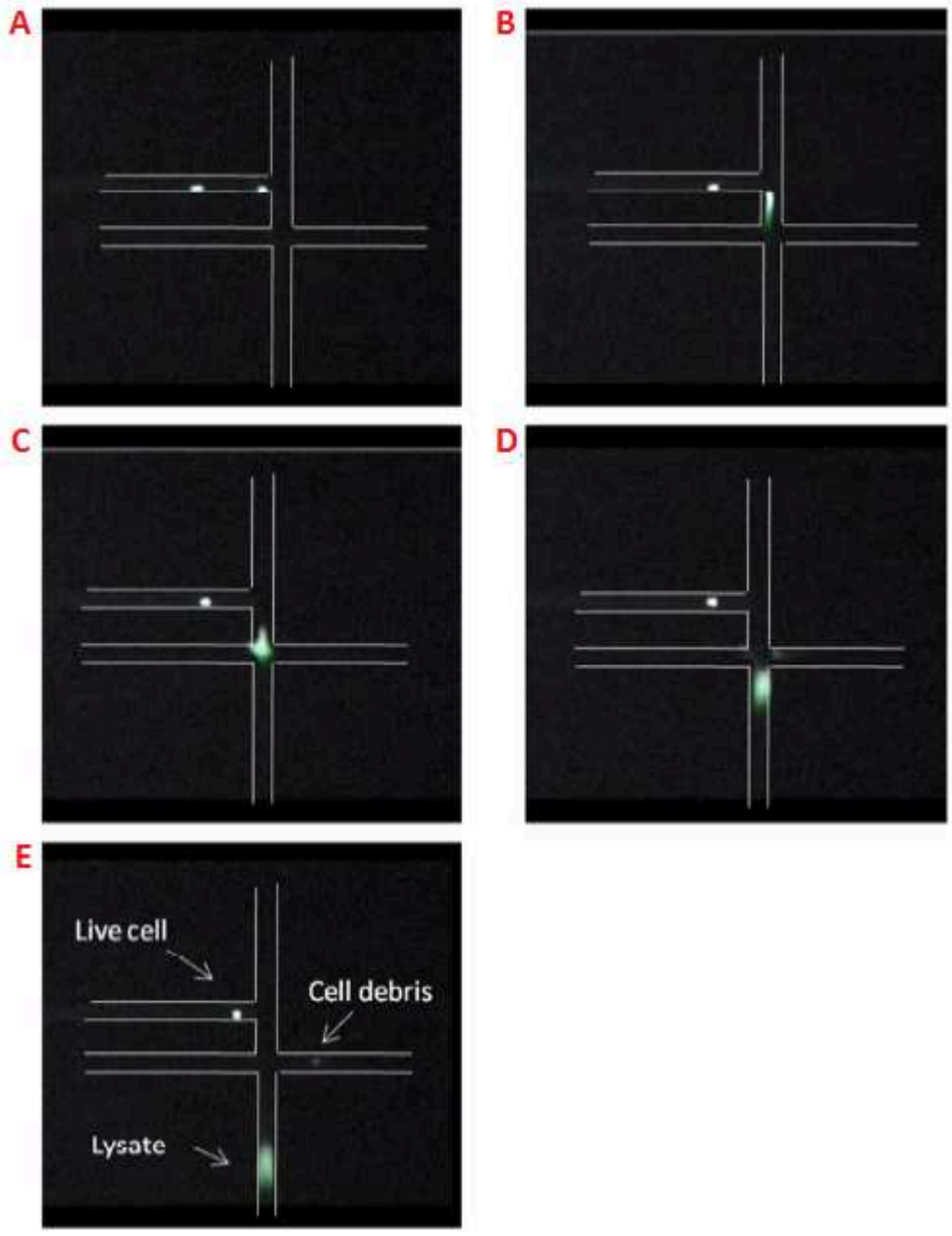

Figure 58 - Still images obtained from a video of Jurkat cells lysing. The cells in frame A are hydrodynamically transported toward the lysis intersection. In frame B, the cells at the intersection encounter an electric field that causes them to lyse. In frames C–E, the cell lysate is electrophoretically transported down the separation channel while the cell debris is shunted to the waste channel.

The first image, **Fig. 58 A**, shows cells approaching the lysis channel. In the second image (**Fig. 58 B**), the cells have entered the lysis channel and are lysed by the electric field. In the next two frames (**Figg. 58 C, 58 D**), the fluorescent lysate is seen traveling

into and down the separation channel electrophoretically toward the anode. The velocity of the lysate was 1.44 mm/s. It took less than 33 ms, the length of time between consecutive video frames, to completely lyse the cell. The cell debris was transported into the waste channel more efficiently with this design than previous in designs (**Fig. 58 E**). In addition to the cell transport redesign, the flow rates on this device were more easily controlled by inserting an adjustable flow splitter into the line between the chip and syringe pump (**Fig. 37 B**).

A major advantage of this new design is that a DC electric field could be used for cell lysis rather than the high voltage AC electric field previously reported. This is important, as the high field AC requires a specialized and expensive generator. In addition, the DC electric field strength necessary for consistent cell lysis and lysate injection was less than half that of the previously reported required AC electric field strength. The constant voltage applied between reservoirs 1 and 4 (**Fig. 37 B**) generated a field strength of ~ 375 V/cm in the cell lysing region of the chip. The significantly lower field strength requirements are due to the substantially longer residence time of the cell in the lysis field and the fact that the cell lysate 1 does not need to change migration direction in order to be injected into the separation channel. The run buffer contained 2% BSA (w/v), which served as a dynamic coating to reduce the adhesion of cell membranes and other biomolecules to the microchip channel surfaces. BSA also substantially reduced the electroosmotic flow in the separation channel. Under these separation conditions, the electrophoretic mobilities of the two negatively charged reporting dyes used for the NO experiments described below were greater than the electroosmotic flow. Therefore, the analytes were detected as they travelled toward the anodic buffer reservoir (reservoir 4 in **Fig. 37 B**) following injection into the separation channel.

When performing very high throughput analysis of single cells, it is crucial that the electrophoretic separation is fast and that the peaks exhibit high separation efficiencies. Unfortunately with this device design, it was not possible to directly determine the number of theoretical plates obtained for the analytes of interest in single cells because the cells entered the intersection randomly during any particular run. Instead, the migration velocities of the 6-CFDA and DAF-FM were calculated from videos of the lysate migration under the same separation conditions as those used to obtain single point separations. The calculated migration velocities (e.g. 1.44 mm/s for 6-CFDA)

from these videos were used to convert the temporal peak variances measured on the electropherograms to spatial variances so that the peak dispersion could be calculated and compared to predicted values. The predicted (or theoretical) peak dispersion values were calculated based upon the published diffusion coefficient of fluorescein together with the peak broadening expected from the parabolic flow generated in the separation channel from the syringe pump.

The fluidic resistances in the channel manifold were designed so that the overall flow out of the separation channel was only about 3% of the flow going into channel 5. The experimentally determined peak dispersion coefficient was 1.1×10^{-5} cm^2/s. The predicted dispersion from diffusion (4.5×10^{-6} cm^2/s) and the hydrodynamic (parabolic) flow (negligible compared to the diffusion) in the separation channel was ~4.5×10^{-6} cm^2/s. The experimentally measured value is only ~2.5 times that of the predicted value. Given the crude and indirect nature of these measurements, the agreement is remarkably good and shows that the separations are behaving as expected.

The optimized microfluidic device described above was then used to determine NO production in a population of individual Jurkat cells.

Cells were stimulated with LPS. Control cells were treated in the same manner, but were not exposed to LPS. **Fig. 59** shows typical electropherograms obtained for native cells.

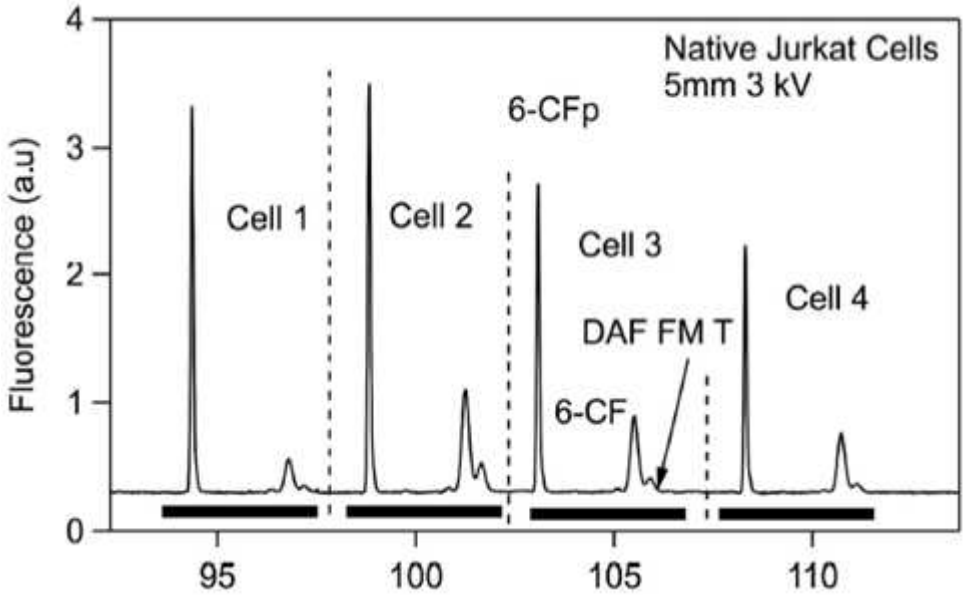

Figure 59 - Electrophoretic separation of dyes released from individual cells. These are 20 s and 30 s segments from a 120 s run. Each cell produced a peak envelope consisting of one tall peak due to partially hydrolyzed 6-CFDA (6-CFp) and a shorter doublet ~3 s later due to fully hydrolyzed 6-CFDA (6-CF) and DAF-FM T.

Fig. 60 shows typical electropherograms obtained for stimulated cells.

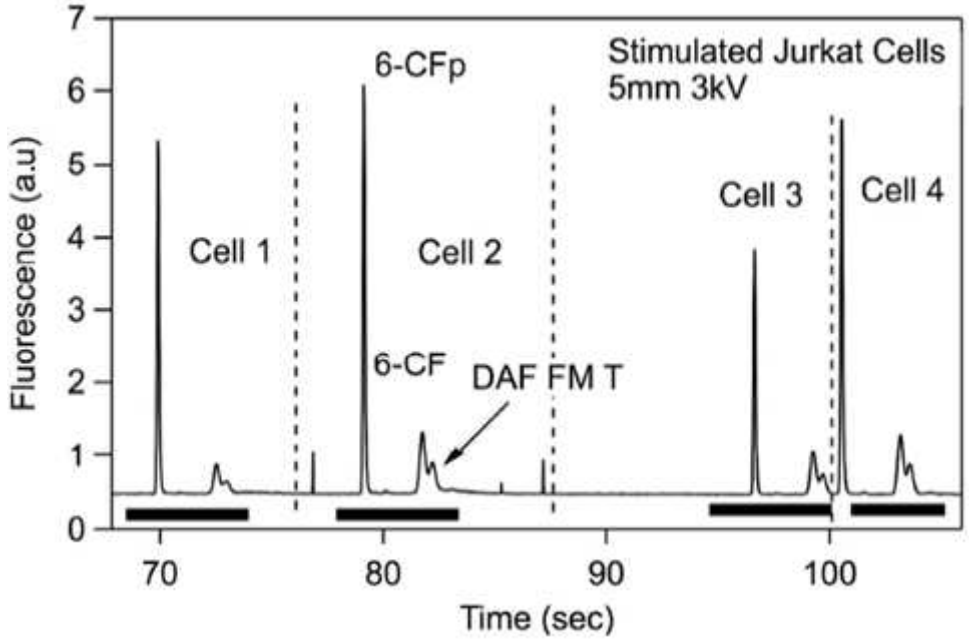

Figure 60 - Electrophoretic separation of dyes released from individual cells. There is a marked increase in DAF-FM T peak height relative to the 6-CF peak following stimulation.

The intracellular production of NO production in the cells was measured using DAF-FMDA. The cells were co-labeled with 6-CFDA, which was used as an internal standard to account for variation in fluorescence intensity when using different microchips and for differences in cell size (volume) as well as variations in esterase activity. The fluorescence yield of 6-CFDA was not affected by the presence of intracellular NO. The analytes present in the cell lysates were detected using laser-induced fluorescence at a distance of 5 mm from the intersection on the separation channel.

Three distinct peaks are observed (**Figg. 59-60**). The first tall peak indicates partially hydrolyzed 6-CFDA (6-CFp). The second peak is the completely hydrolyzed 6-CFDA (6-CF). The last peak is the benzotriole derivative of DAF-FM (DAF-FM T) that corresponds to the NO concentration in the cell. The peak identities were verified by labeling a separate batch of cells with the individual dyes.

The device was then used for the analysis of populations of control and stimulated cells. Due to the lack of a "cell standard," it was not possible to directly quantitate the amount of NO produced in these experiments. However, the ratio of DAF-FM to the products of the 6-CF hydrolysis could be used to evaluate the relative change in NO

production in basal versus stimulated cells. **Table 3** shows the DAF-FM T, 6-CF and 6-CFp peak height and peak area ratios.

Peak area ratio	**6-CF/6-CFp**	**DAF-FM T/6-CF**	**DAF-FM T/6-CFp**	**Number of cells**
Native cells	0.46 (±0.26)	0.39 (±0.34)	0.16 (±0.12)	100
Stimulated cells	0.48 (±0.15)	0.72 (±0.21)	0.34 (±0.12)	100
Mean stimulated/mean native ratio	1.00 (±0.30)	1.80 (±0.40)	2.10 (±0.17)	
Peak height ratio	**6-CF/6-CFp**	**DAF-FM T/6-CF**	**DAF-FM T/6-CFp**	**Number of cells**
Native cells	0.21 (±0.31)	0.26 (±0.08)	0.054 (±0.07)	100
Stimulated cells	0.17 (±0.05)	0.61 (±0.13)	0.10 (±0.03)	100
Mean stimulated/mean native ratio	0.80 (±0.31)	2.30 (±0.15)	1.90 (±0.08)	

Table 3 - The upper table contains the average peak area ratios while the lower table contains the average peak height ratios. The standard deviations for each measurement are reported in parentheses.

As can be seen from this table, the ratio of the two products of 6-CF does not change upon stimulation, but the ratio of DAF-FM T to either of these "internal standards" doubles (**Table 3**).

The addition of LPS resulted in an increase in NO production as shown by the relative increase in the DAF-FM T peak compared to the 6-CF and 6-CFp peaks in **Fig. 60** versus the control cells in **Fig. 59**. A histogram of the distributions of the DAF-FM T/6-CF ratios for 100 stimulated versus 100 control cells is shown in **Figg. 61-62.**

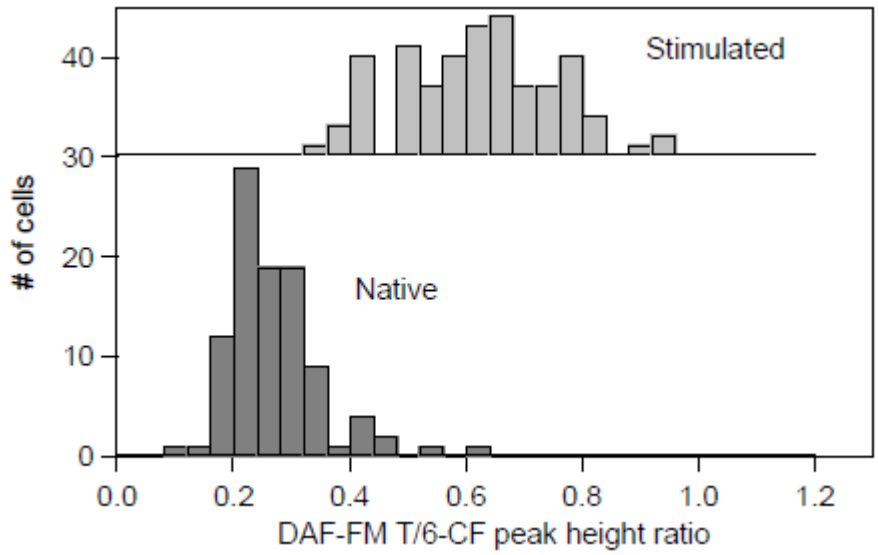

Figure 61 - Histogram of DAF-FM T/6-CF peak area ratios calculated for 100 native cells (dark grey) and stimulated cells (light grey).

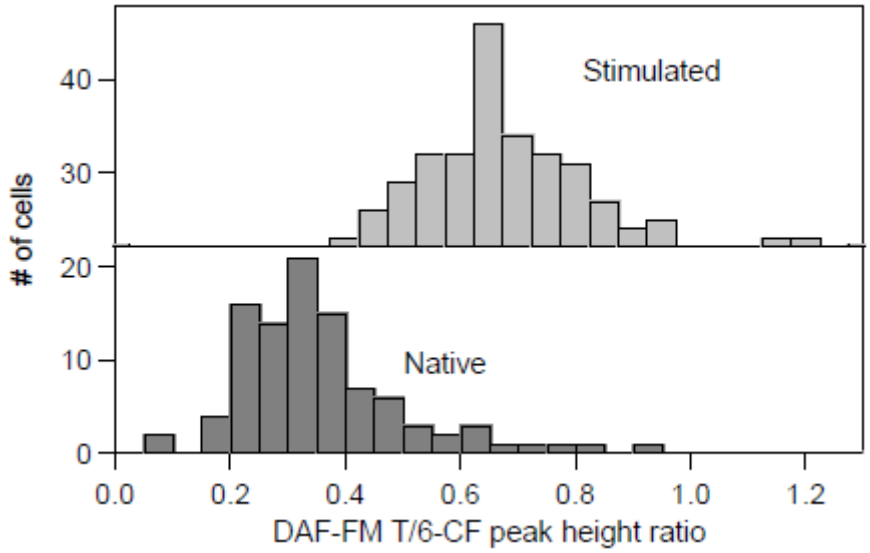

Figure 62 - Histogram of peak height ratios calculated for 100 native cells (dark grey) and stimulated cells (light grey) (same cells of Fig. 59). The peak ratios of cells increase due to increased NO production following stimulation of Jurkat cells with LPS for 3 h.

The relative increase in NO production for the stimulated cells was calculated using equation 1 below:

$$\left(\frac{\left[\frac{\text{DAF-FM T}}{\text{6-CF}}\right]_{\text{stimulated}} - \left[\frac{\text{DAF-FM T}}{\text{6-CF}}\right]_{\text{native}}}{\left[\frac{\text{DAF-FM T}}{\text{6-CF}}\right]_{\text{native}}} \right) \times 100\%$$

Both the peak height and peak area ratios indicate a twofold increase in NO concentration following 3 hrs stimulation of cells with LPS (**Table 3**).

A comparison of the means of two independent samples t-test between the relative NO concentrations in the native and stimulated cells shows the difference to be statistically significant for the both peak height and peak area ratios ($n=199$; $p<0.0005$).

There are a variety of potential interferences that can arise when using DAF-FMDA as a probe molecule for NO. For example DAF-FM can produce a fluorescent species due to photo-oxidation of the probe, contamination of DAF-FM T or formation of interfering products due to dehydroascorbic acid. Also, DAF-FM can produce fluorescence species by superoxide. However, DAF-FM does not produce interfering products due to peroxynitrite (low concentrations, below 10 μM), nitrite and H_2O_2. Although, H_2O_2 can enhance the fluorescence of DAF-FM when NO is present. These issues were addressed in our bulk cell studies paper which was previously published in Analytical Methods [404]. In that study we showed the separation of DAF-FM DHA

(the fluorescent product due to dehydroascorbic acid) from DAF-FM T and that only a negligible peak due to DAF-FM DHA was observed. Under the present separation conditions DAF-FM and DAF-FM T co-migrate; however we observed negligible fluorescence from DAF-FM itself. Additionally, Hoegger's group has shown that DAF-FM can form fluorescence products during DAF-FM freeze-thaw cycles. To prevent these issues we made new DAF-FMDA stock solutions for each set of experiments.

All of the data shown in **Figg. 59-60** were obtained from cells using the same device over the course of sequential 14 runs – 7 for the native cells and 7 for the stimulated cells. At least 20 cells were detected for each run, but 20 cells were not always analyzed due to peak overlap. The results obtained for the video analysis and the diffusion coefficient measurements were obtained using separate devices. We did not perform quantitative device-to-device comparisons in these studies. However, in all cases, a single device could be used multiple times before failing.

Bulk vs Single cell analysis

We have recently published a report on the NO concentration levels in native and stimulated Jurkat bulk cell lysates using microchip electrophoresis with LIF detection [404]. The stimulation and measurement parameters used in these studies were carried out as closely as possible to those used in the previous paper. This makes it possible to compare these single cell analysis results with those obtained previously via bulk cell measurements. The average DAF-FM T/6-CFDA peak height ratios are 2.3±0.15 times greater for the stimulated cells compared to the native cells. The average single cell results are in remarkably close agreement (twofold increase) to the bulk cell analysis results which showed a 2.2±0.2 increase upon LPS stimulation.

In our previous paper the average amount of NO produced per cell was quantitated using a true NO standard with the average native cell producing 0.6±0.1 mM NO and a stimulated cell producing 1.5±0.4 mM NO. Given the similar conditions under which the experiments were performed and the similar increase seen in the DAF-FM T/6-CF peak height and area ratios, it is probable that the average amount on NO in the cells is comparable to these previous results.

NITRITE (NO_2^-) PRODUCTION IN RAW 264.7 CELLS

In order to evaluate the relationship between inflammation and NO production, RAW 264.7 cells were treated/stimulated with LPS alone and together with IFN-γ. Nitrite (NO_2^-) production, the stable end product of nitric oxide metabolism, was measured at 24 and 44 hours. As shown in **Fig. 63** the nitrite production was greater for cells treated with LPS together with IFN-γ both after 24 and 44 hours.

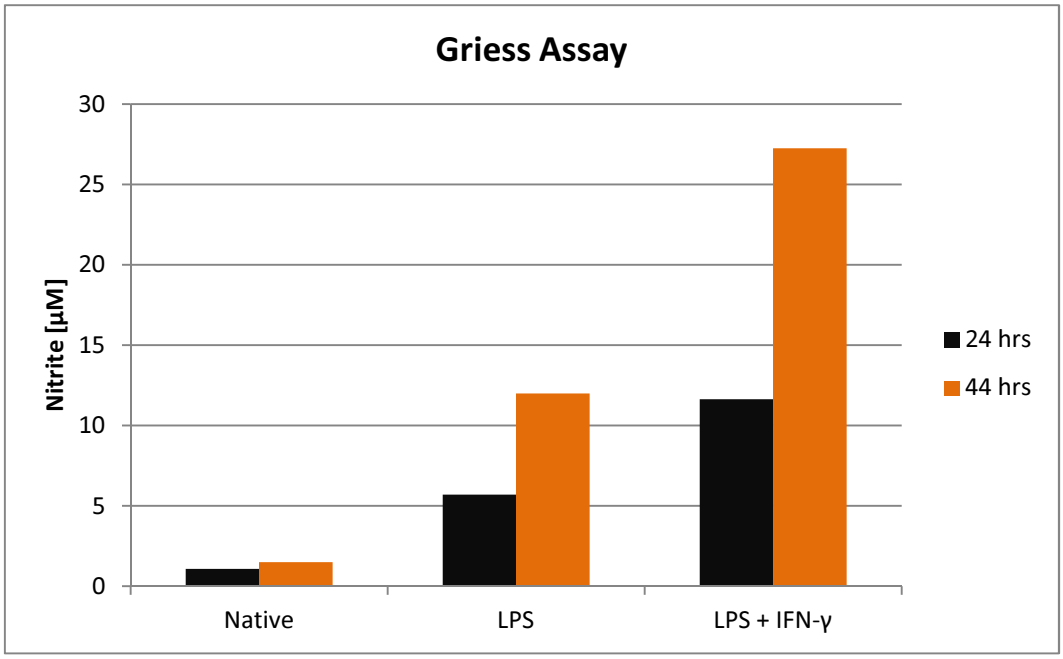

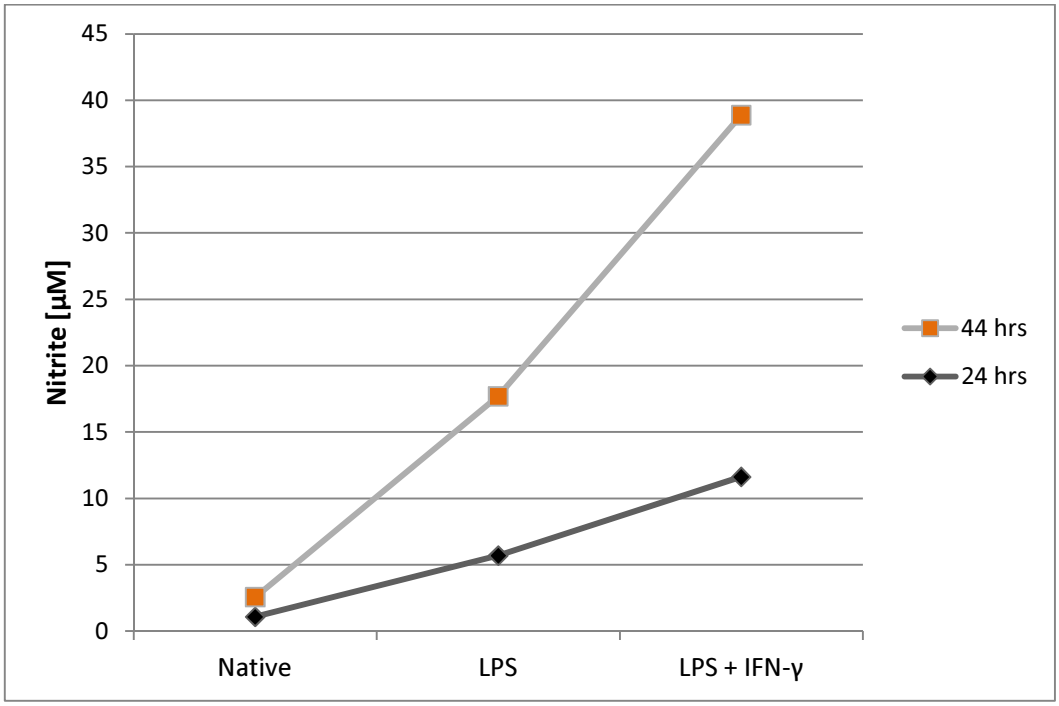

Figure 63 - Production of nitrite in RAW 264.7 cells. Cells were treated with LPS (100 ng/ml) alone or together with IFN-γ (600 U/mL). Levels of nitrite were quantified using Griess reagent after 24 and 44 hrs. Native cells, used such a control, are untreated.

In order to evaluate the relationship between NO production and iNOS activation, two different inhibitors of this enzyme were used. Furthermore, it was examined the effect on nitric oxide production of two other molecules, ascorbic acid and L-carnosine. The following figure (**Fig. 64**) shows the result that was obtained.

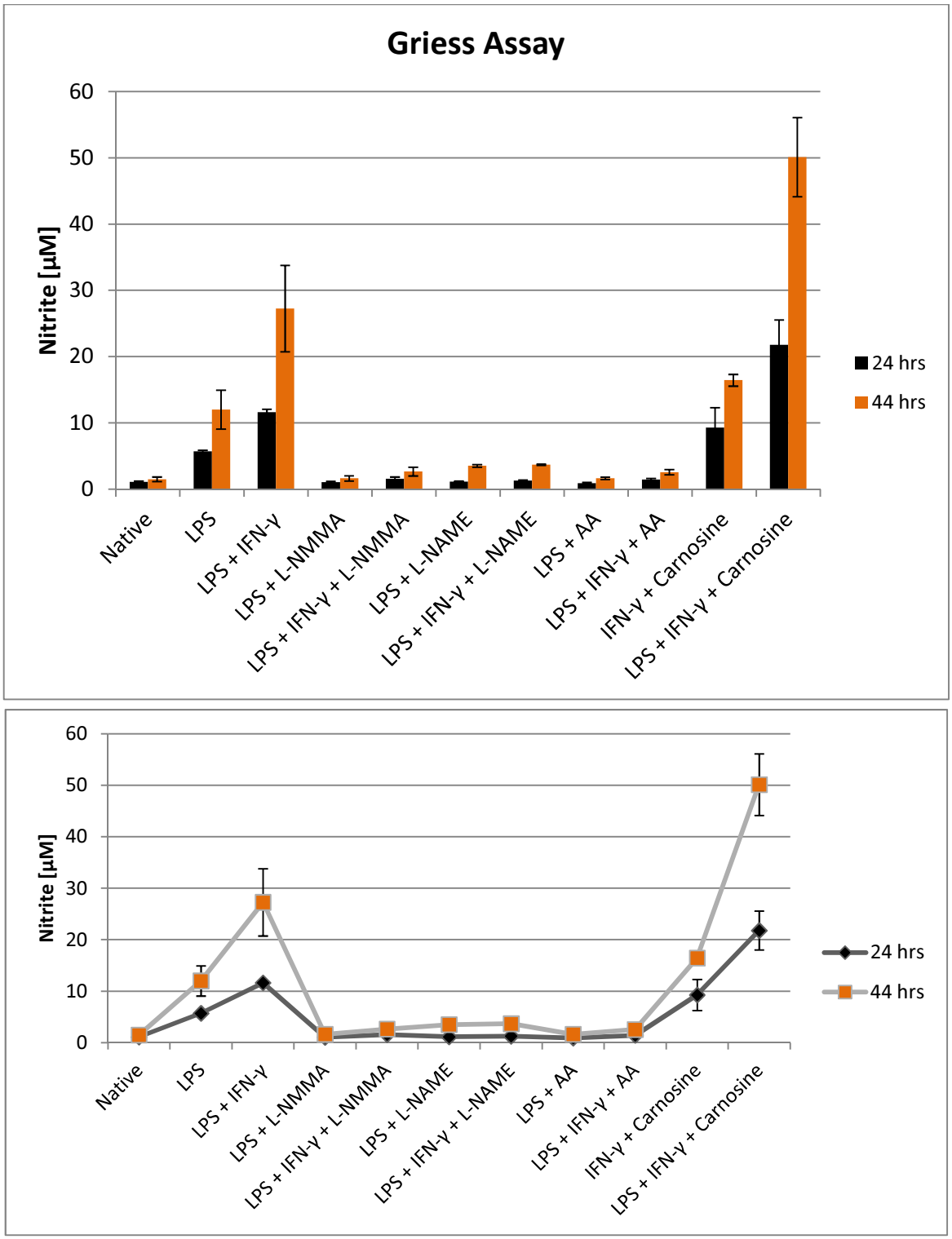

Figure 64 - Production of nitrite in RAW 264.7 cells. Final [ ] in culture: LPS = 100 ng/mL - IFN-γ = 600 U/mL - L-NAME & L-NMMA = 1 mM - Ascorbic acid (AA) = 2 mM - Carnosine: 20 mM. L-NAME, L-NMMA, AA and carnosine were used in pre-treatment (1 h). Native cells, used such a control, are untreated. Data are means ± SEM (n=4) of 3 independent experiments.

As expected the nitrite production in RAW 264.7 cells treated with inhibitors was comparable to the control (untreated cells), confirming that NO production of these cells was dependent of iNOS activation. Even in cells pre-treated with ascorbic acid NO production was very low, suggesting an inhibitory role in respect of NO production or its degradation to nitrite. Interestingly the cells treated with L-carnosine have produced the largest amount of nitrite, suggesting a synergic action between LPS and IFN-γ. Future experiments will be aimed at understanding of this possible synergic action.

Analyzing the pictures of these cells subjected to different treatments, it was observed a marked cellular differentiation in the stimulated samples, especially in the sample treated with LPS, IFN-γ and L-carnosine (**Fig. 65**).

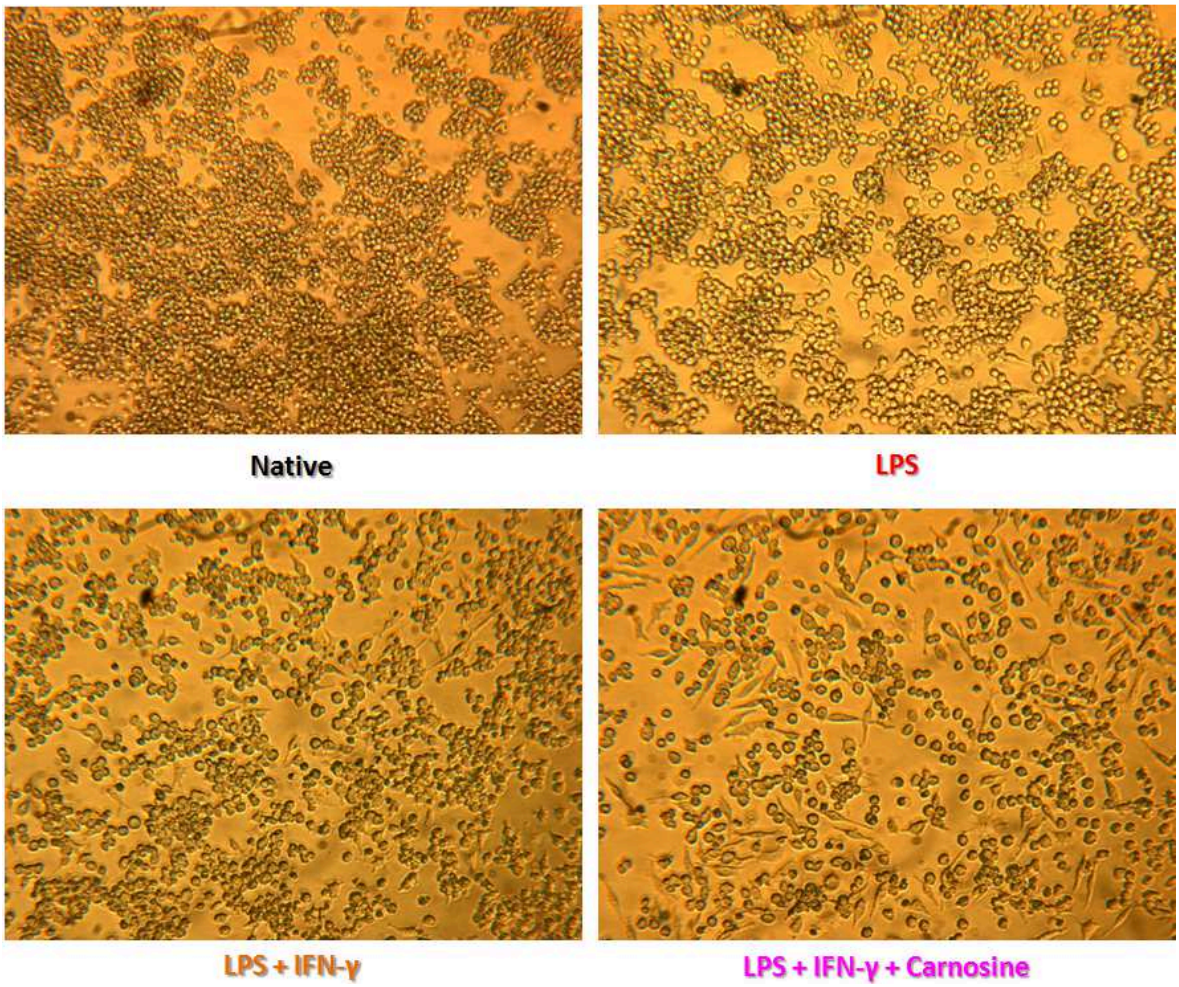

Figure 65 - Pictures obtained with phase contrast microscope showing the possible cell differentiation in response to different treatment.

This suggests a dual role for L-carnosine: promoting cell differentiation and increasing NO production in this type of cells.

Culturing RAW 264.7 cells using 25 cm^2 flask, experiments were carried out to evaluate the difference between nitrite concentrations inside and outside the cell.

Data in **Figg. 66-68** clearly show how the nitrite production is greater outside the cells.

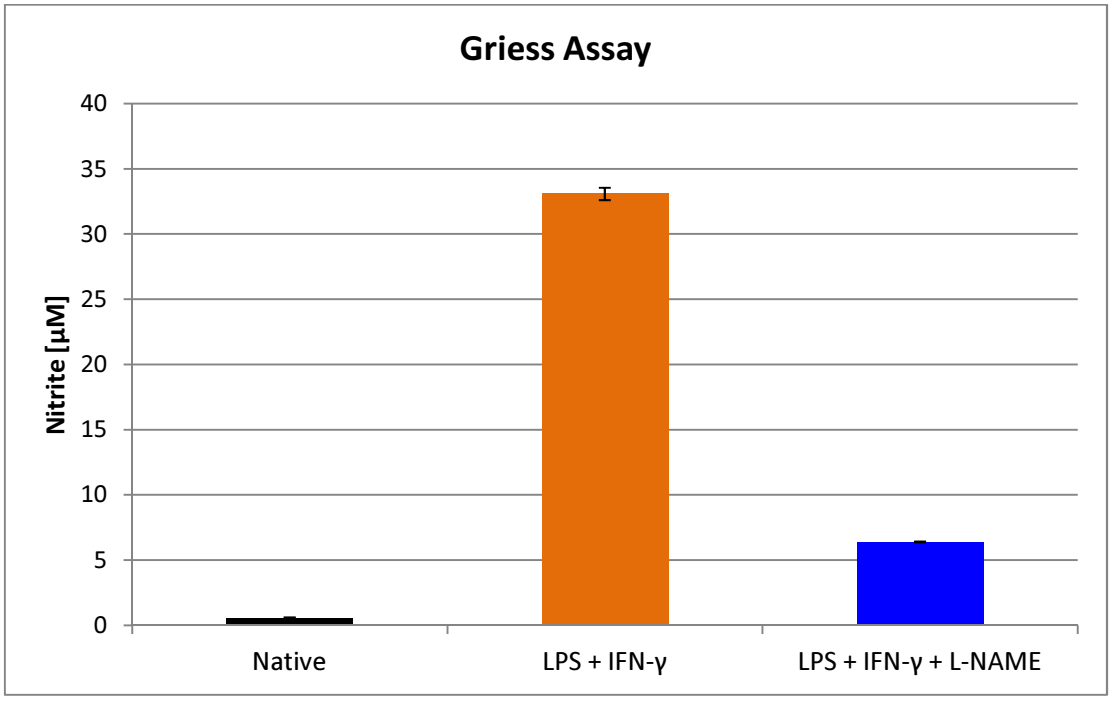

Figure 66 - Nitrite production outside the cell by RAW 264.7 cells. Final [ ] in culture: LPS = 100 ng/mL - IFN-γ = 600 U/mL - L-NAME (pre-treatment 1 h). Native cells, used such a control, are untreated. Stimulation time is 24 hrs. Data are means ± SEM (n=4) of 3 independent experiments.

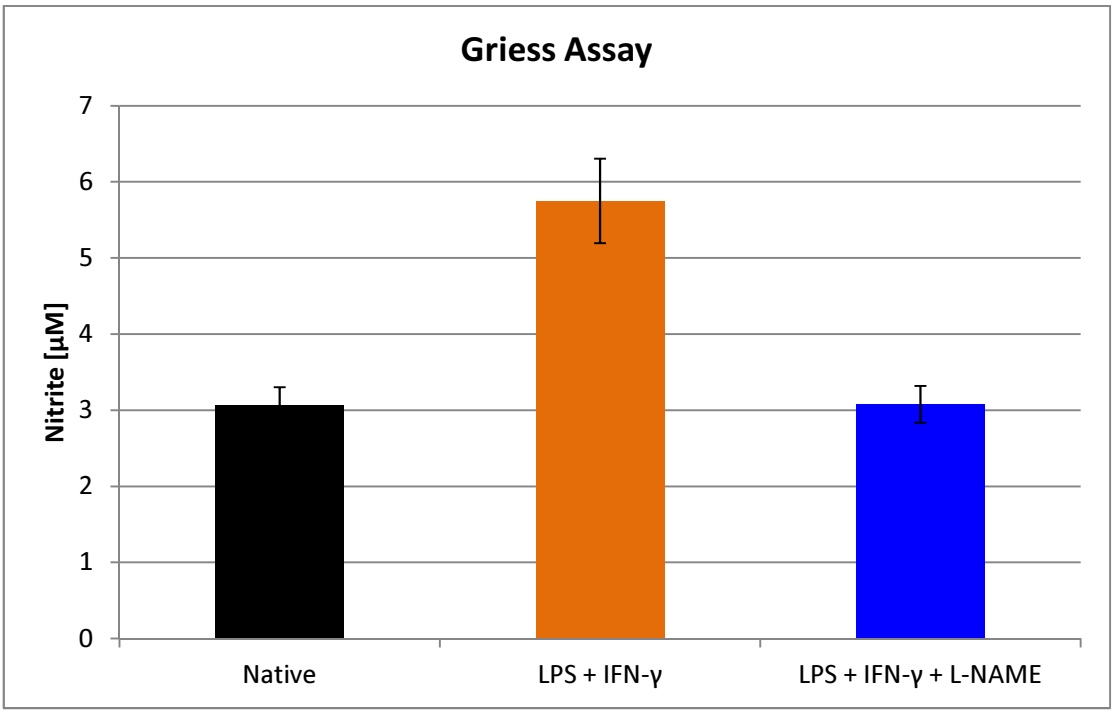

Figure 67 - Nitrite production inside RAW 264.7 cells. Final [ ] in culture: LPS = 100 ng/mL - IFN-γ = 600 U/mL - L-NAME (pre-treatment 1 h). Native cells, used such a control, are untreated. Stimulation time is 24 hrs. Data are means ± SEM (n=4) of 3 independent experiments.

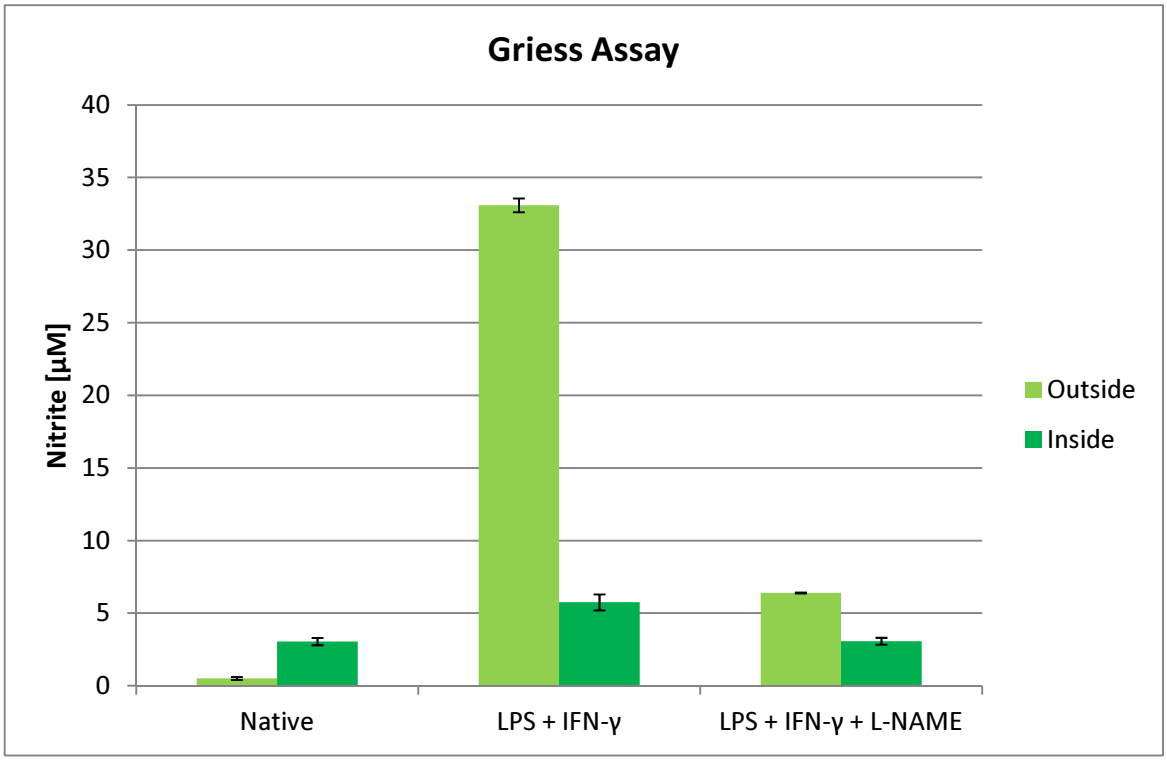

Figure 68 - Different nitrite production inside and outside of RAW 264.7 cells. Final [ ] in culture: LPS = 100 ng/mL - IFN-γ = 600 U/mL - L-NAME (pre-treatment 1 h). Native cells, used such a control, are untreated. Stimulation time is 24 hrs. Data are means ± SEM (n=4) of 3 independent experiments.

Both inside and outside the cell concentration of nitrite is greater for the stimulated cells (LPS together with IFN-γ). In both cases nitrite production is very low for the cells treated with the inhibitor, confirming once again the role of iNOS in nitric oxide and then nitrate production.

The experiments using culture flasks were carried out in anticipation of future experiments to be done using microchip electrophoresis and laser-induced fluorescence detection.

IN VITRO METABOLISM OF DYN A 1-17 IN CENTRAL NERVOUS SYSTEM TISSUES

Elevated concentrations of dynorphin have been implicated in a variety of neurological disorders. Consequently, elucidating the metabolic profile of Dyn A 1-17 in the central nervous system is essential to understanding the role it plays *in vivo*. Toward this end, i*n vitro* metabolism studies were performed with both rat brain and spinal cord slices.

To ascertain that accurate results were attainable in modified PBSA (mPBSA), the stability of Dyn A 1-17 in mPBSA was determined at room temperature and at 37°C over ten hours. The dynorphin concentration remained constant throughout (data not shown). There was no appearance of metabolites over time, however, the Dyn A 1-17

standards did contain peaks for the Dyn A 1-8, 1-13, and 2-17 metabolites even at the initial (t = 0) timepoint. The concentrations of these compounds were constant and did not increase during the stability study (**Figg. 69-70**).

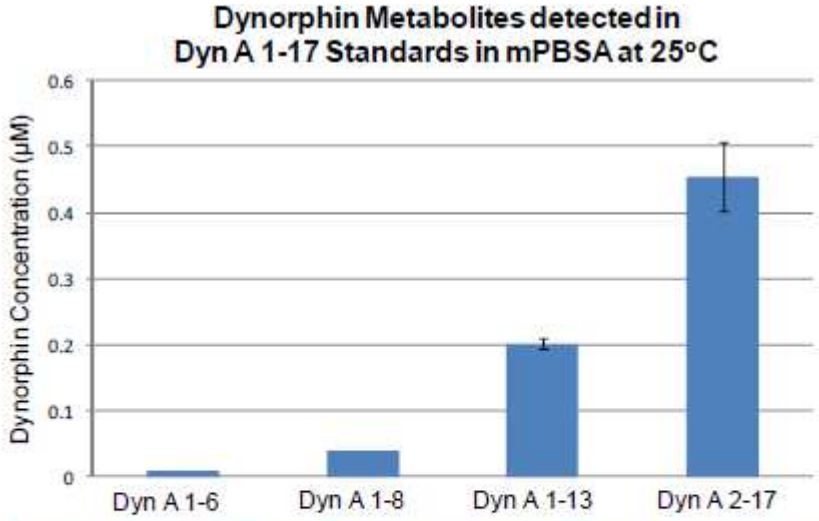

Dynorphin Metabolite	Average Conc (µM)	Standard Deviation
Dyn A 1-6	0.008	0.00018
Dyn A 1-8	0.039	0.00038
Dyn A 1-13	0.202	0.00758
Dyn A 2-17	0.454	0.05171

Figure 69 - Dynorphin metabolite concentrations in Dyn A 1-17 standards (1 µM) in mPBSA at 25°C. Values were constant over time as represented by the standard deviations (n=10).

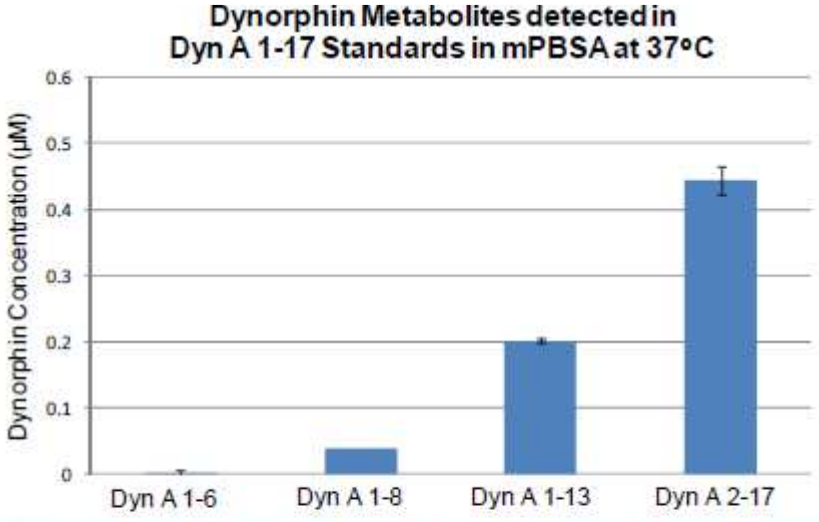

Dynorphin Metabolite	Average Conc (µM)	Standard Deviation
Dyn A 1-6	0.002	0.00053
Dyn A 1-8	0.038	0.00007
Dyn A 1-13	0.202	0.00337
Dyn A 2-17	0.443	0.02070

Figure 70 - Dynorphin metabolite concentrations in Dyn A 1-17 standards (1 µM) in mPBSA at 37°C. Values were constant over time as represented by the standard deviations (n=10).

The presence of dynorphin metabolites in Dyn A 1-17 standards could be contaminants from the synthetic process. The metabolite peaks were seen even when fresh Dyn A 1-17 standards were made and analyzed immediately. The concentrations also did not change over time which would have been expected if the Dyn A 1-17 was undergoing degradation in mPBSA.

If the peaks were due to contaminants from the synthetic process, one would expect an increase in the fragment concentrations when higher Dyn A 1-17 concentrations were used. However, the same concentrations were observed when both 1 µM and 25 µM Dyn A 1-17 stocks were analyzed. Another explanation is that in-source fragmentation is occurring, producing smaller peptidic ions at the electrospray source. This is a commonly reported phenomena when analyzing peptides by electrospray and is especially common for peptides with multiple charge sites. Data for these fragments (1-8, 1-13, and 2-17) is therefore presented as percent increase in concentration during the study duration (4 hours) to account for the initial metabolite concentrations present due to contamination or in-source fragmentation.

For Dyn A 1-6 which is not present as a contaminant, the change in concentration from t =0 to t=240 minutes is plotted.

Once the stability of the parent peptide was established, *in vitro* metabolism could be investigated in rat brain and rat spinal cord samples. The tissue slice was placed in mPBSA and prior to the addition of Dyn A 1-17, a basal sample was collected and analyzed via LC-MS/MS (**Figg. 71-72**).

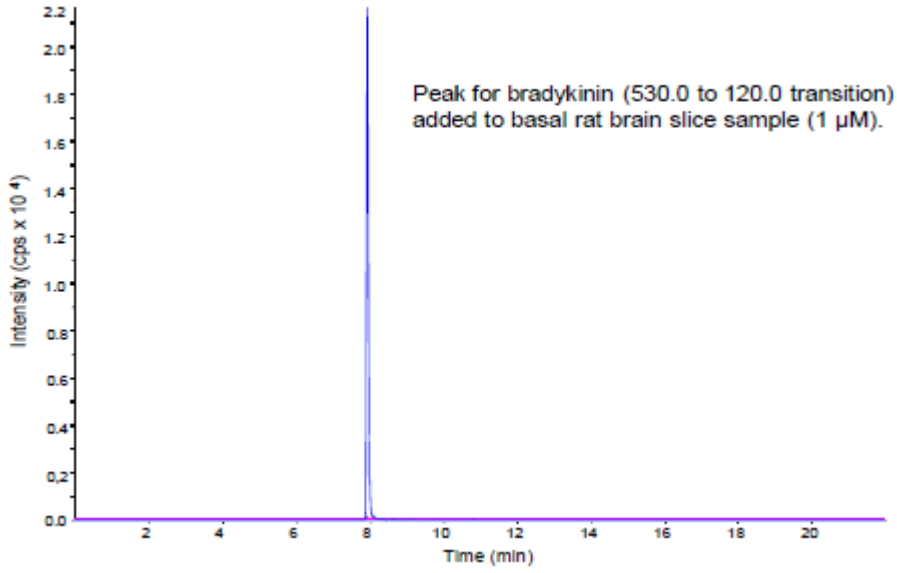

Figure 71 - Basal rat brain slices spiked with 1 µM internal standard (bradykinin). Overlays ofextracted ion chromatograms for Dyn A 1-6, 1-8, 1-13, 1-17, 2-17, and bradykinin. Only one peak is observed for bradykinin.

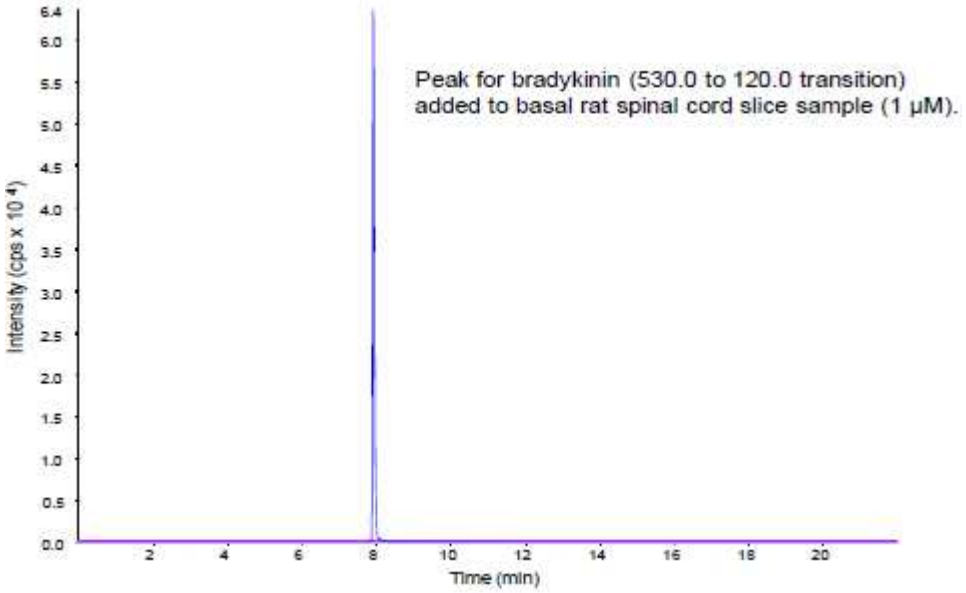

Figure 72 - Rat spinal cord slices spiked with 1 µM internal standard (bradykinin). Overlays ofextracted ion chromatograms for Dyn A 1-6, 1-8, 1-13, 1-17, 2-17, and bradykinin. Only one peak is observed for bradykinin.

No dynorphin peaks were observed in this sample with either tissue.

Dyn A 1-6 was the most abundant metabolite of Dyn A 1-17 in the presence of three separate rat brain slices, although the overall concentrations and time course of metabolism varied as can been seen in **Figg. 73-74**.

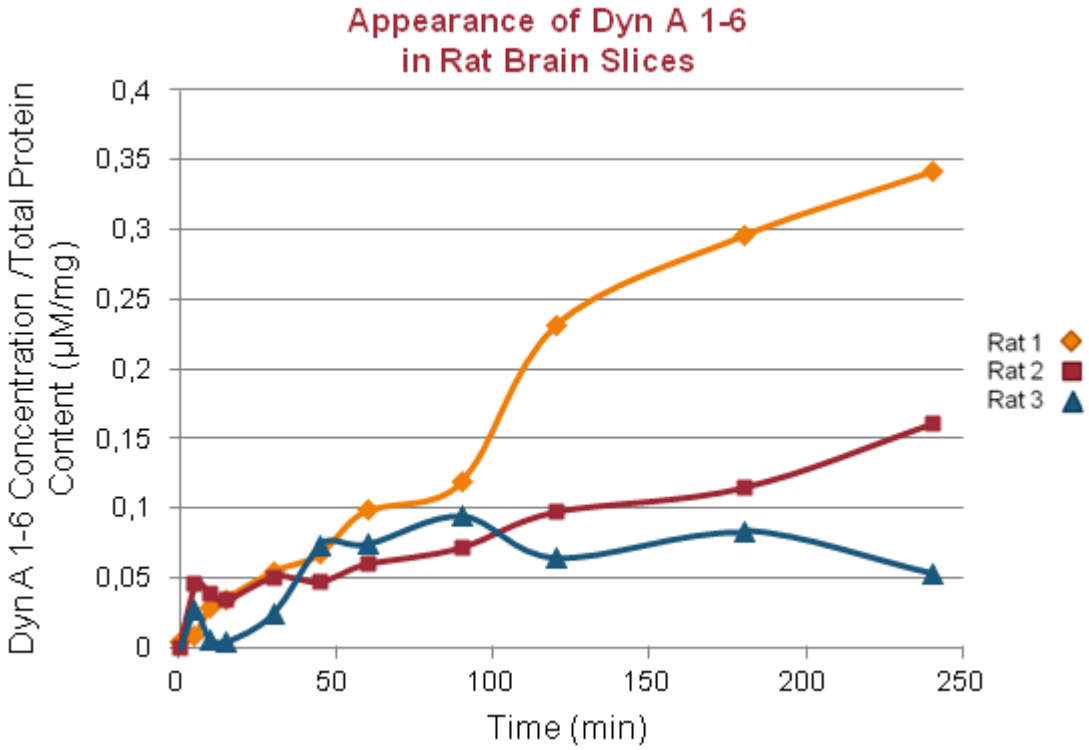

Figure 73 - Appearance of Dyn A 1-6 in rat brain slices. Each graph represents data from 1 rat. Concentrations (µM) are normalized to total protein content.

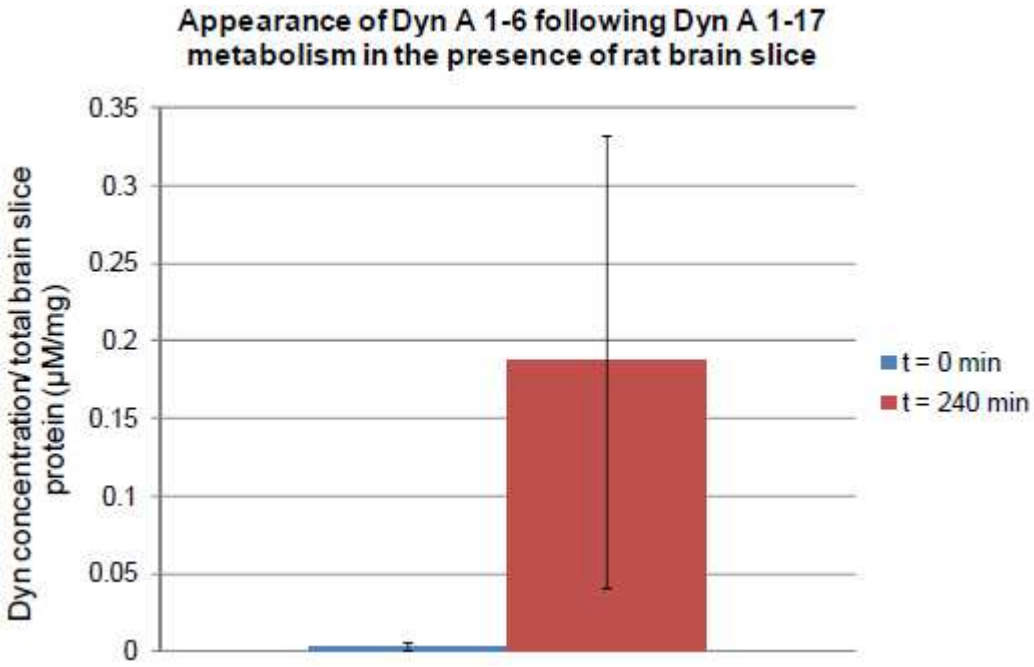

Figure 74 - Appearance of Dyn A 1-6 following Dyn A 1-17 metabolism in the presence of rat brain slices. Bar graph plots the average values (µM peptide/mg of protein) at t=0 and t=240 min, standard deviation as error bars n=3. Experiments performed in mPBSA at 25°C.

Dyn A 1-13 and Dyn A 2-17 were produced to a much lesser extent than Dyn A 1-6, exhibiting 23.0% and 27.8% increases, respectively, from the initial levels observed due to in-source fragmentation. Dyn A 1-8 did not significantly increase over time. The average percent increase for Dyn A 1-8, 1-13, and 2-17 following 4 hour incubation with rat brain slices is summarized in **Table 4**.

Dynorphin Metabolite	Average Percent Increase
Dyn A 1-8	2.01% (+/- 1.40)
Dyn A 1-13	23.0% (+/- 4.65)
Dyn A 2-17	27.8% (+/- 11.2)

Table 4 - Average percent increase of dynorphin metabolites 4 hour following incubation of Dyn A 1-17 with rat brain slices. Standard deviations in parentheses, n=3.

The presence of Dyn A 1-6 as a metabolite in rat brain was previously confirmed by copper complexation with capillary electrophoretic separation and UV detection.

In addition to investigating the metabolism of Dyn A 1-17 in rat brain slices, the metabolism in rat spinal cord slices was also investigated. Again Dyn A 1-6 was observed as the most abundant metabolite. The time course of Dyn A 1-6 appearance was even more varied than in the rat brain samples.

In the first rat (**Fig. 75**, blue diamonds), the Dyn A 1-6 appears to undergo additional metabolism itself after two hours in the presence of rat spinal cord, shown by the decrease in concentration after the two hour sample.

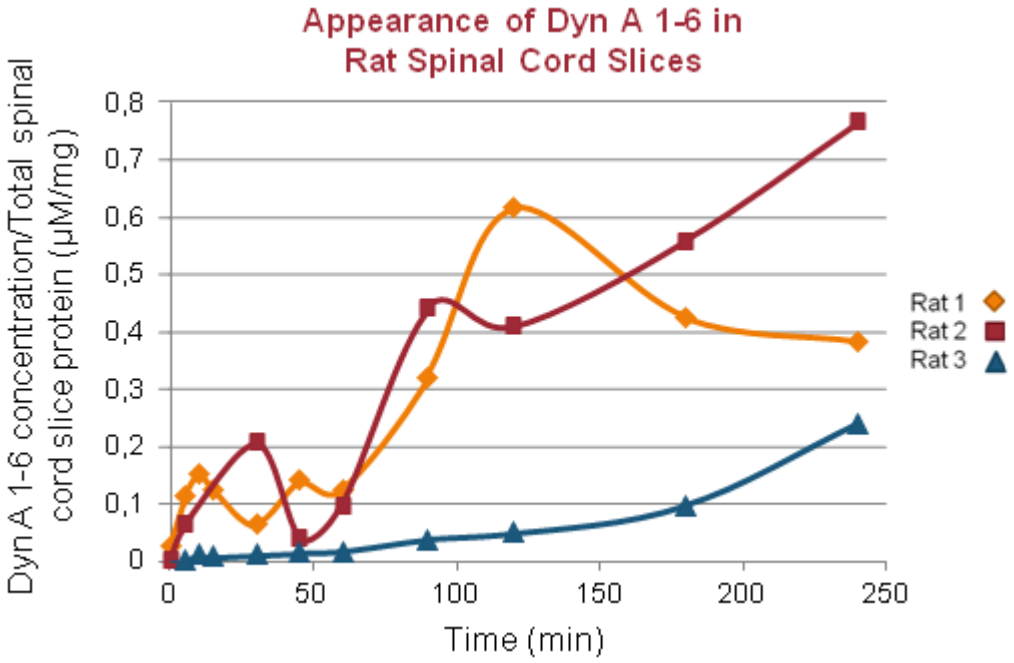

Figure 75 - Appearance of Dyn A 1-6 in rat spinal cord slices. Each graph represents data from 1 rat. Concentrations (µM) are normalized to total protein content.

In the third rat (**Fig. 75**, green triangles), Dyn A 1-6 is only produced to a small degree (less than 0.1 µM/mg of protein) until just after 2 hours when a rise in the metabolite concentration occurs. Dyn A 1-13 and 2-17 were also produced, only to a much lesser degree. Again, an increase in Dyn A 1-8 concentration was not observed.

The average percent increase for Dyn A 1-8, 1-13, and 2-17 following 4 hour incubation with rat spinal cord slices is summarized in **Table 5**.

Dynorphin Metabolite	Average Percent Increase
Dyn A 1-8	1.04% (+/- 0.14)
Dyn A 1-13	35.6% (+/- 20.8)
Dyn A 2-17	17.4% (+/- 0.88)

Table 5 - Average percent increase of dynorphin metabolites 4 hour following incubation of Dyn A 1-17 with rat spinal cord slices. Standard deviations in parentheses, n=3.

Some of the differences observed here can be attributed to inter-animal variability. Factors such as the age and weight of the animal can alter their metabolism. The isolation of the spinal cord was also a more tedious surgery. Unlike the brain (which is easily removed as a whole organ and then sliced in a reproducible way), often the

spinal cord was removed in small segments. Therefore, there was more variability with regard to the section of the spinal cord that was used in each experiment. Additionally, the viability of the tissues over the course of the study also plays a significant role in these studies. Rat central nervous system tissues are known to degrade more rapidly than the CNS tissues of other mammalian species (bovine and human for example). This would explain the increase in variability observed at the later timepoints of the metabolism studies.

Appearance of Dyn A 1-6 following Dyn A 1-17 metabolism in the presence of rat spinal cord slice is shown in **Fig. 76**.

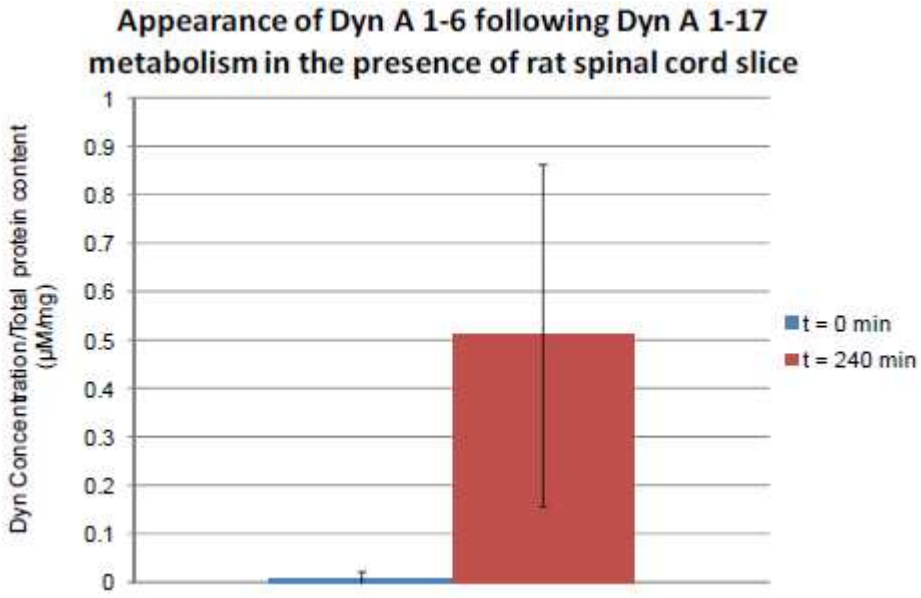

Figure 76 - Appearance of Dyn A 1-6 following Dyn A 1-17 metabolism in the presence of rat spinal cord slices. Bar graph plots the average values (µM peptide/mg of protein) at t=0 and t=240 min, standard deviation as error bars n=3. Experiments performed in mPBSA at 25°C.

IN VITRO METABOLISM OF DYN A 1-17 IN THE PRESENCE OF BBMECs

In addition to investigating the metabolism of Dyn A 1-17 in the presence of rat brain and spinal cord, the metabolism in the presence of BBMECs was also explored. Wells without added Dyn A 1-17 were used as a control, and no dynorphin peaks were observed in the control wells throughout the duration of the experiment (data not shown). Percent increase in each of the metabolites was again calculated to account for the initial levels of fragmentation produced at the electrospray source.

The time course of Dyn A 1-17 metabolism is seen in **Fig. 77**.

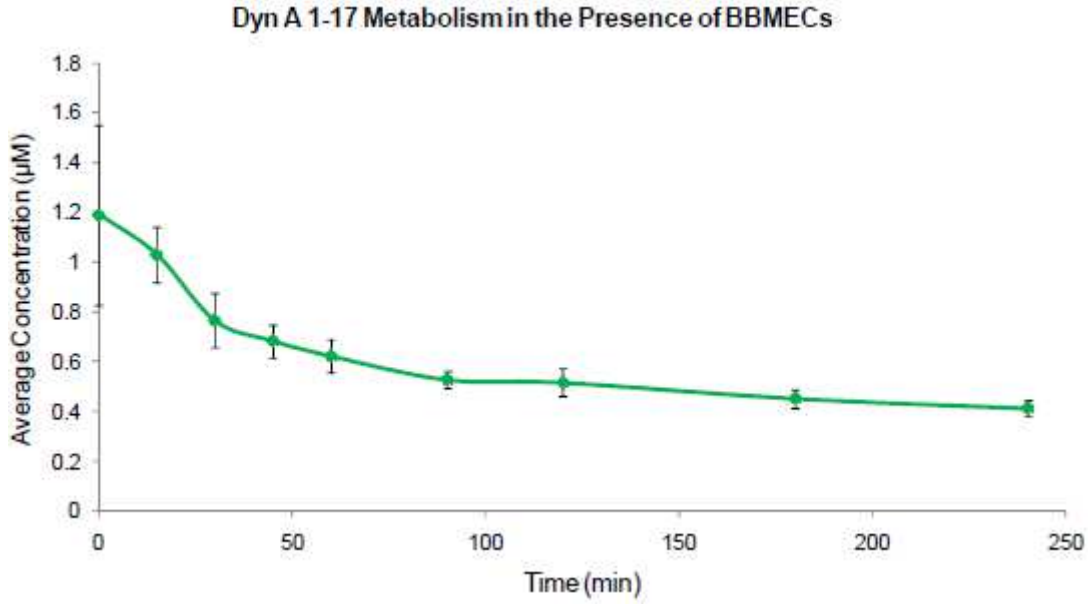

Figure 77 - Metabolism of Dyn A 1-17 in the presence of BBMECs following a 1 µM spike (n=3). Experiment performed in mPBSA at 37 °C.

A clear decrease in Dyn A 1-17 concentration over time is apparent. In order to identify the appearance of metabolites over time, LC-MS/MS data is presented as percent increase over the duration of each four hour study. No appreciable increase in Dyn A 1-8, 1-13, or 2-17 concentrations were observed as summarized in **Table 6**.

Dynorphin Metabolite	Average Percent Change
Dyn A 1-8	2.19% (+/- 0.503)
Dyn A 1-13	-0.869% (+/- 1.31)
Dyn A 2-17	-1.15% (+/- 0.903)

Table 6 - Average percent increase of dynorphin metabolites 4 hour following incubation of Dyn A 1-17 with BBMECs. Standard deviations in parentheses, n=3.

Low amounts of the peptides were present for the duration of the study due to in-source fragmentation; however, in each of the wells, the concentration did not change over time. The concentration of Dyn A 1-6 however did increase over time. The presence of Dyn A 1-6 as a major metabolite of 1-17 agrees well with the previously reported metabolism in the rat brain and rat spinal cord. Therefore characterizing the transport of this metabolite at the blood brain barrier could contribute to a better understanding of the role dynorphin may play in neuropathic pain and other neurological disorders.

Appearance of Dyn A 1-6 in the presence of BBMECs following incubation with 1 µM Dyn A 1-17 is shown in **Fig. 78**.

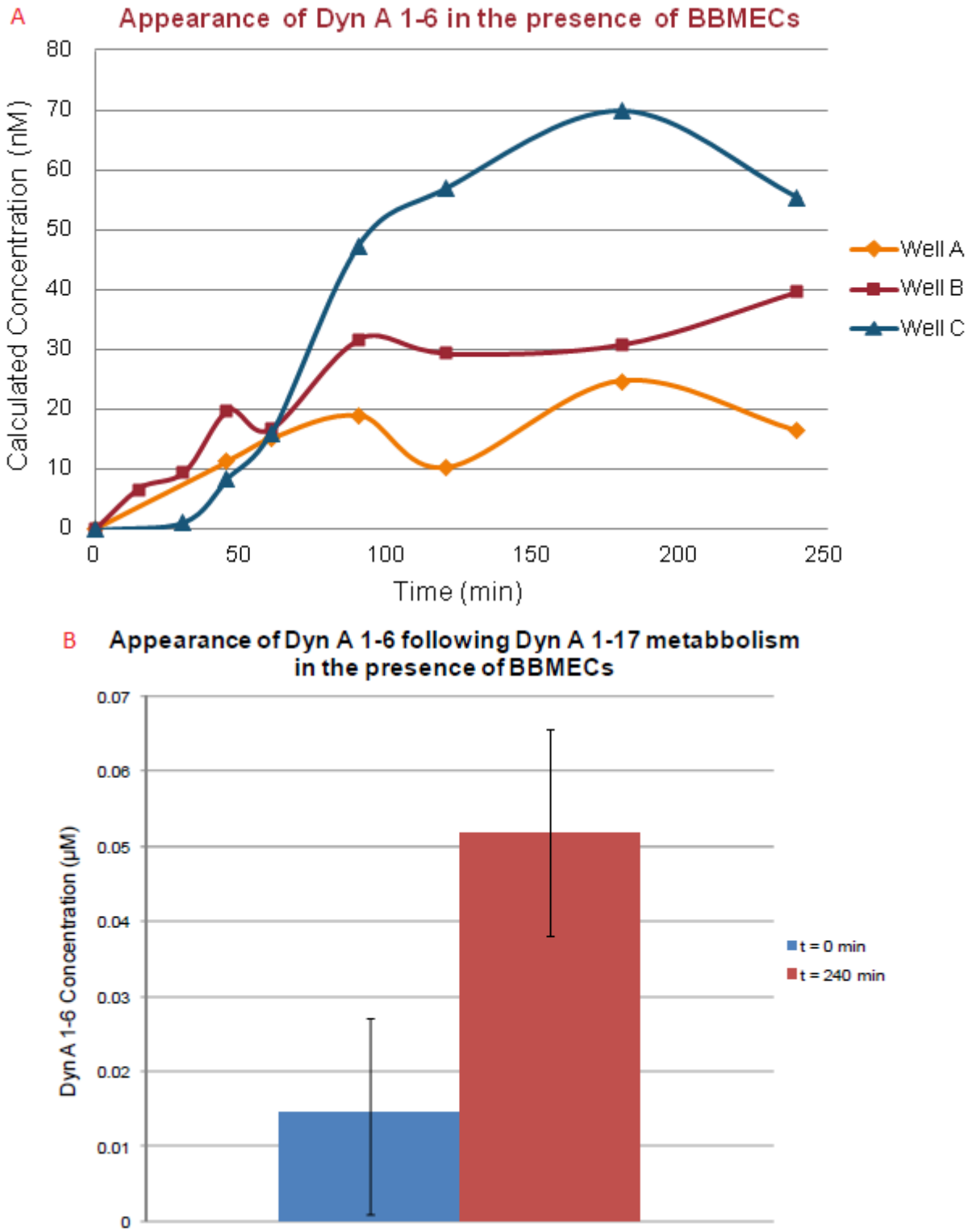

Figure 78 - Appearance of Dyn A 1-6 in the presence of BBMECs following incubation with 1 µM Dyn A 1-17. Each trace is 8data from 1 well of a 12 well cell culture plate (A). Average concentration (n=3) in the initial sample (t=0 min timepoint, blue) and the concentration following a 4 hour incubation (t=240 min, red) (B). Experiment performed in mPBSA at 37°C.

BLOOD BRAIN BARRIER PERMEABILITY OF DYN A 1-6, A MAJOR METABOLITE OF DYN A 1-17

Dyn A 1-6 has been identified as a major metabolite of the parent peptide Dyn A 1-17 in both the central nervous system (brain and spinal cord) as well as in peripheral tissues (blood and plasma). For this reason, the BBB permeability of Dyn A 1-6 was investigated, using BBMECs grown on polycarbonate membranes and mounted in Side-by-Side™ diffusion chambers. Fluorescein was utilized as a low permeability control following all experiments to examine monolayer integrity.

Dyn A 1-6 permeability was screened by the above method. Both the directional and temperature dependence of Dyn A 1-6 permeability were determined. The apparent permeability coefficient of Dyn A 1-6 was calculated to be $P_{app}=6.59x10^{-5}$ cm/s ($\pm 1.74x10^{-5}$, n=4), in the apical to basolateral direction, and $P_{app}=6.43x10^{-5}$ cm/s ($\pm 1.61x10^{-5}$, n=4), in the basolateral to apical direction. There was no difference in the permeability based on direction (**Fig. 79**).

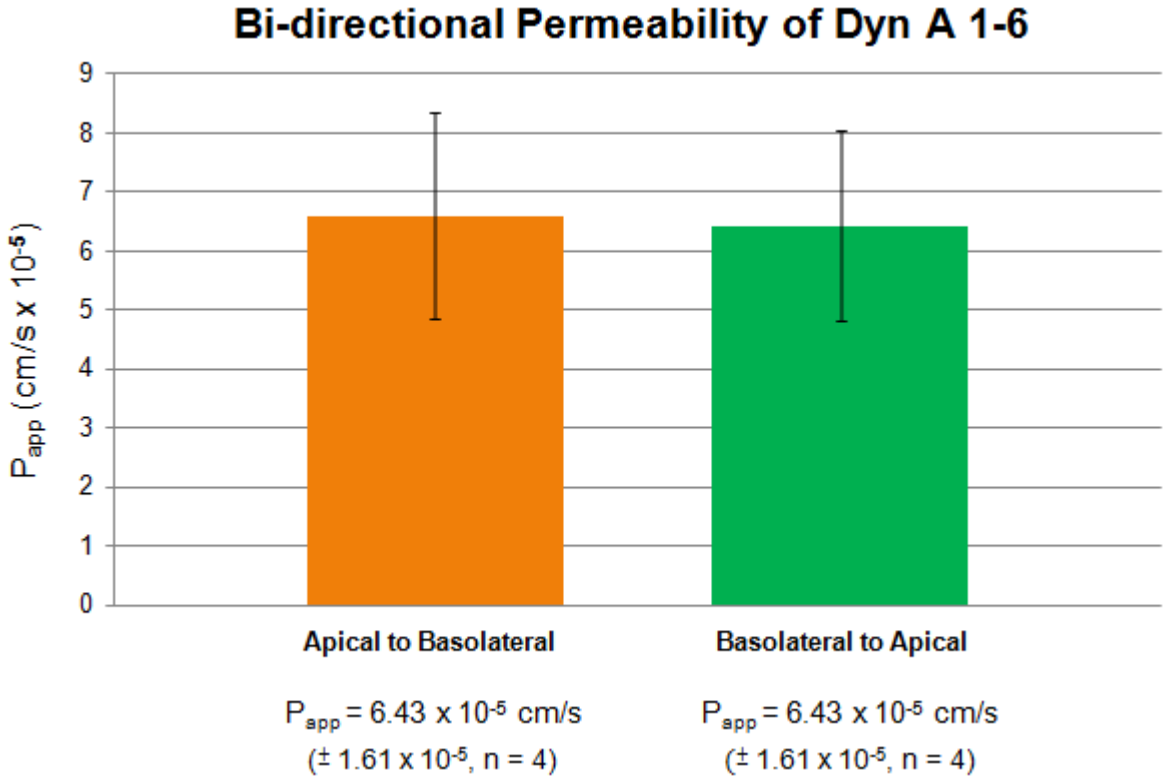

Figure 79 - Bi-directional apparent permeability coefficients of Dyn A 1-6 (n=4 in each direction).

A decrease in permeability was observed at 4°C, P_{app}=1.11x10^{-5} cm/s (± 2.90x 0^{-6}, n=4, p<0.005) indicative of a carrier-mediated transport system (**Fig. 80**).

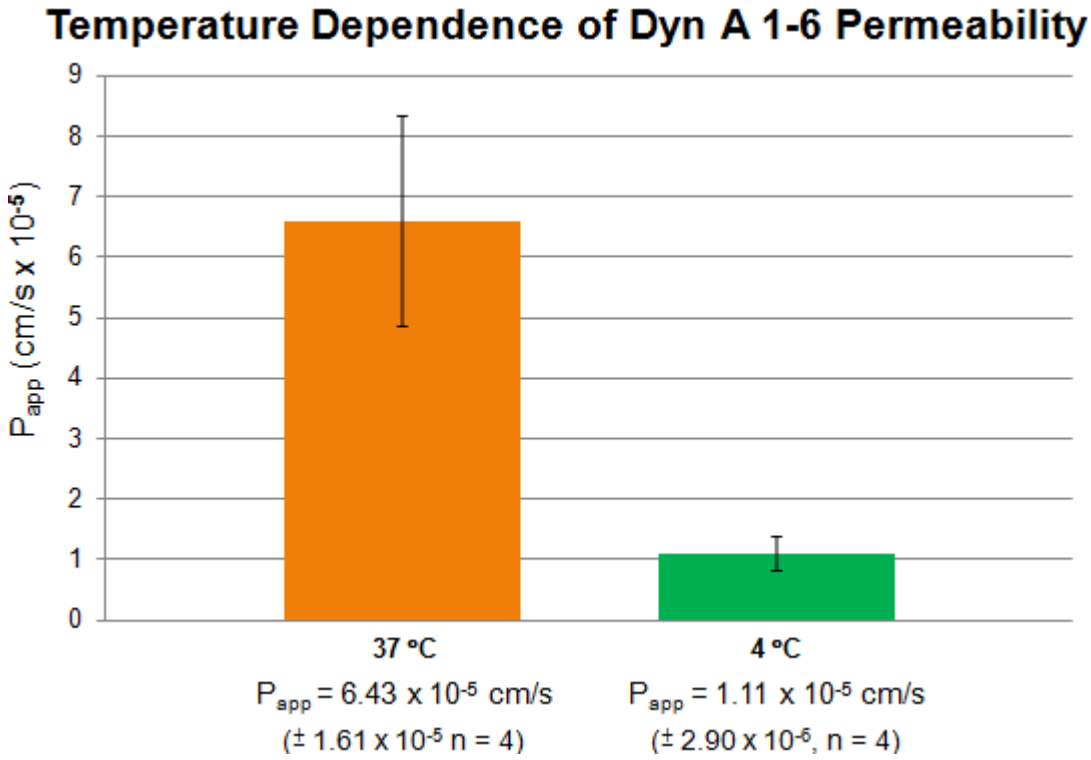

Figure 80 - Temperature dependence of the apical to basolateral transport of Dyn A 1-6 (n=4 at each temperature) p<0.005.

Fluorescein was utilized as a control following the end of each experiment. Values for fluorescein permeability are presented in **Fig. 81**.

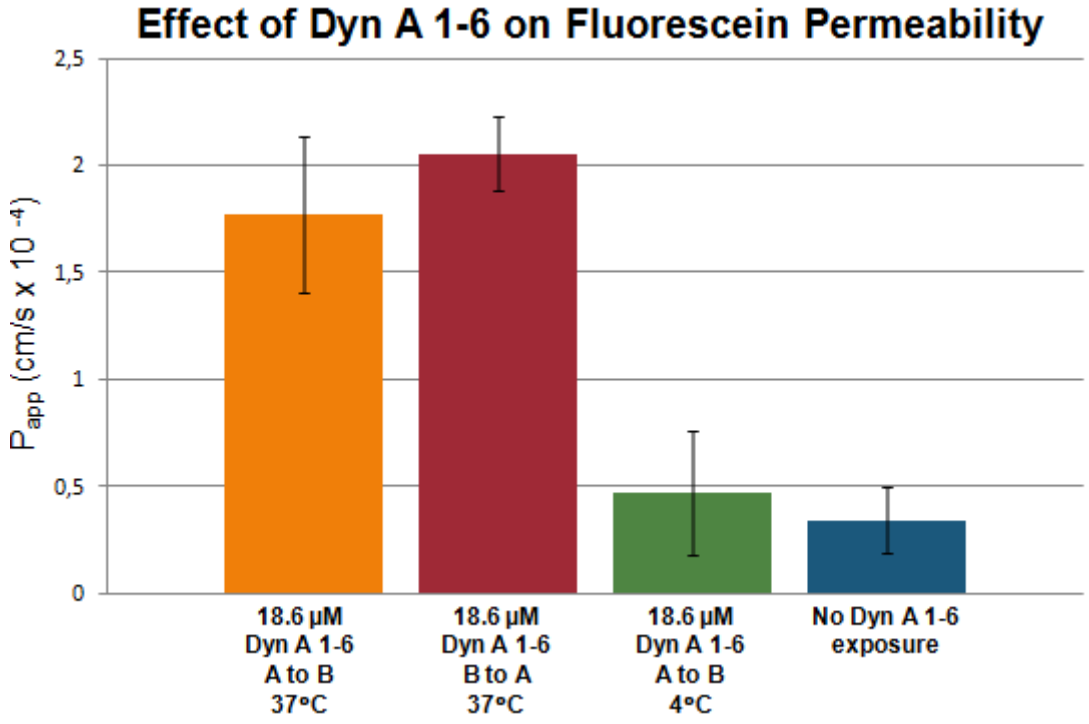

Figure 81 - Effect of pre-treatment with 18.6 µM Dyn A 1-6 on the BBB permeability of the low molecular weight, low permeability marker, fluorescein (10 µM), n=4.

An interesting observation was made when the fluorescein permeability controls were analyzed following studies with Dyn A 1-6. It was found that the permeability values for fluorescein were increased following the Dyn A 1-6 exposure at 37°C. However, at 4°C the permeability coefficient of fluorescein was not affected by the peptide. This effect was further investigated by incubating mounted monolayers for 2 hours in mPBSA at 37°C. Following the 2 hour incubation, 0, 20, and 100 µL of mPBSA were removed and replaced with Dyn A 1-6 resulting in final concentrations in the chamber of 0, 18.6, and 46.6 µM. The fluorescein permeability increased in a linear fashion with increasing exposure to Dyn A 1-6, R^2= 0.9995..

The permeability values for Dyn A 1-6 in the apical to basolateral and basolateral to apical directions fall along this line, as shown by the purple and orange data points in **Fig. 82**, suggesting that this peptide is responsible for increasing BBB permeability.

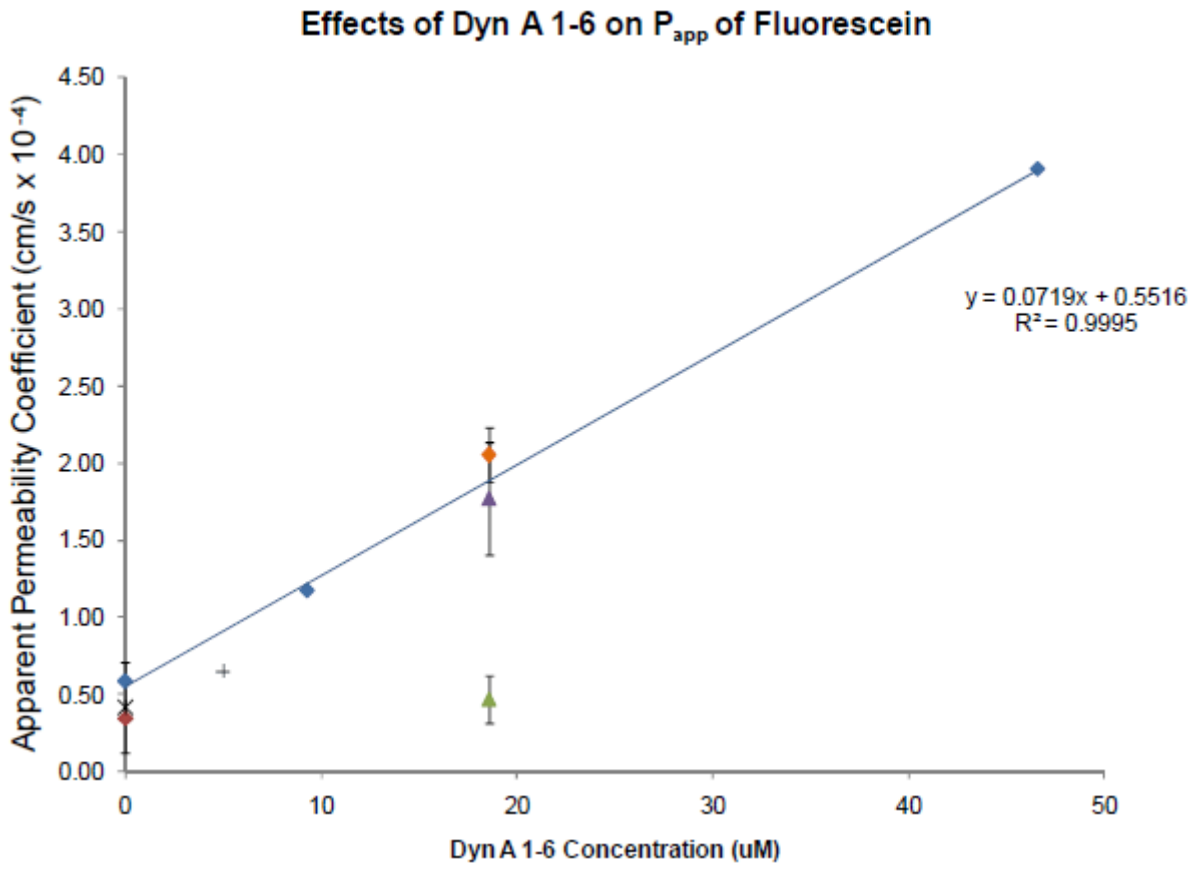

Figure 82 - Effect of pre-treatment with varying Dyn A 1-6 concentrations (blue diamond) on the BBB permeability of the low molecular weight, low permeability marker, fluorescein (10 µM). Fluorescein permeability without Dyn A 1-6 incubation (red diamond), fluorescein permeability following 240 min Dyn A 1-6 pretreatment A to B (purple triangle) and B to A (orange diamond), and fluorescein permeability following 120 min Dyn A 1-6 pretreatment at 4°C (green triangle). Also shown are literature values for the permeability of fluorescein alone (x) and following pre-treatment with leucine-enkephalin (+).

A similar phenomenon was observed by Thompson and Audus with the opioid peptide leucine enkephalin, and the reported values for fluorescein permeability both with and without leucine enkephalin pretreatment are also plotted in **Fig. 82**.

DISCUSSION

Data obtained in our experiment show that Aβ25-35 after incubation at 37°C, spontaneously forms amorphous or fibrillary aggregates. In presence of copper Aβ25-35 fibrillogenesis undergoes changes, tightly linked to the time of incubation, especially in the shift from one species to another. These changes may be related to the toxicity degree measured after treatment of neuroblastoma cell cultures (SH-SY5Y). Cellular toxicity increase, induced by incubation with copper, may be explained with a slowdown in the evolution toward non-toxic structures, and a consequent stabilization of oligomeric aggregates, notoriously much more toxic than fibrillary species.

In our experiments it was seen that the incubation favors the formation of β-sheet structures by hA17-29. The state of aggregation changes according to incubation time. The presence of copper in solution slows the fibrillogenesis process, and favors the stabilization of oligomeric species, instead other factors such as zinc and ribose favor the formation of large aggregates. The neuroblastoma cells viability decreases in relation to incubation time of the peptide fragment. The pre-incubation in the presence of copper further increases the toxicity of the peptide. This decrease of viability could also depend on the formation of toxic free radical species produced as a result of Fenton reactions.

The use of conditioned medium from RBE4 has allowed us to highlight the key role of the interactions between endothelial and neuronal cells in the proper functioning of the "neurovascular unit". The brain endothelial cells may in fact produce potent neuroprotective factors. The combined use of antibodies to block specific membrane receptors has allowed the identification of such factors may be actually involved in the protection against neurotoxicity induced by amyloid peptides. It is known that the conditioned medium from endothelial cells contains several factors, including VEGF. In our experiments blocking the receptor Flk-1 with a specific antibody, it was found the protective effect of the conditioned medium to be eliminated, demonstrating the involvement of VEGF in neuroprotection due to endothelial cell conditioned medium.

Among the possible reasons for the protective effect of conditioned medium from RBE4 the production of αB-crystallin has been taken into consideration. The production of αB-crystallin has been shown directly proportional to the concentration of Aβ25-35 peptide used to treat cell cultures. This is in agreement with literature data

in which increased production of HSP, necessary for the proper folding of proteins and for the cell protection, is connected to events of cellular stress. The αB-crystallin has cytoprotective effect by inhibiting protein aggregation, and disrupting the proteolytic activity of caspase 3. It protects against oxidative stress. *In vitro* it inhibits the fibrils formation by different amyloidogenic proteins, including the β-amyloid. In addition, αB-crystallin plays a key role in the expression and excretion of VEGF, thus participating, even if indirectly, to the neuroprotective mechanisms.

A microchip electrophoresis method using DAF-FMDA and 6-CFDA with LIF detection was described for the quantitation of intracellular NO concentrations in bulk cell lysates. This method was used to quantitate intracellular concentrations of NO in native and stimulated Jurkat cells. It was found that the average intracellular NO concentrations for LPS-stimulated and native Jurkat cells were 1.5 mM and 0.6 mM, respectively. These results provide an average value of NO production per cell.

We have developed an integrated glass/PDMS hybrid microfluidic device for high throughput analysis of single cells. The device uses a new channel manifold design to significantly improve the reliability and robustness of the cell lysis and lysate injection. Intracellular detection of NO in single cells was accomplished using DAF-FMDA and 6-CFDA. The single cell analysis system was used to determine the increase in NO production following stimulation with LPS. A three-hour stimulation of the cells with LPS resulted in a 2-fold increase in NO production. A comparison of bulk and single cell NO measurements was performed, and the average NO production in single cells compared well to the increase measured at the bulk cell level. In future studies, we will incorporate electrodes in the bulk and single cell analysis chips for the simultaneous detection of NO, peroxynitrite as well as other molecules that play an important role in inflammation including glutathione, ascorbic acid and nitrotyrosine by microchip electrophoresis with amperometric detection.

The influence of several factors on the production of nitric oxide by macrophages was investigated. It was seen that both the stimulation with LPS alone or together with IFN-γ leads to increased production of nitrates (therefore NO) compared to the control. Furthermore, it has been established the role of iNOS in the production of NO. Our experiments have also shown that L-carnosine , which is involved in many cellular

processes, has a dual role: it increases the production of nitrite and promotes cell differentiation.

In our experiments we used the Griess assay to measure nitrite in both inside and outside the cell. We have shown that under stress conditions within the stimulated cells have a higher concentration of nitrates when compared to the control (untreated cells). Also the production of nitrates outside of stimulated cells was much greater than the amount of nitrates inside.

The metabolism of Dyn A 1-17 has been characterized in the presence of rat brain and spinal cord slices as well as in the presence of BBMECs, an *in vitro* model of the BBB. Dyn A 1-6 was found to be the predominant metabolite in each of these systems. The transport of this metabolite across the BBB was then characterized and was found to be bi-directional. Dyn 1-6 transport was decreased at 4°C indicating energy (ATP) driven transport mechanism. The metabolite was also found to increase the permeability of the blood brain barrier to a low molecular weight, low permeability control substance, fluorescein. Such effects suggest a role of this dynorphin metabolite in the opening of the blood brain barrier, and potentially a role of the metabolite in the neurotoxic effects of Dyn A 1-17. Further studies would be necessary to determine the mechanism by which this opening occurs.

BIBLIOGRAPHY

[1] Carrell RW and Lomas DA (1997) *Lancet* 350, 134-138.

[2] Kelly JW (1996) *Curr. Opin. Struct. Biol.* 6, 11-17.

[3] Thomas PJ, Qu BH and Pedersen PL (1995) *Trends Biochem. Sci.* 20, 456-459.

[4] Soto C (1999) *J. Mol. Med.* 77, 412-418.

[5] Carrell RW and Gooptu B (1998) *Curr. Opin. Struct. Biol.* 8, 799-809.

[6] Gaggelli E, Kozlowski H, Valensin D and Valensin G. (2006) *Chem. Rev.* 106, 1995-2044

[7] Stefani M (2004) *Biochimica et Biophysica Acta* 1739, 5-25

[8] Johnson WG (2000) *J. Anat.* 196, 609-616.

[9] Glenner GG (1980) *N. Engl. J. Med.* 302, 1283-1292.

[10] Sipe JD (1992) *Ann. Rev. Biochem.* 61, 947-975.

[11] Serpell LC, Sunde M, Benson MD, Tennent GA, Pepys MB and PE Fraser (2000) *J. Mol. Biol.* 300, 1033-1039.

[12] Sunde M, Serpell LC, Bartham M, Fraser PE, Pepys MB and Blake CF (1997) *J. Mol. Biol.* 273, 729-739.

[13] Gillmore JD, Hawkins PN and Pepys MB (1997) *Br. J. Haematol.* 99, 245-256.

[14] Westermark P (1995) *Scand. J. Rheumatol.* 24, 327-329.

[15] Price DL, Sisodia SS and Borchelt DR (1998) *Science* 282, 1079-1083.

[16] Gurney ME (2000) *Bioessays* 22, 297-304.

[17] Price DL, Wong PC, Markowska AL, Lee MK, Thinakaren G, Cleveland DW, Sisodia SS and Borchelt DR (2000) *Ann. N.Y. Acad. Sci.* 920, 179-191.

[18] Araki S, Yi S, Murakami T, Watanabe S, Ikegawa S, Takahashi K and Yamarnura K (1994) *Mol. Neurobiol.* 8, 15-23.

[19] Emilien G, Maloteaux JM, Beyreuther K and Masters CL (2000) *Arch. Neurol.* 57, 176-181.

[20] Janson J, Soeller WC, Roche PC, Nelson RT, Torchia AJ, Kreutter DK and Butler PC (1996) *Proc. Natl. Acad. Sci. USA* 93, 7283-7288.

[21] Weissmann C, Fischer M, Raeber A, Bueler H, Sailer A, Shmerling D, Rulicke T, Brandner S and Aguzzi A (1998) *Rev. Sci. Tech.* 17, 278-290.

[22] Van Leuven F (2000) *Prog. Neurobiol.* 61, 305-312.

[23] Duff K (1998) *Curr. Opin. Biotechnol.* 9, 561-564.

[24] Alzheimer A (1907) *Psychiatrie* und *Psychisch-Gerichtliche Medizin* 64, 146-148.

[25] Glenner GG and Wong CW (1984) *Biochem. Biophys. Res. Commun.* 120, 885-890.

[26] Masters CL, Simms G, Weinman NA, Multhaup G, McDonald BL and Beyreuther K (1985) *Proc. Natl. Acad. Sci. USA* 82, 4245-4249.

[27] Selkoe DJ (2004) *Nat. Cell. Biol.* 6, 1054-1061.

[28] Rozemuller JM, Eikelenboom P and Stam FC (1986) *Virchows Arch. B. Cell. Pathol.* 51, 247-254.

[29] Wyss-Coray T (2006) *Nature Med.* 12, 1005-1015.

[30] Markesbery WR (1997) *Free Radic. Biol. Med.* 23, 134-147.

[31] McGeer P., Rogers J and McGeer EG (2006) *J. Alzheimers Dis.* 9, 271-6.

[32] Griffin WST, Stanley LC, Ling C, MacLeod V, Perrot LJ, White CL III, Araoz C (1989) *Proc. Natl. Acad. Sci. USA* 86, 7611-7615

[33] Rogers J, Luber-Narod J, Styren SD, Civin WH (1988) *Neumbiol. Aging* 9, 339-349.

[34] McGeer PL, Schulzer M, McGeer EG (1996). *Neurology* 47, 425-432.

[35] Rogers J, Coopers NR, Webster S, Schultz J, McGeer PL, Styren SD, Civin WH, Brachova L, Bradt B, Ward P, Liebberburgh I (1992) *Proc. Natl. Acad. Sci. USA* 89, 10016-10020.

[36] Mrak RE, Sheng JG, Griffin WST (1995) *Human Pathol.* 26, 816-823.

[37] Mrak E, Griffin WST (2005) *J. Alzheimers Dis*. 8, 369-375

[38] Mrak RE, Griffin WST (2007) *J. Neuropathol. Exp. Neural.* 66, 683-686.

[39] Bauer J, Strauss S, Schreiter-Gasser U, Ganter U, Schlegel P, Witt I, Yolk B and Berger M (1987) *FEBS Lett.* 285, 525-526.

[40] Luterman JD, Haroutunian V, Yemul S, Ho L, Purohit D, Aisen PS, Mohs R, Pasinetti GM (2000) *Arch. Neurol.* 57, 1153-1160.

[41] Wood JA, Wood PL, Ryan R, Graff-Radford NR, Pilapil C, Robitaille Y, Quiron R (1993) *Brain Res.* 629, 245-252.

[42] Du Yan S, Zhu H, Fu J, Yan SF, Roher A, Tourtellotte WW, Rajavashisth T, Chen X, Godman GC, Stern D and Schmidt AM (1997) *Proc. Natl. Acad. Sci. USA.* 94, 5296-5301.

[43] Van der Wai EA, Gomez-Pinilla F, Cotman CW (1993) *Neuroreport.* 4, 69-72.

[44] Hensley K, Fedynyshyn J, Ferre S, Floyd RA, Bordon B, Grammas P, Hamdheydari L, Mhatre MC, Mou S, Pye QN, Stewart CA, West MS, West S and Williamson KS (2003) *Neurobiol. Dis.* 14, 74-80.

[45] Hensley K, Abd El-Moaty H, Hunter J, Mhatre MC, Mou S, Nguyen K, Potapova T, Pye QN, Qi M, rice H, Stewart CA, Stroukoff K and West MS (2006) *J. Neuminflam.* 3, 2-10.

[46] Gabbita SP, Robinson KA, Stewart CA, Floyd RA and Hensley K (2000) *Arch. Biochem. Biophys.* 376, 1-13.

[47] Fuller S, Steele M, Imholz P and Munch G Mutat (2010) *Mutat. Res.* 690, 40-9.

[48] Hensley K, Floyd RA, Zheng NY, Nael R, Robinson KA, Nguyen X, Pye QN, Stewart CA, Geddes J, Markesbery WR, Patel E, Johnson GV and Bing G (1999) *J. Neurochem.* 72, 2053-2058.

[49] Lorton D, Schaller J, Lala A and De Nardin E (2000) *Neurobiol. Aging* 21, 463-473.

[50] Yan SD, Chen X, Fu J, Chen M, Zhu H, Roher A, Slattery T, Zhao L, Nagashima M, Morser J, Migheli A, Nawroth P, Stem D and Schmidt AM (1996) *Nature* 382, 685-691.

[51] El Khoury JB, Moore KJ, Means TK, Leung J, Terada K, Toft M, Freeman MW and Luster AD (2003) *J. Exp. Med.* 197, 1657-1666.

[52] Adlard PA and Bush AI (2006) *J. Alzheimers Dis.* 10, 145-163.

[53] Gorlovoy P, Larionov S, Pham TT and Neumann H (2009) *FASEB J.* 23, 2502-2513.

[54] Bryan KJ, Zhu Z, Harris PL, Perry G, Castellani RJ, Smith MA and Casadesus G (2008) *Mol. Neurodegener.* 3, 13.

[55] Allinson TM, Parkin ET, Turner AJ and Hooper NM (2003) *J. Neurosci. Res.* 74, 342-352.

[56] Vassar R, Bennett BD, Babu-Khan S, Kahn S, Mendiaz EA, Denis P, Teplow DB, Ross S, Amarante P, Loeloff R, Luo Y, Fisher S, Fuller J, Edenson S, Lile J, Jarosinski MA, Biere AL, Curran E, Burgess T, Louis JC, Collins F, Treanor J, Rogers G and Citron M (1999) *Science* 286, 735-741.

[57] Hussain I, Powell D, Howlett DR, Tew DG, Meek TD, Chapman C, Gloger IS, Murphy KE, Southan CD, Ryan DM, Smith TS, Simmons DL, Walsh FS, Dingwall C and Christie G (1999) *Mol. Cell. Neurosci.* 14, 419-427.

[58] Sinha S, Anderson JP, Barbour R, Basi GS, Caccavello R, Davis D, Doan M, Dovey HF, Frigon N, Hong J, Jacobson-Croak K, Jewett N, Keim P, Knops J, Lieberburg I, Power M, Tan H, Tatsuno G, Tung J, Schenk D, Seubert P, Suomensaari SM, Wang S, Walker D, Zhao J, McConlogue L and John V (1999) *Nature* 402, 537-540.

[59] Wolfe MS, Xia W, Ostaszewski BL, Diehl TS, Kimberly WT and Selkoe DJ (1999) *Nature* 398, 513-517.

[60] Steiner H, Winkler E, Edbauer D, Prokop S, Basset G, Yamasaki A, Kostka M and Haass C (2002) *J. Biol. Chem.* 277, 39062-39065.

[61] Francis R, McGrath G, Zhang J, Ruddy DA, Sym M, Apfeld J, Nicoll M, Maxwell M, Hai B, Ellis MC, Parks AL, Xu W, Li J, Gurney M, Myers RL, Himes CS, Hiebsch R, Ruble C, Nye JS and Curtis D (2002) *Dev. Cell.* 3, 85-97.

[62] Levitan D, Lee J, Song L, Manning R, Wong G, Parker E and Zhang L (2001) *Proc. Natl. Acad. Sci. USA* 98, 12186-12190.

[63] Yu G, Nishimura M, Arawaka S, Levitan D, Zhang L, Tandon A, Song YQ, Rogaeva E, Chen F, Kawarai T, Supala A, Levesque L, Yu H, Yang DS, Holmes E, Milman P, Liang Y, Zhang DM, Xu DH, Sato C, Rogaev E, Smith M, Janus C, Zhang Y, Aebersold R, Farrer LS, Sorbi S, Bruni A, Fraser P and St George-Hyslop P (2000) *Nature* 407, 48-54.

[64] Kojro E and Fahrenholz F (2005) *Subcell. Biochem.* 38, 105-127.

[65] Haass C, Hung AY, Schlossmacher M., Teplow DB and Selkoe DJ (1993) *J. Biol. Chem.* 268, 3021-3024.

[66] Jarrett JT, Berger EP and Lansbury PT Jr (1993) *Biochem.* 32, 4693-4697.

[67] Younkin SG (1998) *J. Physiol. Paris* 92, 289-292.

[68] St George-Hyslop, PH and Petit A (2005) *C. R. Biol.* 328, 119-130.

[69] Haass C, Lemere CA, Capell A, Citron M, Seubert P, Schenk D, Lannfelt L and Selkoe DJ (1995) *Nature Med.* 1, 1291-1296.

[70] Nilsberth C, Westlind-Danielsson A, Eckman CB, Condron MM, Axelman K, Forsell C, Stenh C, Luthman J, Teplow DB, Younkin SG, Näslund J and Lannfelt L (2001) *Nature Neurosci.* 4, 887-893.

[71] Guo Q, Fu W, Sopher BL, Miller MW, Ware CB, Martin GM and Mattson MP (1999) *Nature Med.* 5, 101-106.

[72] Jankowsky JL, Fadale DJ, Anderson J, Xu GM, Gonzales V, Jenkins NA, Copeland NG, Lee MK, Younkin LH, Wagner SL, Younkin SG and Borchelt DR (2004) *Hum. Mol. Genet.* 13, 159-170.

[73] Rovelet-Lecrux A, Hannequin D, Raux G, Le Meur N, Laquerrière A, Vital A, Dumanchin C, Feuillette S, Brice A, Vercelletto M, Dubas F, Frebourg T and Campion D (2006) *Nature Genet.* 38, 24-26.

[74] Cabrejo L, Guyant-Maréchal L, Laquerrière A, Vercelletto M, De la Fournière F, Thomas-Antérion C, Verny C, Letournel F, Pasquier F, Vital A, Checler F, Frebourg T, Campion D and Hannequin D (2006) *Brain* 129, 2966-2976.

[75] Gyure KA, Durham R, Stewart, WF, Smialek JE and Troncoso JC (2001) *Arch. Pathol. Lab. Med.* 125, 489-492.

[76] Mori C, Spooner ET, Wisniewsk KE, Wisniewski TM, Yamaguch H, Saido TC, Tolan DR, Selkoe DJ and Lemere CA (2002) *Amyloid* 9, 88-102.

[77] Gouras GK, Tsai J, Naslund J, Vincent B, Edgar M, Checler F, Greenfield JP, Haroutunian V, Buxbaum JD, Xu H, Greengard P and Relkin NR (2000) *Am. J. Pathol.* 156, 15-20.

[78] Chui DH, Tanahashi H, Ozawa K, Ikeda S, Checler F, Ueda O, Suzuki H, Araki W, Inoue H, Shirotani K, Takahashi K, Gallyas F and Tabira T (1999) *Nature Med.* 5, 560-564.

[79] Knobloch M, Konietzko U, Krebs DC and Nitsch RM (2006) *Neurobiol. Aging* 28, 1297-306

[80] Kuo YM, Beach TG, Sue LI, Scott S, Layne KJ, Kokjohn TA, Kalback WM, Luehrs DC, Vishnivetskaya TA, Abramowski D, Sturchler-Pierrat C, Staufenbiel M, Weller RO and Roher AE (2001) *Mol. Med.* 7, 609-618.

[81] Li QX, Maynard C, Cappai R, McLean CA, Cherny RA, Lynch T, Culvenor JG, Trevaskis J, Tanner JE, Bailey KA, Czech C, Bush AI, Beyreuther K and Masters CL (1999) *J. Neurochem.* 72, 2479-2487.

[82] Lord A, Kalimo H, Eckman C, Zhang XQ, Lannfelt L and Nilsson LN (2006) *Neurobiol. Aging* 27, 67-77.

[83] Oakley H, Cole SL, Logan S, Maus E, Shao P, Craft J, Guillozet-Bongaarts A, Ohno M, Disterhoft J, Van Eldik L, Berry R and Vassar R (2006) *J. Neurosci.* 26, 10129-10140.

[84] Oddo S, Caccamo A, Shepherd JD, Murphy MP, Golde TE, Kayed R, Metherate R, Mattson MP, Akbari Y and LaFerla FM (2003) *Neuron* 39, 409-421.

[85] Wirths O, Multhaup G, Czech C, Blanchard V, Moussaoui S, Tremp G, Pradier L, Beyreuther K and Bayer TA (2001) *Neurosci. Lett.* 306, 116-120.

[86] Kinoshita A, Fukumoto H, Shah T, Whelan CM, Irizarry MC and Hyman BT (2003) *J. Cell Sci.* 116, 3339-3346.

[87] Breen KC, Bruce M and Anderton BH (1991) *J. Neurosci. Res.* 28, 90-100.

[88] Sabo SL, Ikin AF, Buxbaum JD. and Greengard P (2001) *J. Cell Biol.* 153, 1403-1414.

[89] Xu H, Greengard P and Gandy S (1995) *J. Biol. Chem.* 270, 23243-23245.

[90] Mizuguchi M, Ikeda K and Kim SU (1992) *Brain Res.* 584, 219-225.

[91] Bu G, Cam J and Zerbinatti C (2006) *Ann. N. Y. Acad. Sci.* 1086, 35-53.

[92] Deane R, Du Yan S, Submamaryan RK, LaRue B, Jovanovic S, Hogg E, Welch D, Manness L, Lin C, Yu J, Zhu H, Ghiso J, Frangione B, Stern A, Schmidt AM, Armstrong DL, Arnold B, Liliensiek B, Nawroth P, Hofman F, Kindy M, Stern D and Zlokovic B (2003) *Nature Med.* 9, 907-913.

[93] Nagele, RG, D'Andrea MR, Anderson WJ and Wang HY (2002) *Neurosci.* 110, 199-211.

[94] Yazawa H, Yu ZX, Takeda, Le Y, Gong W, Ferrans VJ, Oppenheim JJ, Li CC and Wang JM (2001) *FASEB J.* 15, 2454-2462.

[95] Wang HY, Lee DH, D'Andrea MR, Peterson PA, Shank RP and Reitz AB (2000) *J. Biol. Chem.* 275, 5626-5632.

[96] Yan SD, Chen X, Fu J, Chen M, Zhu H, Roher A, Slattery T, Zhao L, Nagashima M, Morser J, Migheli A, Nawroth P, Stern D and Schmidt AM.(1996) *Nature* 382, 685-691.

[97] Sasaki N, Toki S, Chowei H, Saito T, Nakano N, Hayashi Y, Takeuchi M and Makita Z (2001) *Brain Res.* 888, 256-262.

[98] Tian ZF, Zhang ZM, Li YH, Zhao S and Wang X (2011) *Zhonghua Yi Xue Za Zhi.* 91, 2143-7.

[99] Snyder EM, Nong Y, Almeida CG, Paul S, Moran T, Choi EY, Nairn AC, Salter MW, Lombroso PJ, Gouras GK and Greengard P (2005) *Nature Neurosci.* 8, 1051-1058.

[100] Bi X, Gall CM, Zhou J and Lynch G (2002) *Neurosci.* 112, 827-840.

[101] Cleary JP, Walsh DM, Hofmeister JJ, Shankar GM, Kuskowski MA, Selkoe DJ and Ashe KH (2005) *Nature Neurosci.* 8, 79-84.

[102] Walsh DM,. Klyubin I, Fadeeva JV, Cullen WK, Anwyl R, Wolfe MS, Rowan MJ, Selkoe DJ (2002) *Nature* 416, 535-539.

[103] Lesne S, Koh MT, Kotilinek L, Kayed R, Glabe CG, Yang A, Gallagher M and Ashe KH. (2006) *Nature* 440, 352-357.

[104] Walsh DM, Tseng BP, Rydel RE, Podlisny MB and Selkoe DJ (2000) *Biochem.* 39, 10831-10839.

[105] Yamamoto N, Igbabvoa U, Shimada Y, Ohno-Iwashita Y, Kobayashi M, Wood WG, Fujita SC and Yanagisawa K (2004) FEBS Lett. 569, 135-139.

[106] D'Andrea MR, Nagele RG, Wang HY, Peterson PA and Lee DH (2001) *Histopathology* 38, 120-134.

[107] Oddo S, Billings L, Kesslak JP, Cribbs DH abd LaFerla FM *Neuron* (2004) 43, 321-332.

[108] Oddo S, Caccamo A, Smith IF, Green KN and LaFerla FM (2006) *Am. J. Pathol.* 168, 184-194.

[109] Wegiel J, Kuchna I, Nowicki K, Frackowiak J, Mazur-Kolecka B, Imaki H, Wegiel J, Mehta PD, Silverman WP, Reisberg B, Deleon M, Wisniewski T, Pirttilla T, Frey H, Lehtimäki T, Kivimäki T, Visser FE, Kamphorst W, Potempska A, Bolton D, Currie JR and Miller DL. (2007) *Acta Neuropathol. (Berl)* 113, 389-402.

[110] Green KN, Martinez-Coria H, Khashwji H, Hall EB, Yurko-Mauro KA, Ellis L and LaFerla FM (2007) *J. Neurosci.* 27, 4385-4395.

[111] Hashimoto M, Tanabe Y, Fujii Y, Kikuta T, Shibata H and Shido O (2005) *J. Nutr.* 135, 549-555.

[112] Lim GP, Calon F, Morihara T, Yang F, Teter B, Ubeda O, Salem N Jr, Frautschy SA and Cole GM (2005) *J. Neurosci.* 25, 3032-3040.

[113] Gasparini L, Gouras GK, Wang R, Gross RS, Beal MF, Greengard P and Xu H (2001) *J. Neurosci.* 21, 2561-2570.

[114] Tierney LM (2002) Current Medical Diagnosis and Treatment, 2002. New York: Lange Medical Books/McGraw-Hill.

[115] Olokoba AB, Obateru OA and Olokoba LB (2012) *Oman Med. J.* 27, 269-73.

[116] Patlak M (2002) *FASEB J.* 16, 1853.

[117] Chen L, Magliano DJ and Zimmet PZ (2011) *Nat. Rev. Endocrinol.* 8, 228-36.

[118] Genetic basis of type 1 and type2 diabetes, obesity, and their complications. Advances and emerging opportunities in diabetes research: a Strategic Planning report of the DMICC.

[119] Azevedo M and Alla S (2008) *Int. J. Diabetes. Dev. Ctries* 28, 101-108.

[120] Zimmet P, Alberti KG and Shaw J. (2001) *Nature* 414, 782-787.

[121] Department of Health and Human Services. Centres for Disease Control and Prevention, 2011. National diabetes fact sheet: national estimates and general information on diabetes and prediabetes in the United States, 2011.

[122] Das SK and Elbein SC (2006) Cellscience 2, 100-131.

[123] Kahn CR (1994) *Diabetes* 43, 1066-1084.

[124] Robertson RP (1995) *J. Lab. Clin. Med.* 125, 560-564.

[125] Fujioka K (2007) *JAAPA*; suppl. 3-8.

[126] Hu FB, Manson JE, Stampfer MJ, Colditz G, Liu S, Solomon CG and Willett WC (2001) *N. Engl. J. Med.* 345, 790-797.

[127] Prevalence of overweight and obesity among adults with diagnosed Diabetes United States, 1988-1994 and 1999-2000. Centers for Disease Control and Prevention (CDC) (November 2004) MMWR. Morbidity and Mortality Weekly Report; 53(45): 1066-1068.

[128] Rother KI (2007) N. Engl. J. Med. 356, 1499-1501.

[129] McCarthy MI (2010) N. Engl. J. Med. 363, 2339-2350.

[130] Walley AJ, Blakemore AI and Froguel P (2006) *Hum. Mol. Genet.* 15, R124-R130.

[131] Camastra S, Bonora E, Del Prato S, Rett K, Weck M and Ferrannini E (1999) *Int. J. Obes. Relat. Metab. Disord.* 23, 1307-1313.

[132] Alberti KG, Zimmet P and Shaw J (2005) Lancet 366, 1059-1062.

[133] Powers AC Diabetes mellitus. In: Fauci AS, Braunwauld E, Kasper DL, Hauser SL, Longo DL, Jameson JL, Loscalzo J (eds). Harrison's Principles of Internal Medicine.17th ed, New York, McGraw-Hill; 2008: 2275-2304.

[134] Jack L Jr, Boseman L and Vinicor F (2004) *Geriatrics* 59, 14-17.

[135] Lovejoy JC (2002) Curr. Diab. Rep. 2, 435-440.

[136] Westermark P, Andersson A and Westermark GT (2011) *Physiol. Rev.* 91, 795-826.

[137] Krampert M, Bernhagen J, Schmucker J, Horn A, Schmauder A, Brunner H, Voelter W and Kapurniotu A (2000) *Chem. and Biol.*, 7, 855-871.

[138] Martin C (2006) *Diabetes Educ.* 32, 101-104.

[139] Kogire M, Ishizuka J, Thompson JC and Greeley GH (1991) *Pancreas* 6, 459-463.

[140] Degano P, Silvestre RA, Salas M, Peiro E and Marco J (1993) *Regul. Pep.*, 43, 91-96.

[141] Rink TJ, Beaumont K, Koda J and Young A (1993) *Trends in Pharmacol. Sci.*, 14, 113-118.

[142] Zhu T, Wang Y, He B, Zang J, He Q and Zhang W (2011) *Diabetes Metab. Res. Rev.* 27, 28-34.

[143] Cooper GJS (1994) *Endocr. Reviews* 15, 163-201.

[144] Kruger DF, Gatcomb PM and Owen SK (1999) *Diabetes Educ.* 25, 389-397.

[145] Silvestre RA, Rodrıguez-Gallardo J, Jodka C, Parkes DG, Pittner RA, Young AA and Marco J. (2001) *Am. J. of Phyiol. Endocrinol. Metab.* vol. 280, E443-E449.

[146] Akesson B, Panagiotidis G, Westermark P and Lundquist I (2003) *Regul. Pept.* 111, 55-60.

[147] Hull RL, Andrikopoulos S, Verchere CB, Vidal J, Wang F, Cnop M, Prigeon RL and Kahn SE (2003) *Diabetes* 52, 372-379.

[148] Hoppener JW, Jacobs HM, Wierup N, Sotthewes G, Sprong M, de Vos P, Berger R, Sundler F and Ahrén B. (2008) *Exp. Diabetes Res.* 2008, 697035.

[149] Kodali R and Wetzel R (2007) *Curr. Opin. Struc. Biol.* 17, 48-57.

[150] Jaikaran S and Clark A (2001) *Biochim. Biophys. Acta* 1537, 179-203.

[151] Howard CF Jr (1978) *Diabetes* 27, 357-364.

[152] Yano BL, Hayden DW and Johnson KH (1981) *Vet. Pathol.*, 18, 621-627.

[153] Betsholtz C, Christmanson L, Engstrom U, Rorsman F, Svensson V, Johnson KH, Westermark P (1989) *FEBS Lett.* 251, 261-265.

[154] Johnson KH, O'Brien TD, Betsholtz C, Westermark P (1992) *Lab. Invest.* 66, 522-535.

[155] Smith PE, Brender JR and Ramamoorthy A (2009) *J. Am. Chem. Soc.* 131, 4470-8.

[156] Westermark P, Engstrom U, Johnson KH, Westermark GT and Betsholtz C (1990) *Proc. Natl. Acad. Sci. USA* 87, 5036-5040.

[157] Tenidis K, Waldner M, Bernhagen J, Fischle W, Bergmann M, Weber M, Merkle ML, Voelter W, Brunner H and Kapurniotu A (2000) *J. Mol. Biol.* 295, 1055-1071.

[158] Scrocchi LA, Chen Y, Waschuk S, Wang F, Cheung S, Darabie AA, McLaurin J and Fraser PE (2002) *J. Mol. Biol.* 318, 697-706.

[159] Abedini A, Raleigh DP (2005) *Biochemistry* 44, 16284-16291.

[160] Li Y, Xu W, Mu Y and Zhang JZ (2013) *J. Chem. Phys.* 139, 055102.

[161] Jaikaran ET, Higham CE, Serpell LC, Zurdo J, Gross M, Clark A and Fraser PE (2001) *J. Mol. Biol.* 308, 515-525.

[162] Kajava AV, Aebi U and Steven AC (2005) *J. Mol. Biol.* 348, 247-252.

[163] Luca S, Yau WM, Leapman R and Tycko R (2007) *Biochemistry* 46, 13505-13522.

[164] Shim SH, Gupta R, Ling YL, Strasfeld DB, Raleigh DP and Zanni MT (2009) *Proc. Natl. Acad. Sci. USA* 106, 6614-6619.

[165] Gazit E (2002) *FASEB J.* 16, 77-83.

[166] Lansbury PT and Caughey B (1995) *Chem. Biol.*, 2, 1-5.

[167] Kayed R, Bernhagen J, Greenfield N, Sweimeh K, Brunner H, Voelter W and Kapurniotu A (1999) J. *Mol. Biol.* 287, 781-796.

[168] Goldsbury C, Kistler J, Aebi U, Arvinte T and Cooper GJS (1999) *J. Mol. Biol.* 285, 33-39.

[169] Benzinger TLS, Gregory DM, Burkoth TS, Miller-Auer H, Lynn DG, Botto RE and Meredith SC (2000) *Biochemistry* 39, 3491-3499.

[170] Tycko R (2004) *Curr. Opin. Struct. Biol.* 14, 96-103.

[171] Jayasinghe SA and Langen R (2005) *Biochemistry* 44, 12113-12119,.

[172] Nelson R, Sawaya MR, Balbirnie M (2005) *Nature* 435, 773-778.

[173] Mattson MP and Goodman Y (1995) *Brain Res.* 676, 219-224.

[174] Mirzabekov TA, Lin MC and Kagan BL (1996) *J. Biol. Chem.* 271, 1988-1992.

[175] Tomiyama T, Kaneko H, Kataoka KI, Asano S and Endo N (1997) *Biochem. J.* 322, 859-865.

[176] Kapurniotu A, Bernhagen J, Greenfield N, Al-Abed Y, Teichberg S, Frank RW, Voelter W and Bucala R (1998) *Eur. J. Biochem.* 251, 208-216.

[177] Bai JZ, Saafi EL, Zhang S and Cooper GJS (1999) *Biochem. J.* 343, 53-61.

[178] Hiddinga HJ and Eberhardt NL *Am. J. Pathol.*. 154, 1077-1088 (1999).

[179] Kapurniotu A, Schmauder A and Tenidis K (2002) *J. Mol. Biol.* 315, 339-350.

[180] Tatarek-Nossol M, Yan LM, Schmauder A, Tenidis K, Westermark G and Kapurniotu A (2005) *Chem. Biol.* 12, 797-809.

[181] Yan LM, Velkova A, Tatarek-Nossol M, Andreetto E and Kapurniotu A. (2007) *Angew. Chem. Int. Ed. Engl*. 46, 1246-1252.

[182] Janson J, Ashley RH, Harrison D, McIntyre S and Butler PC (1999) *Diabetes* 48, 491-498.

[183] Anguiano M, Nowak RJ and Lansbury PT (2002) *Biochemistry* 41, 11338-11343.

[184] Kayed R, Sokolov Y, Edmonds B, McIntire TM, Milton SC, Hall JE and Glabe CG (2004) *J. Biol. Chem.* 279, 46363-46366.

[185] Konarkowska B, Aitken JF, Kistler J, Zhang S and Cooper GJS (2006) *FEBS J.* 273, 3614-3624.

[186] Zhao J, Yu X, Liang G and Zheng J (2011) *Biomacromolecules* 12, 210-20.

[187] Ritzel RA, Meier JJ, Lin CY, Veldhuis JD and Butler PC (2007) *Diabetes* 56, 65-71.

[188] Aitken JF, Loomes KM, Scott DW, Reddy S, Phillips AR, Prijic G, Fernando C, Zhang S, Broadhurst R, L'Huillier P and Cooper GJ (2010) *Diabetes* 59, 161-171.

[189] Meier JJ, Kayed R, Lin CY, Gurlo T, Haataja L, Jayasinghe S, Langen R, Glabe CG, Butler PC (2006) *Am. J. Physiol. Endocrinol. Metab.* 291, E1317-E1324.

[190] Lorenzo A, Razzaboni B, Weir GC and Yankner BA (1994) *Nature* 368, 756-760.

[191] Sciacca MFM, Pappalardo M, Attanasio F, Milardi D, La Rosa C and Grasso DM (2010) *New J. Chem.* 34, 200-207.

[192] Demuro A, Mina E, Kayed R, Milton SC, Parker I and Glabe CG (2005) *J. Biol. Chem.* 280, 17294-17300.

[193] Knight JD and Miranker AD (2004) *J. Mol. Biol.* 341, 1175-1187.

[194] Lopes DHJ, Meister A, Gohlke A, Hauser A, Blume A and Winter R (2007) *Biophys. J.* 93, 3132-3141.

[195] Sparr E, Engel MFM, Sakharov DV, Sprong M, Jacobs J, de Kruijff B, Höppener JW and Killian JA (2004) *FEBS Lett.* 577, 117-120.

[196] Engel MFM, Yigittop H, Elgersma RC, Rijkers DT, Liskamp RM, de Kruijff B, Höppener JW and Antoinette Killian J (2006) *J. Mol. Biol.* 356, 783-789.

[197] Engel MFM, Khemt´emourian L, Kleijer CC, Meeldijk HJ, Jacobs J, Verkleij AJ, de Kruijff B, Killian JA and Höppener JW (2008) *Proc. Natl. Acad. Sci. USA* 105, 6033-6038.

[198] Schubert D, Behl C, Lesley R, Brack A, Dargusch R, Sagara Y and Kimura H (1995) *Proc. Natl. Acad. Sci. US*, 92, 1989-1993.

[199] Zhang S, Liu J, Saafi EL and Cooper GJS (1999) *FEBS Lett.* 455, 315-320.

[200] Zhang S, Liu J, MacGibbon G, Dragunow M and Cooper GJS (2002) *J. Mol. Biol.* 324, 271-285.

[201] Huang CJ, Haataja L, Gurlo T, Butler AE, Wu X, Soeller WC and Butler PC *Am. J. Physiol. Endocrinol. Metab.* (2007) 293, E1656-E1662.

[202] Zhang S, Liu H, Yu H and Cooper GJS (2008) *Diabetes* 57, 348-356.

[203] Huang CJ, Gurlo T, Haataja L, Costes S, Daval M, Ryazantsev S, Wu X, Butler AE and Butler PC (2010) *J. Biol. Chem.* 285, 339-348.

[204] Gurlo T, Ryazantsev S, Huang CJ, Yeh MW, Reber HA, Hines OJ, O'Brien TD, Glabe CG and Butler PC (2010) *Am. J. Pathol.* 176, 861-869.

[205] Lim YA, Rhein V, Baysang G, Meier F, Poljak A, Raftery MJ, Guilhaus M, Ittner LM, Eckert A and Götz J (2010) *Proteomics* 10, 1621-1633.

[206] Jiang P, Li W, Shea JE and Mu Y (2011) *Biophys. J* 100, 2076-2076.

[207] Smoliga JM, Baur JA and Hausenblas HA (2011) *Mol. Nutr. Food Res.* 55, 1129-1141.

[208] Abedini A, Meng F and Raleigh DP (2007) *J. Am. Chem. Soc.* 129, 11300-11301.

[209] Hayashi T, Asai T and Ogoshi H (1997) *Tetrahedron Lett.* 38, 3039-3042.

[210] Kong MF, King P, Macdonald IA, Stubbs TA, Perkins AC, Blackshaw PE, Moyses C and Tattersall RB (1997) *Diabetologia* 40, 82-88.

[211] Kong MF, Stubbs TA, King P, Macdonald IA, Lambourne JE, Blackshaw PE, Perkins AC and Tattersall RB (1998) *Diabetologia* 41, 577-583.

[212] Thompson R, Pearson L, Schoenfeld S and Kolterman O (1997) *Diabetologia* 40, 1397-1397.

[213] Thompson RG, Pearson L, Schoenfeld SL and Kolterman OG (1998) *Diabetes Care* 21, 987-993.

[214] Thompson RG, Gottlieb A, Organ K, Koda J, Kisicki J and Kolterman OG (1997) *Diabet. Med.* 14, 547-555.

[215] Thompson RG, Pearson L and Kolterman OG (1997) *Diabetologia* 40, 1278-1285.

[216] Cao P, Abedini A, Wang H, Tu LH, Zhang X, Schmidt AM and Raleigh DP (2013) *Proc. Natl. Acad. Sci. USA* 110, 19279-84.

[217] Caillon L, Lequin O and Khemtémourian L (2013) *Biochim. Biophys. Acta* 1828, 2091-8.

[218] Hollander P, Ratner R, Fineman M, Strobel S, Shen L, Maggs D, Kolterman O and Weyer C (2003) *Diabetes, Obes. Metab.* 5, 408-414.

[219] Weyer C, Maggs D, Ruggles J, Fineman M, Burrell T and Kolterman O (2003) *Diabetologia* 46, A295-A295.

[220] Maggs DG, Fineman M, Kornstein J, Burrell T, Schwartz S, Wang Y, Ruggles JA, Kolterman OG and Weyer C (2004) *Diabetes Metab. Res. Rev.* 20, 55-60.

[221] Ratner RE, Dickey R, Fineman M, Maggs DG, Shen L, Strobel SA, Weyer C and Kolterman OG (2004) *Diabetic Med.* 21, 1204-1212.

[222] Ryan GJ, Jobe LJ and Martin R (2005) *Clin. Ther.* 27, 1500-1512.

[223] Ryan G, Briscoe TA and Jobe L (2008) *Drug Des. Devel. Ther.* 2, 203-214.

[224] Miklossy J, Qing H, Radenovic A, Kis A, Vileno B, Làszló F, Miller L, Martins RN, Waeber G, Mooser V, Bosman F, Khalili K, Darbinian N and McGeer PL (2010) Neurobiol. Aging 31, 1503-1515.

[225] Hebda JA and Miranker AD. (2009) *Annu. Rev. Biophys.* 38, 125-52.

[226] Masad A, Tabner BJ, Mayes J and Allsop D. (2011) *Free Radic. Biol. Med*. 15, 869-75.

[227] Wild S, Roglic G, Green A, Sicree R and King H (2004) *Diabetes Care* 27, 1047-1053.

[228] Ferri CP, Prince M, Brayne C, Brodaty H, Fratiglioni L, Ganguli M, Hall K, Hasegawa K, Hendrie H, Huang Y, Jorm A, Mathers C, Menezes PR, Rimmer E, Scazufca M; Alzheimer's Disease International (2005) *Lancet* 366, 2112-2117.

[229] Götz J, Ittner LM, Schonrock N and Cappai R (2008) *Neuropsychiatr. Dis. Treat.* 4, 1033-1042.

[230] Marzban L, Park K and Verchere CB (2003) *Exp. Gerontol.* 38, 347-351.

[231] Hoppener JW,and Lips CJ (2006) *Int. J. Biochem. Cell Biol.* 38, 726-736.

[232] Shimizu T, Matsuoka Y and Shirasawa T (2005) *Biol. Pharm. Bull.* 28, 1590-1596.

[233] Sargaeva NP, Lin C and O'Connor PB (2009) *Anal. Chem.* 81, 9778-9786.

[234] Dunkelberger EB, Buchanan LE, Marek P, Cao P, Raleigh DP and Zanni MT (2012) *J. Am. Chem. Soc.* 134, 12658-12667.

[235] Guo JL and Lee VM (2011) *J. Biol. Chem.* 286, 15317-15331.

[236] Watanabe A, Takio K and Ihara Y (1999) *J. Biol. Chem.* 274, 7368-7378.

[237] Gorn AH, Flannery MR, Jenkins NA, Gilbert DJ, Copeland NG, Tapp DR, Krane SM and Goldring SR (1994). *Endocrinology* 135, 2635-2643.

[238] Ueda T, Ugawa S, Saishin Y and Shimada S (2001) *Brain Res. Mol. Brain Res.* 93, 36-45.

[239] Yang F, Lim GP, Begum AN, Ubeda OJ, Simmons MR, Ambegaokar SS, Chen PP, Kayed R, Glabe CG, Frautschy SA and Cole GM (2005) *J. Biol. Chem.* 280, 5892-5901.

[240] Jhamandas JH and MacTavish D (2004) *J. Neurosci.* 24, 5579-5584.

[241] White A., Maher F, Brazier MW, Jobling MF, Thyer J, Stewart LR, Thompson A, Gibson R, Masters CL, Multhaup G, Beyreuther K, Barrow CJ, Collins SJ and Cappai R (2003) *Brain Res.* 966, 231-244.

[242] Wright S, Malinin NL, Powell KA, Yednock T, Rydel RE and Griswold-Prenner I (2007) *Neurobiol. Aging* 28, 226-237.

[243] Götz J, Lim YA and Eckert A (2013) *Front. Aging Neurosci.* 5, 38.

[244] Jhamandas JH , Li Z, Westaway D, Yang J, Jassar S and MacTavish D (2011) *Am. J. Pathol.* 178, 140-149.

[245] Morfis M, Tilakaratne N, Furness SG, Christopoulos ., Werry TD, Christopoulos A and Sexton PM (2008) *Endocrinology* 149, 5423-5431.

[246] Poyner DR, Sexton PM, Marshall I, Smith DM, Quirion R, Born W, Muff R, Fischer JA and Foord SM (2002) *Pharmacol. Rev.* 54, 233-246

[247] Fu W, Ruangkittisakul A, MacTavish, D, Shi JY, Ballanyi,K. and Jhamandas JH (2012) *J. Biol. Chem.* 287, 18820-18830.

[248] Cao D, Lu H, Lewis TL and Li L (2007) *J. Bio.Chem.* 282, 36275-36282.

[249] Li ZG, Zhang W and Sima AA (2007) *Diabetes* 56, 1817-1824.

[250] Qiu WQ and Folstein MF (2006) *Neurobiol. Aging* 27, 190-198.

[251] Leissring MA, Farris W, Chang AY, Walsh DM, Wu X, Sun X, Frosch MP and Selkoe DJ (2003) *Neuron* 40, 1087-1093.

[252] Farris W, Mansourian S, Leissring MA, Eckman EA, Bertram L, Eckman CB, Tanzi RE and Selkoe DJ (2004) *Am. J. Pathol.* 164, 1425-1434.

[253] Quan W, Jo EK and Lee MS (2013) *Diabetes Obes. Metab.* 15, 141-51.

[254] Lim YA, Ittner LM, Lim Y and Götz J (2008) *FEBS Lett.* 582, 2188-2194.

[255] Ritzel RA and Butler PC (2003) *Diabetes* 52, 1701-1708.

[256] Mucke L and Selkoe DJ (2012) *Cold Spring Harb. Perspect. Med.* 2:a006338.

[257] Lee CC, Sun Y and Huang HW (2012). *Biophys.J.* 102, 1059-1068.

[258] Nicolls MR, D'Antonio JM, Hutton JC, Gill RG, Czwornog JL and Duncan MW (2003) *J. Proteome Res.* 2, 199-205.

[259] David DC, Ittner L., Gehrig P, Nergenau D, Shepherd C, Halliday G *et al*. (2006) *Proteomics* 6, 6566-6577.

[260] Freshney RI. Culture of Animal Cells: A Manual of Basic Technique, 5th ed. New York: Wiley Liss; 2005.

[261] Goss JR, O'Malley ME, Zou L, Styren SD, Kochanek PM and DeKosky ST (1998) *Exp. Neurol.* 149, 301-9.

[262] Lamarche F, Signorini-Allibe N, Gonthier B and Barret L (2004) *Alcohol* 33, 127-38.

[263] Griffin S, Clark JB and Canevari L (2005) *J Neurochem* 95, 1015-22.

[264] Mahesh VB, Dhandapani KM and Brann DW (2006) *Mol. Cell. Endocrinol.* 246, 1-9.

[265] Yan J, Tan T and Huang Q (2013) *Chin. J. Traumatol.*16, 3-9.

[266] Boulton M and Dayhaw-Barker P (2001) *Eye (Lond)* 15:, 384-389.

[267] Marneros AG, Fan J, Yokoyama Y, Gerber HP, Ferrara N, Crouch RKand Olsen BR (2005) *Am. J. Pathol.* 167, 1451-1459.

[268] Tombran-Tink J and Barnstable CJ (2003) *Nat. Rev. Neurosci.* 4, 628-636.

[269] Hollborn M, Bringmann A, Faude F, Wiedemann P and Kohen L (2006) *Biochem. Biophys. Res. Commun.* 344, 912-919.

[270] Wenzel A, Grimm C, Samardzija M and Reme CE (2005) *Prog. Retin. Eye. Res.* 24, 275-306.

[271] Sun X, Cheng L and Lu G (2008) *Cell. Research* 18, s125.

[272] Xue H, Lu B and Lai M (2008) *J. Transl. Med. 6*, 52.

[273] Righetti PG, Castagna A, Antonucci F, Piubelli C, Cecconi D, Campostrini N and Zanusso G, Monaco S (2003) *Clin. Chem. Lab. Med. 41*, 425-438.

[274] Zhong L, Roybal J, Chaerkady R, Zhang W, Choi K, Alvarez CA, Tran H, Creighton CJ, Yan S, Strieter RM, Pandey A and Kurie JM (2008) *Cancer Res.* 68, 7237-7245.

[275] Volmer MW, Stuhler K, Zapatka M, Schoneck A, Klein-Scory S, Schmiegel W, Meyer HE and Schwarte-Waldhoff I (2005) *Proteomics*, 5, 2587-2601.

[276] Gronborg M, Kristiansen TZ, Iwahori A, Chang R, Reddy R, Sato N, Molina H, Jensen ON, Hruban RH, Goggins MG, Maitra A and Pandey A (2006) *Mol. Cell. Proteomics*, 5, 157-171.

[277] Weiss JV, Klein-Scory S, Kübler S, Reinacher-Schick A, Stricker I, Schmiegel W and Schwarte-Waldhoff I (2010) *Int. J. Cancer.* 128, 1384-92

[278] Klee EW and Sosa CP (2007) *Drug Discov. Today*, 12, 234-240.

[279] Nickel W (2010) *Curr. Opin. Biotechnol*. 5, 621-626.

[280] Andre F, Schartz NE, Movassagh M, Flament C, Pautier P, Morice P, Pomel C, Lhomme C, Escudier B, Le Chevalier T, Tursz T, Amigorena S, Raposo G, Angevin E and Zitvogel L. (2002) *Lancet* 360, 295-305.

[281] Gunawardana CG, Kuk C, Smith CR, Batruch I, Soosaipillai A and Diamandis EP (2009) *J. Proteome Res.* 8, 4705-4713.

[282] Radomski MW, Palmer RMJ and Moncada S (1990) *Proc. Natl. Acad. Sci. USA.* 87, 5193.

[283] Carroll JS, Ku CJ, Karunarathne W and Spence DM (2007) *Anal. Chem.* 79, 5133.

[284] Kelleher ZT, Potts EN, Brahmajothi MV, Foster MW, Auten RL, Foster WM and Marshall HE (2011) *Am. J. Physiol. Lung Cell. Mol. Phys.* 301, L327.

[285] Vazquez-Torres A, Stevanin T, Jones-Carson J, Castor M, Read RC and Fang FC (2008) *Methods Enzymol.* 437, 521.

[286] Ballard RA, Truog WE, Cnaan A, Martin RJ, Ballard PL, Merrill JD, Walsh MC, Durand DJ, Mayock DE, Eichenwald EC, Null DR, Hudak ML, Puri AR, Golombek SG, Courtney SE, Stewart DL, Welty SE, Phibbs RH, Hibbs AM, Luan X, Wadlinger SR, Asselin JM and Coburn CE (2006) *N. Engl. J. Med.* 355, 343-353.

[287] Frostell CG, Blomqvist H, Hedenstierna G, Lundberg J and Zapol WM (1993) *Anesthesiology* 78, 427-435.

[288] Frostell D, Fratacci MD, Wain JC, Jones R and Zapol WM (1991) *Circulation* 83, 2038-2047.

[289] Ichinose F, Roberts JD Jr and Zapol WM (2004) *Circulation* 109, 3106-3111.

[290] Kinsella JP (2006) *Curr. Opin. Pediatr.* 18, 107-111,.

[291] Kinsella JP, Cutter GR, Walsh WF, Gerstmann DR, Bose CL, Hart C, Sekar KC, Auten RL, Bhutani VK, Gerdes JS, George TN, Southgate WM, Carriedo H, Couser RJ, Mammel MC, Hall DC, Pappagallo M, Sardesai S, Strain JD, Baier M and Abman SH (2006) *N. Engl. J. Med.* 355, 354-364.

[292] Sekar K (2006) *J. Perinatol.* 26, S4-S23.

[293] Beckman JS (1996) *Chem. Res. Toxicol.* 9, 836-44,.

[294] Beckman JS. The physiological and pathological chemistry of nitric oxide. In: Nitric Oxide: Principles and Actions, edited by Lancaster JR. Orlando, FL: Academic (1996) p. 1-82.

[295] Butler AR, Megson IL and Wright PG (1998) *Biochim. Biophys. Acta* 1425, 168-176.

[296] Joshi MS, Ferguson TB Jr, Han TH, Hyduke DR, Liao JC, Rassaf T, Bryan N, Feelisch M and Lancaster JR Jr (2002) *Proc. Natl. Acad. Sci. USA* 99, 10341-10346.

[297] Moncada S, Palmer RMJ and Higgs EA (1991) *Pharmacol. Rev.* 43, 109-142.

[298] Ambs S, Merriam WG, Ogunfusika MO, Bennett WP, Ishibe N, Hussain SP, Tzeng EE, Geller DA, Billiar TR and Harris CC (1998) *Nat. Med.* 12, 1371-1376.

[299] Grisham MB, Jourd'heuil D and Wink DA (1999) *Gastrointest. Liver Physiolo1.* 39, 315-321.

[300] Kanner J, Harel S and Granit R (1991) *Arch. Biochem. Biophys.* 289, 130-136.

[301] Pacher P, Beckman JS and Liaudet L (2007) *Physiol. Rev.* 87, 315.

[302] Szabo C, Ischiropoulos H and Radi R (2007) *Nat. Rev. Drug Discovery* 6, 662.

[303] Cameron B and Landreth GE (2010) *Neurobiol. Dis.* 37, 503.

[304] Jenner P (2003) *Ann. Neurol.* 53, S26-36.

[305] Subapriya R, Kumaraguruparan R, Ramachandran CR and Nagini S (2002) *Clin. Biochem.* 35, 489-493.

[306] Tamir S and Tannenbaum SR (1996) *Biochim. Biophys. Acta* 1288, F31-F36.

[307] Bouchier-Hayes L, Lartigue L and Newmeyer DD (2005) *J. Clin. Invest.* 115, 2640-2647.

[308] Newmeyer DD and Ferguson-Miller S (2003) *Cell* 112, 481-490.

[309] Sharma VS, Traylor TG, Gardiner R and Mizukami H (1987) *Biochemistry* 26, 3837-3843.

[310] Traylor TG and Sharma VS (1992) *Biochemistry* 31, 2847-2849.

[311] Wise DL and Houghton G (1968) *Chem. Eng. Sci.* 23, 1211-1216.

[312] Tsoukias NM and Popel AS (2002) *Am. J. Physiol. Heart Circ. Physiol.* 282, H2265-H2277.

[313] Wood J and Garthwaite J (1994) *Neuropharmacology* 33, 1235-1244.

[314] Lancaster JR (1994) *Proc. Natl. Acad. Sci. USA* 91, 8137-8141.

[315] Tsoukias NM, Kavdia M and Popel AS (2004) *Am. J. Physiol. Heart Circ. Physiol.* 286, H1043-H1056.

[316] East SJ and Garthwaite J (1991) *Neurosci. Lett.* 123, 17-19.

[317] Southam E, East SJ and Garthwaite J (1991) *J. Neurochem.* 56, 2072-2081.

[318] Hillier BJ, Christopherson KS, Prehoda KE, Bredt DS and Lim WA (1999) *Science* 284, 812-815,.

[319] Brown TH, Chapman PF, Kairiss EW and Keenan CL (1988) *Science* 242, 724-728.

[320] Boulton CL, Southam E and Garthwaite J (1995) *Neuroscience* 69, 699-703.

[321] Schuman EM and Madison DV (1991) *Science* 254, 1503-1506.

[322] Gally JA, Montague PR, Reeke GN Jr and Edelman GM (1990) *Proc. Natl. Acad. Sci. USA* 87, 3547-3551.

[323] Brüning G (1993) *J. Neurosci. Res.* 36, 580-587.

[324] Gouge RC, Marshburn P, Gordon BE, Nunley W and Huet-Hudson YM (1998) *Biol. Reprod.* 58, 875-879.

[325] Kalb RG and Agostini J (1993) *Neuroscience* 57, 1-8.

[326] Miyado T, Wakida S, Aizawa H, Shibutani Y, Kanie T, Katayama M, Nose K and Shimouchi A (2008) *J. Chromatogr. A* 1206, 41.

[327] Miyado T, Tanaka Y, Nagai H, Takeda S, Saito K, Fukushi K, Yoshida Y, Wakida S and Niki E (2006) *J. Chromatogr. A* 1109, 174.

[328] Mao H, Chen B, Wang W, Zhuang P, Zong M and Xu Z (2011) *Microchem. J.* 97, 291.

[329] Ye X, Kim W, Rubakhin SS and Sweedler JV (2007) *J. Neurochem.* 101, 632.

[330] Gomes A, Fernandes E and Lima JLFC (2006) *J. Fluoresc.* 16, 119.

[331] Nagano T (2010) *Proc. Jpn. Acad., Ser. B Phys. Biol. Sci.* 86, 837.

[332] McQuade LE and Lippard SJ (2010) *Curr. Opin. Chem. Biol.* 14, 43.

[333] Ye X, Rubakhin SS and Sweedler JV (2008) *Analyst* 133, 423.

[334] Kim WS, Ye X, Rubakhin SS and Sweedler JV (2006) *Anal. Chem.* 78, 1859.

[335] Ye X, Xie F, Romanova EV, Rubakhin SS and Sweedler JV (2009) *ACS Chem. Neurosci.* 1, 182.

[336] Goto M, Sato K, Murakami A, Tokeshi M and Kitamori T (2005) *Anal. Chem.* 77, 2125.

[337] Cardoso FL, Brites D and Brito MA (2010) *Brain Res. Rev.* 64, 328-63.

[338] Abbott NJ, Roennbaeck L and Hansson E (2006) *Nat. Rev. Neurosci.* 7, 41-53.

[339] Abbott NJ, Patabendige AA, Dolman DE, Yusof SR and Begley DJ (2010 *Neurobiol. Dis.* 37, 13-25.

[340] Jain AJ and SK (2011) *Curr. Nanosci.* 7, 21-36.

[341] Jeffrey P and Summerfield S (2010) *Neurobiol. Dis.* 37, 33-37.

[342] Vangilder RL, Rosen CL, Barr TL and Huber JD (2011) *Pharmacol. Ther.* 130, 239-47.

[343] Lok J, Gupta P, Guo S, Kim WJ, Whalen MJ, van Leyen K and Lo EH (2007) *Neurochem. Res.* 32, 2032-45.

[344] Ransohoff RM and Perry VH (2009) *Annu. Rev. Immunol.* 27, 119-45.

[345] Mangas-Sanjuan V, Gonzalez-Alvarez M, Gonzalez-Alverez I and Bermejo M (2010) *Ther. Deliv.* 1, 535-62.

[346] Nag S, Kapadia A and Stewart DJ (2011) *Neuropathol. Appl. Neurobiol.* 37, 3-23.

[347] Abbott NJ, Dolman DEM and Patabendige AK (2008) *Curr. Drug Metab.* 9, 901-10.

[348] Bentivoglio M, Mariotti R and Bertini G (2011) *Brain Res. Rev.* 66, 152-73.

[349] Civelli O, Douglass J, Goldstein A and Herbert E (1985) *Proc. Natl. Acad. Sci. USA* 82, 4291-4295.

[350] Evans CJ, Hammond DL and Frederickson RCA (1988) The opioid peptides. In The Opiate Receptors (G. W. Pasternak, Ed.), pp. 23-71. Humana, Clifton, New Jersey.

[351] Goldstein A, Tachibana S, Lowney LI, Hunkapiller M and Hood L (1979) *Proc. Natl. Acad. Sci. USA* 76, 6666-6670.

[352] Kakidani H, Furutani Y, Takahashi H, Noda M, Morimoto Y, Hirose T, Asai M, Inayama S, Nakanishi S and Numa S (1982) *Nature* 298, 245-249.

[353] Yakovleva T, Marinova Z, Kuzmin A, Seidah NG, Haroutunian V, Terenius L and Bakalkin G (2006) *Neurobiol. Aging* 14, 1700-8.

[354] Klintenberg R and Andren PE (2005) *J. Mass Spectrom.* 40, 261-70.

[355] Lai J, Ossipov MH, Vanderah TW, Malan JTP and Porreca F (2001) *Mol. Interv.* 1, 160-7.

[356] Knoll AT and Carlezon Jr WA (2010) *Brain Res.* 1314, 56-73.

[357] Shirayama Y, Ishida H, Iwata M, Hazama G, Kawahara R and Duman RS (2004) *J. Neurochem.* 90, 1258-68.

[358] Hauser KF, Aldrich JV, Anderson KJ, Bakalkin G, Christie MJ, Hall ED, Knapp PE, Scheff SW, Singh IN, Vissel B, Woods AS, Yakovleva T and Shippenberg TS (2005) *Front. Biosci.* 10, 216-35.

[359] Hauser KF, Knapp PE and Turbek CS *Exp. Neurol.* (2001) 168, 78-87.

[360] Nardo L, Soong Y, Wu D, Young IR, Walker D and Szeto HH (2002) *Am. J. Physiol. Endocrinol. Metabol.* 282, 1301-7.

[361] Bakshi R, Ni RX and Faden AI (1992) *Brain Res.* 580, 255-264.

[362] Chen L, Gu Y and Huang LY (1995) *J. Neurosci.* 15, 4602-4611.

[363] Chen L, Gu Y and Huang LY (1995) *J. Physiol. (London)* 482, 575-581.

[364] Chen L and Huang LY (1992) *Nature* 356, 521-523.

[365] Dubner R and Ruda MA (1992) *Trends Neurosci.* 15, 96-103.

[366] Faden AI (1992) *J. Neurosci.* 12, 425-429.

[367] Laughlin TM, Vanderah TW, Lashbrook J, Nichols ML, Ossipov M, Porreca F and Wilcox GL (1997) *Pain* 72, 253-260.

[368] McIntosh TK, Fernyak S, Yamakami I and Faden AI (1994) *Am. J. Physiol.* 267, R665-72.

[369] Shukla VK and Lemaire S (1994) *Trends Pharmacol. Sci.* 15, 420-424.

[370] Vanderah TW, Laughlin T, Lashbrook JM, Nichols ML, Wilcox GL, Ossipov MH, Malan TPJ and Porreca F (1996) *Pain* 68, 275-281.

[371] Bakshi R, Newman AH and Faden AI (1990) *J. Neurosci.* 10, 3793-3800.

[372] Isaac L, O'Malley TVZ, Ristic H and P Stewart (1990) *Brain Res.* 531, 83-87.

[373] Long JB, Martinez-Arizala A, Echevarria EE, Tidwell RE and Holaday JW (1988) *Eur. J. Pharmacol.* 153: 45-54.

[374] Skilling SR, Sun X, Kurtz HJ and Larson AA (1992) *Brain Res.* 575, 272-278.

[375] Faden AI (1993) *Crit. Rev. Neurobiol.* 7, 175-186.

[376] Faden AI and Salzman S (1992) *Trends. Pharmacol. Sci.* 13, 29-35.

[377] Hu WH, Zhang CH, Yang HF, Zheng YF, Liu N, Sun XJ, Jen J and Jen MF (1998) *Eur. J. Pharmacol.* 342, 325-332.

[378] Long JB, Kinney RC, Malcolm DS, Graeber GM and Holaday JW (1986) *NIDA Res. Monogr.* 75, 524-526.

[379] Long JB, Rigamonti DD, Oleshansky MA, Wingfield CP and Martinez-Arizala A (1994) *J. Pharmacol. Exp. Ther.* 269, 358-366.

[380] Oleshansky MA and JB Long (1991) *Soc. Neurosci. Abstr.* 17, 1268.

[381] Walker JM, Moises HC, Coy DH, Baldrighi G and Akil H (1982) *Science* 218, 1136-1138.

[382] Walker JM, Moises HC, Coy DH, Young EA, Watson SJ and Akil H (1982) *Life Sci.* 31, 1821-1824.

[383] Walker JM, Tucker DE, Coy DH, Walker BB and Akil H (1982) *Eur. J. Pharmacol.* 85, 121-122.

[384] Caudle RM and Dubner R (1998) *Neuropeptides* 32, 87-95.

[385] Caudle RM and Isaac L (1988) *Brain Res.* 443, 329-332.

[386] Gentile NT and McIntosh TK (1993) *Ann. Emer. Med.* 22, 1028-1034.

[387] Hauser KF, Foldes JK and Turbek CS (1999) *Exp. Neurol.* 160, 361-375.

[388] Shukla VK and Lemaire S (1992) *J. Psychiatry Neurosci.* 17, 106-119.

[389] Chen L and Huang LY (1998) *J. Pharmacol. Exp. Ther.* 284, 826-831.

[390] Shukla VK, Prasad JA and Lemaire S (1997) *J. Pharmacol. Exp. Ther.* 283, 604-610.

[391] Lai SL, Gu Y and Huang LY (1998) *Neurosci. Lett.* 247, 115-118.

[392] Porreca F, Ossipov MH, Hruby VJ, Malan TP Jr and Lai J (1998) *Int. Narc. Res. Conf.* 29: 31-31.

[393] Kuhnline CD and Lunte SM *J. Sep. Sci.* (2010) 33, 2506-14.

[394] Reed B, Zhang Y, Chait BT and Kreek MJ (2003) *J. Neurochem.* 86, 815-23.

[395] Chou JZ, Chait BT, Wang R and Kreek MJ (1996) *Peptides* 17, 983-90.

[396] Chou JZ, Kreek MJ and Chait BT (1994) *J. Am. Soc. Mass Spectrom.* 5, 10-6.

[397] Yu J, Butelman ER, Woods JH, Chait BT and Kreek MJ (1996) *J. Pharmacol. Exp. Ther.* 279, 507-14.

[398] Aldrich JV, Patkar KA, Chappa AK, Fang W, Audus KL, Lunte SM, Carey AN and McLaughlin JP Development of Centrally Acting Peptide Analogs: Structure-Transport Studies and Pharmacological Evaluation of. Analogs of the Opioid Peptide Dynorphin A. In: Wilce, J., editor. Proceedings of the 4th International Peptide Symposium, Wilce, J Ed, 2007. Cairns, Queensland, Australia: 2007. www.peptideoz.org, M 64

[399] LeVine H 3rd (1993) *Protein Sci.* 2, 404-10.

[400] Hulvey MK, Frankenfeld CN and SM Lunte *Anal. Chem.* (2010) 82, 1608.

[401] Duffy DC, McDonald JC, Schueller OJA and Whitesides GM. (1998) *Anal. Chem.* 70, 4974.

[402] Balcerczyk A, Soszynski M and Bartosz G (2005) *Free Radical Biol. Med.* 39, 327.

[403] Audus KL and Borchardt RT (1986) *Pharmaceutical Research* 3, 81-87.

[404] Mainz ER, Gunasekara DB, Caruso G, Jensen DT, Hulvey MK, Fracassi dSJA, Metto EC, Culbertson AH, Culbertson CT and Lunte SM (2012) *Anal. Methods* 4, 414.

ACKNOWLEDGMENTS

I might be listed as the author on this thesis, but it was not a solitary effort by any means. There are many people without whom, this work would not have been possible and for all of them I am truly grateful.

First, I would like to thank my advisor, Prof. Vincenzo Giuseppe Nicoletti for allowing me to work in his lab during my time at University of Catania. Thank you for listening to my interests and then assigning me a project that not only nurtured those interests but challenged me. Because of you I am a better scientist, teacher, and presenter. Thank you for always seeing the positive side in my work!!

I would like to thank Prof. Guccione Salvatore for believing in me and for giving me the chance to make a great experience abroad.

I also must gratefully acknowledge Dr. Susan M. Lunte for welcoming me into her lab for sixteen months and teaching me a plethora of things about MCE and LIF. My experience in your lab was an amazing opportunity and I truly appreciate all of your mentorship. I also must thank your Program Coordinator Gary Webber, his help and his kindness were fundamental in the time spent in Lawrence.

I would like to thank Prof. Roberto Avola… he was both a Professor and a great friend for me!

A special note of thanks to people who have helped me in the lab or contributed to this project directly: Donatella Distefano, Paolo Parlascino, Giuseppe Malfa, Sonia Grasso, Irina Naletova, Ryan Grigsby, Anne Regel, Tom Linz, Jessica Creamer, David Scott, Dulan Gunasekara, Derek Jensen, Emilie Mainz, Jose Alberto Fracassi da Silva, Joe Siegel, Rachel Saylor, Nathan Oborny, Abdullah Al-Hossaini, Jeff Bauman, and Pann Pichetsurnthorn.

Thanks to my wonderful fiancee Claudia and my best friend Antonio for having always been at my side.

Thank you to all my family, without them my life would be nothing...I love you so much!!!